Enabling Technologies for Direct Detection Optical Phase Modulation Formats

Xian Xu

Department of Electrical & Computer Engineering
McGill University
Montréal, Canada

October 2009

A thesis submitted to the Faculty of Graduate Studies & Research in partial fulfillment of the requirements of the degree of Master of Engineering

Abstract

Phase modulation formats are believed to be one of the key enabling techniques for next generation high speed long haul fiber-optic communication systems due to the following main advantages: (1) with a balanced detection, a better receiver sensitivity over conventional intensity modulation formats, e.g., a ~3-dB sensitivity improvement using differential phase shift keying (DPSK) and a ~1.3-dB sensitivity improvement using differential quadrature phase shift keying (DQPSK); (2) excellent robustness against fiber nonlinearities; (3) high spectrum efficiency when using multilevel phase modulation formats, such as DQPSK. As the information is encoded in the phase of the optical field, the phase modulation formats are sensitive to the phase-related impairments and the deterioration induced in the phase-intensity conversion. This consequently creates new challenging issues. The research objective of this thesis is to depict some of the challenging issues and provide possible solutions.

The first challenge is the cross-phase modulation (XPM) penalty for the phase modulated channels co-propagating with the intensity modulated channels. The penalty comes from the pattern dependent intensity fluctuations of the neighboring intensity modulated channels being converted into phase noise in the phase modulation channels. We propose a model to theoretically analyze the XPM penalty dependence on the walk off effect. From this model, we suggest that using fibers with large local dispersion or intentionally introducing some residual dispersion per span would help mitigate the XPM penalty.

The second challenge is the polarization dependent frequency shift (PDf) induced penalty during the phase-intensity conversion. The direct detection DPSK is usually demodulated in a Mach-Zehnder delay interferometer (DI). The polarization dependence of DI introduces a PDf causing a frequency offset between the laser's frequency and the transmissivity peak of DI, degrading the demodulated DPSK signal. We found that PDf ratio, defined as PDf/FSR, plays a predominant role in determining the performance of

the demodulator. We further investigate on the PDf induced penalty for a 40-GHz DPSK demodulator on a 40-Gb/s return-to-zero (RZ)-DPSK signal to study PDf incurred optical filtering effect and spectrum distortion. Degradation for the RZ signal has been found in the presence the PDf.

The third challenge is fiber dispersion induced inter-symbol interference for the phase modulated signals. Traditionally the dispersion is compensated using dispersion compensation fibers (DCF). Recently emerged electronic dispersion compensation (EDC) not only avoids the attenuation that would be introduced by DCF, but also is capable of simultaneously compensating the chromatic dispersion (CD) and polarization mode dispersion (PMD). We investigate on EDC's CD and PMD compensation capabilities for the direct detection return-to-zero (NRZ)-DPSK signal. The simulation results show that around 300-ps/nm CD and 10-ps differential group delay (DGD) can be compensated by employing EDC. However, compared with the on-off keying (OOK) signal, the EDC is actually less effective with the DPSK signal. The investigation is extended to the RZ-DPSK signal and found out the decision feedback equalizer (DFE) exhibits better performance with the RZ-DPSK signal.

Sommaire

La modulation de phase est considérée comme l'une des technologies clés pour la prochaine génération des systèmes de communication optiques à haut débit et longue portée, en raison des avantages suivants: (1) A l'aide d'une modulation en phase suivi d'un détecteur balancé, nous obtenus une meilleure sensibilité du récepteur comparé aux formation de modulation en intensité conventionnels, par exemple, une amélioration de la sensibilité de ~3-dB en utilisant une modulation en modulation déplacement phase différentielle (DPSK) et une amélioration de la sensibilité de ~1.3-dB en utilisant une modulation en modulation déplacement phase en quadrature (DQPSK); (2) une tolérance accrue aux effets non-linéaires de la fibre; (3) une efficacité spectrale élevée, si l'on considère les formats de modulation de phase à plusieurs niveaux, comme par exemple la modulation en DQPSK. Puisque l'information est encodée par des changements de phase, ces formats de modulation sont sensibles aux dégradations liées à la phase du signal et aux détériorations provoquées par le processus de conversion phase-intensité. L'objectif de cette thèse est d'identifier les principaux défis associés à leur mise en œuvre, et de proposer des moyens de mitigation.

Le premier défi concerne la pénalité de transmission engendrée par la modulation de phase croisée (XPM), affectant les canaux modulés en phase qui sont adjacents aux canaux à modulation d'intensité. Dans ce cas, la dégradation de performance est provoquée par le fait que les fluctuations d'intensité des canaux voisins modulés en intensité, sont converties en bruit de phase pour les canaux utilisant la modulation de phase. Nous proposons un modèle théorique pour analyser l'effet du phénomène de walk-off et son influence sur les pénalités provoquées par la XPM. À partir de ce modèle, nous suggérons que l'utilisation de fibres optiques avec une dispersion locale importante ou l'ajout d'une certaine quantité de dispersion résiduelle à chaque section permettrait d'atténuer la pénalité XPM.

Le deuxième défi est associé au décalage de fréquence dépendant de la polarisation (PDf), qui survient lors de la conversion phase-intensité. La modulation en DPSK repose

sur l'utilisation au récepteur d'un interféromètre à délai (DI) Mach-Zehnder dont la sensibilité à la polarisation provoque du PDf, ce qui en retour cause un décalage entre la fréquence d'émission du laser et la sensibilité maximale du DI, dégradant ainsi la qualité du signal DPSK démodulé. Nous avons trouvé que le ratio PDf, définit comme étant PDf/FSR, joue un rôle primordial dans la détermination des performances du démodulateur. Nous étudions également l'influence de l'effet de filtrage optique induit par le PDf pour un démodulateur 40-GHz DPSK sur un signal 40-Gb/s RZ-DPSK. Une dégradation de performance est observée lorsque l'effet de filtrage induit par le PDf est présent.

Le troisième défi pour les formats de modulation de phase est l'interférence entre symboles provoquées par la dispersion de la fibre. Traditionnellement, la dispersion est compensée en utilisant des modules de compensation de dispersion (DCF). Des techniques plus récentes font appel à des systèmes de compensation de dispersion électroniques (EDC). Ceux-ci, en plus d'éviter l'atténuation induite par les DCF, peuvent simultanément compenser la dispersion chromatique (CD) et la dispersion de polarisation (PMD). Nous étudions les performances de systèmes EDC appliqués à la compensation de la CD et de la PMD, pour un signal NRZ-DPSK en détection directe. Les résultats de simulations indiquent qu'environ 300-ps/nm de CD et 10-ps de DGD peuvent être compensées par l'utilisation de systèmes EDC. Par contre, l'efficacité des EDC est moindre pour les systèmes de modulation par phase que pour les systèmes OOK. Un signal RZ-DPSK est également considéré et l'étude présentée met en relief que l'égaliseur de décision rétroactif (DFE) est plus performant avec ce type de modulation.

Acknowledgements

This thesis would not have been accomplished without the help of many people. First and foremost, I wish to express my deepest thanks to my supervisor, Professor David V. Plant, for introducing me to the exciting research field - ultra high data rate long haul optical communication systems, and providing constant encouragement and guidance to support my research work. I would also like to thank him for providing me with generous financial support so that I could come to McGill University for my graduate studies.

I would like to express my sincere gratitude to my co-supervisor, Professor Odile Liboiron-Ladouceur, for teaching me a lot in optical communications, making me develop from a beginner to an independent researcher. I am also very grateful to her for always carefully reviewing my publication and thesis drafts with patience, providing professional and valuable advices and comments, and correcting my presentations.

I would like to express my appreciation to Dragos Cotruta for working together on the re-circulating loop design and the experiment on polarization dependent frequency shift. I am really impressed by his ideas towards the research, the life and the society.

I am indebted to Benoît Châtelain for helping me a lot in the adaptive equalizer design and the digital signal processing, and giving many valuable suggestions. I really enjoy the frequent discussions among us about various topics in optical communications.

I am grateful to the following professors that have taught me the lifetime-benefited knowledge at the graduate level: Prof. Martin Rochette (Nonlinear fiber optics, Lightwave technology), Prof. Lawrence R. Chen (Lightwave technology); Prof. Jan Bajcsy (Introduction to digital communications); Prof. Lorne Mason (Telecommunication network analysis); Prof. Zetian Mi (Optoelectronic devices); and Prof. Ishiang Shih (Pysical basis of semiconductor devices); Prof. Frederic Nabki (RF microelectronics).

I gratefully acknowledge the help from the administrative and support staffs. Special thanks go to Joshua Schwartz and Christopher Rolston for ordering the parts we need in the experiments.

I would like to thank Zhaobing Tian, Yongyuan Zang, Mathieu Chagnon, Chen Chen, Bhavin Shastri, Ming Zeng, Mohammad Pasandi, Javad Haghighat, Kai Sun, Jifang Qiu, and Guannan Zheng for their help and advices both in experiments and in life. I was fortunate to work with all my past and present colleagues in the Photonic Systems Group.

Last but not least, I would like to say "I love you" to my parents, who dedicate their whole lives to raise me up, who always support my decisions, and who let me go abroad, thousands of miles away from them, for the upliftment of me! Lu, thanks for your love.

Xian Xu

Octorber, 2009

Contribution of Authors

The work presented in this thesis has been published or to be published in the following conference proceedings:

[1] **Xu X.**, Liboiron-Ladouceur O. and Plant D.V., 2008, "XPM penalty mitigation for a 42.7-Gb/s DQPSK channel co-propagating with 10.7-Gb/s OOK channels using SSMF and dispersion map," The 21st Annual Meeting of the IEEE Lasers and Electro-Optics Society (LEOS 2008), WH4.

[2] **Xu X.**, Tian Z., Liboiron-Ladouceur O. and Plant D. V., 2010, "Suppression of XPM-Induced nonlinear phase shifts using a walk-off effect in DQPSK/OOK hybrid systems," submitted to The Conference on Lasers and Electro-Optics and The Quantum Electronics and Laser Science Conference (CLEO/QELS) 2010.

[3] Cotruta D., **Xu X.**, Liboiron-Ladouceur O. and Plant D. V., 2009, "Polarization dependent frequency shift induced BER penalty in DPSK demodulators," The 22nd Annual Meeting of the IEEE Lasers and Electro-Optics Society (LEOS 2009), WM1.

In [2], I co-authored a paper with my colleague Zhaobing Tian. I conceived the idea, built the model, conducted the simulation and wrote the paper. Zhaobing gave a lot of useful suggestions to polish the model and helped me with the simulation.

In [3], I co-authored a paper with my colleague Dragos Cotruta. Both of us made substantial contributions to the paper. Dragos measured the PDf for the 10-GHz DI and proposed the measurement of the PDf for the 40-GHz DI. I proposed to compare the PDf effect between NRZ and RZ formats. We conceived the experiment strategy, conducted the experiment and wrote the paper together.

Other publications that is not directly related to this thesis:

[4] Chatelain B., Jiang Y., Roberts K., **Xu X.**, Cartledge J. C. and Plant D. V., 2010, "Impact of pulse shaping on SPM Tolerance in electronically pre-compensated optical systems," accepted to The Optical Fiber communication/National Fiber Optic Engineers Conference (OFC/NFOEC) 2010.

List of Acronyms

ASE	amplified spontaneous emission
AWG	arrayed waveguide grating
AWGN	additive white Gaussian noise
BER	bit error ratio
BERT	bit error rate tester
BPF	bandpass filter
CD	chromatic dispersion
CDR	clock data recovery
DCF	dispersion compensation fiber
DFB	distributed feedback laser
DFE	decision feedback equalizer
DGD	differential group delay
DI	delay interferometer
DPSK	differential phase shift keying
DQPSK	differential quadrature phase shift keying
DSF	dispersion-shifted fiber
DWDM	dense wavelength division multiplexing
EDC	electronic dispersion compensation
EDFA	erbium-doped fiber amplifier
FEC	forward error correction
FFE	feed-forward equalizer
FIR	finite impulse response
FSR	free spectral range
FWM	four-wave mixing
GVD	group velocity dispersion
ISI	inter-symbol interference
ITU-T	International Telecommunication Union -Telecommunication

	Standardization Sector
LEAF	large effective area fiber
LMS	least-mean-square
MLSE	maximum likelihood sequence estimator
MSE	mean square error
MZM	Mach-Zehnder modulator
NRZ	non-return-to-zero
NZDSF	non-zero dispersion-shifted fiber
OEO	optical-electrical-optical
OFDM	orthogonal frequency-division multiplexing
OOK	on-off keying
OPC	optical phase conjugation
OSA	optical spectrum analyzer
OSNR	optical signal to noise ratio
PC	polarization controller
PDf	polarization dependent frequency shift
PDL	polarization dependent loss
PDM	polarization division multiplexing
PMD	polarization mode dispersion
PRBS	pseudo-random bit sequence
QAM	quadrature amplitude modulation
RDPS	residual dispersion percentage per span
RLS	recursive least-square
ROADM	reconfigurable optical add-drop multiplexer
RZ	return-to-zero
SBS	stimulated Brillouin scattering
SNR	signal to noise ratio
SOP	state of polarization
SPM	self-phase modulation
SRS	stimulated Raman scattering
SSMF	standard single mode fibers

VOA	variable optical attenuator
WDM	wavelength division multiplexing
XPM	cross phase modulation

Table of Contents

Chapter 1 Introduction 1
1.1 Challenging Issues in Fiber-optic Communication Systems 1
1.1.1 Fiber loss 2
1.1.2 Noises 2
1.1.3 Fiber chromatic dispersion 3
1.1.4 Polarization related effects 4
1.1.5 Fiber nonlinearities 5
1.2 Advanced Key Enable Technologies 7
1.2.1 Advance optical modulation formats 7
1.2.2 Electronic dispersion compensation 8
1.3 Thesis Research Challenges and Objects 9
1.4 Thesis Overview 10
References 12
Chapter 2 XPM Penalty Mitigation for a 40-Gb/s DQPSK Channel Co-propagating with 10-Gb/s OOK Channels 14
2.1 Introduction 14
2.2 XPM penalty for the DQPSK channels in the co-propagation 15
2.2.1 Performance evaluation metric 15
2.2.2 Characterization of the XPM penalty for the DQPSK channels 17
2.3 Review of current approaches 19
2.4 Model of XPM mitigation approach based on walk off effect 20
2.4.1 Physical model of the XPM penalty for the DQPSK channel 20
2.4.2 Physical model of our XPM mitigation approach 21
2.4.3 Mathematical modeling of the XPM penalty's dependence on walk off effect 22
2.4.4 Analytical simulations of the dependence of XPM induced differential phase shift on walk off effect 24
2.5 System simulation demonstration 33

2.6 Summary 38
References 39
Chapter 3 Polarization Dependent Frequency Shift Induced Penalty in DPSK Demodulator 42
3.1 Introduction 42
3.2 Model of PDf in a DPSK demodulator 43
3.3 Experiment on polarization dependent frequency shift induced penalty for DPSK demodulator 50
3.3.1 Experiment Setup 50
3.3.2 Methodology 51
3.3.3 Experiment Result 53
3.4 Summary 57
Chapter 4 Electronic Dispersion Compensation for Direct Detection Phase Modulation Formats 60
4.1 Introduction 60
4.2 History of electronic dispersion compensation 61
4.3 Principle of Electronic Dispersion Post-compensation 62
4.3.1 Types of adaptive equalizers 63
4.3.2 Coefficients Adaptation algorithm 65
4.4 Performance study of electronic dispersion compensation for phase modulated optical communication systems 67
4.4.1 Simulation setup 67
4.4.2 Equalizer parameters 69
4.4.3 Simulation result 74
4.5 Summary 80
References 81
Chapter 5 Conclusion & Future Work 84
5.1 Summary 84
5.2 Future work 86

List of Figures

Figure 1.1 Channel capacity limit, evaluated in spectral efficiency, versus input power density for channels without and with fiber nonlinearity.. 6

Figure 2.1 Channel plan example for the co-propagation of 40-Gb/s DQPSK channels and 10-Gb/s OOK channels over the same fiber.. 15

Figure 2.2 Simulated XPM penalty for a DQPSK channel when co-propagating with 16 adjacent OOK channels and with 16 adjacent DQPSK channels, respectively. 18

Figure 2.3 The Q factor of the DQPSK channel and the OOK channels when increasing the OOK launch power per channel while keeping the DQPSK channel launch power constant. 19

Figure 2.4 Illustration of the walk off between the OOK channel and the DQPSK channel in LEAF and SSMF.. 21

Figure 2.5 Illustration of the walk off between the OOK channel and the DPSK channel for different dispersion schemes. 22

Figure 2.6 The XPM induced differential phase shift for the DQPSK channel transmitted over LEAF and SSMF.. 26

Figure 2.7 Probability density of the XPM induced differential phase shift for the DQPSK channel transmitted over LEAF and SSMF. The inset figure shows the profile of the probability density.. 26

Figure 2.8 Standard deviation (Std) of XPM-induced differential phase variance versus residual dispersion percentage per span and its corresponding number of walk off bits in the nearest pair of neighboring OOK channels (n_{c1}) for different number of adjacent OOK channels.. 28

Figure 2.9 The XPM induced differential phase shift for the DQPSK channel transmitted in a link with and without residual dispersion. 29

Figure 2.10 Probability density of the XPM induced differential phase shift for the DQPSK channel transmitted in a link with and without residual dispersion. The inset figure shows the profile of the probability density. 29

Figure 2.11 The XPM induced differential phase shift for the DQPSK channel transmitted in a link with different residual dispersion. 30
Figure 2.12 Probability density of the XPM induced differential phase shift for the DQPSK channel transmitted in a link with different residual dispersion. The inset figure shows the profile of the probability density. 31
Figure 2.13 Standard deviation of XPM-induced differential phase variance versus n_{c1} for different fiber types. 31
Figure 2.14 Comparison of standard deviations of XPM-induced differential phase variance in LEAF versus n_{c1} between the model in [24] and our model. 32
Figure 2.15 Standard deviation of XPM-induced differential phase variance versus n_{c1} for different channel plans 33
Figure 2.16 Schematic of the hybrid system setup. 34
Figure 2.17 Q penalty on the DQPSK channel versus OOK channel launch power. 35
Figure 2.18 The different dispersion compensation schemes and their corresponding transmission performances for the DQPSK channel co-propagating over LEAF fibers. . 36
Figure 2.19 The different dispersion compensation schemes and their corresponding transmission performances for the DQPSK channel co-propagating over SSMF fibers. . 36
Figure 2.20 The XPM penalty for the DQPSK channel transmitted over different fibers with different dispersion compensation schemes. 37
Figure 2.21 OOK launch power per channel at DQPSK 3-dB Q penalty. 38
Figure 3.1 Schematic of a fiber-based DPSK demodulator. 43
Figure 3.2 The frequency response at the constructive and destructive ports for two orthogonal SOP of a DI with FSR=10-GHz and measured PDf=1-GHz. 44
Figure 3.3 The spectrum profile of the received DPSK signal after the DI and the PDf induced penalty. 45
Figure 3.4 The transmissivity at the constructive port of the DIs with FSR=10-GHz and FSR=40-GHz for different SOP. 46
Figure 3.5 The comparison of the spectrum of the demodulated signal at the constructive port of the DIs with FSR=10-GHz and FSR=40-GHz and the PDf induced penalty. 47
Figure 3.6 The spectrum profile of the received RZ-DPSK signal after the DI and the PDf induced penalty. 49

Figure 3.7 The comparison of the PDf induced penalty for the DIs with FSR=10-GHz and FSR=11-GHz. 50
Figure 3.8 Schematic of the experiment setup. 51
Figure 3.9 Set of SOPs that uniformly cover the Poincaré sphere. 52
Figure 3.10 The aligning process and the PDf measurement. 53
Figure 3.11 BER versus frequency detuning for the fast and slow polarization axis for the10-GHz and 40-GHz DI and the zoom-in at the frequency range of -2-GHz to 2-GHz. 54
Figure 3.12 Comparison between the 40-Gb/s NRZ-DPSK and RZ-DPSK signals, both modulated and demodulated spectrums at no frequency shift. 55
Figure 3.13 Comparison between the 40-Gb/s NRZ-DPSK and RZ-DPSK signals, both modulated and demodulated spectrums at a frequency shift of 11.425-GHz. 56
Figure 3.14 BER versus frequency detuning for the 40-Gb/s NRZ-DPSK and RZ-DPSK signals for the fast and slow polarization axis of a 40-GHz DI and the zoom-in at the frequency range of -2-GHz to 2-GHz 57
Figure 4.1 Model for a typical baseband communication system. 62
Figure 4.2 Schematic of FIR filter. 63
Figure 4.3 Schematic of FFE equalizer. 65
Figure 4.4 Schematic of DFE equalizer. 65
Figure 4.5 Simulation setup. 67
Figure 4.6 BER versus OSNR at an accumulate CD of 1280-ps/nm for the unequalized signal and the equalized signal from the equalizers with different samples per bit.......... 71
Figure 4.7 BER versus OSNR at an accumulate CD of 1280-ps/nm for the unequalized signal and the equalized signal from the equalizers with 5 taps, 7 taps and 9 taps. 72
Figure 4.8 The convergence speed and variance dependence on the step size of tap weights 73
Figure 4.9 The MSE before a FFE equalizer which compensates the dispersion of 1280-ps/nm. 74
Figure 4.10 The MSE after a FFE equalizer which compensates the dispersion of 1280-ps/nm. 74
Figure 4.11 The required OSNR at BER=10^{-3} versus accumulative CD for the

NRZ-DPSK signal without equalization, with the FFE equalization and with the DFE equalization. 75
Figure 4.12 The signal eye diagrams at an accumulative CD of 1280-ps/nm and the OSNR of 13-dB.. 76
Figure 4.13 The required OSNR@BER=10^{-3} versus DGD for the NRZ-DPSK signal without equalization, with the FFE equalization and with the DFE equalization. 76
Figure 4.14 The signal eye diagrams at a DGD of 60-ps and the OSNR of 10-dB. 77
Figure 4.15 The required OSNR at BER=10^{-3} versus accumulative CD for the NRZ-DPSK signal and the NRZ-OOK signal without equalization, with the FFE equalization and with the DFE equalization. 78
Figure 4.16 The eye diagrams for the NRZ-OOK signal at an accumulative CD of 1280-ps/nm and the OSNR of 17-dB. 78
Figure 4.17 The required OSNR at BER=10^{-3} versus accumulative CD for the NRZ-DPSK signal and the RZ-DPSK signal without equalization, with the FFE equalization and with the DFE equalization. 79
Figure 4.18 The eye diagrams for the RZ-DPSK signal at an accumulative CD of 1280-ps/nm and the OSNR of 14-dB. 80

List of Tables

Table 1.1 Summary of the evolution of the fiber loss over different wavelength regions. . 2

Table 2.1 Simulation parameters. 25

Table 3.1 The comparison of PDf induced penalty and the PDf ratio for DIs with different FSR 48

Table 3.2 The PDf induced penalty ratio dependence on the FSR of the DI. 50

Chapter 1 Introduction

1.1 Challenging Issues in Fiber-optic Communication Systems

Last century witnessed the revolution of communication systems, driven by the emergence and development of the computers and the Internet. The two questions that naturally arisen were: (1) Is there an upper bound of the channel capacity that a communication link can reach? (2) If there is such a limit, how to approach this limit? In 1948, Shannon proposed the channel capacity limit for the memory-less bandlimited channels in the presence of additive white Gaussian noise (AWGN) [1]. In his theory, for a given channel with a signal power of S and a noise power of N, the channel capacity (C) is related to the channel bandwidth (B) and signal-to-noise ratio (S/N) through the formula: $C = B \cdot \log_2\left(1+\frac{S}{N}\right)$. For a given bandwidth, the spectral efficiency, defined as C/B, is usually used instead of channel capacity. It is related to the S/N by: $S_{eff} = \frac{C}{B} = \log_2\left(1+\frac{S}{N}\right)$. Since then, the communication systems engineers have always been making attempts to approach the Shannon limit with a tolerable complexity.

Prior to the introduction of fiber-optic communications, microwave communication systems evolved considerably during the decade of the 1950s and the 1960s. In the late 1960s, microwave systems were able to operate at a bit rate of up to 200-Mb/s and closed to the fundamental limit [2]. Therefore further research efforts were put into looking for new kinds of medium that would provide a larger system capacity. It was realized in the 1950s that optical waves could increase the system capacity by several orders of magnitude because of its high carrier frequency. However, fiber-optic communication systems did not come true until the 1970s when the room temperature compact coherent optical source – semiconductor laser and low-loss optical fiber were available [2]. After the first successful field trial in Chicago in 1977, fiber-optic communication systems were commercially deployed in 1980 [3][4]. However, there were still several challenging issues for such systems.

1.1.1 Fiber loss

Coming from the material absorption of silica and the Rayleigh scattering [5], the fiber loss leads to a reduction in intensity of the light beam with respect to distance transmitted in a fiber. In order to correctly distinguish the signal from the noises, optical receiver needs a certain minimum amount of signal power. Therefore, for early fiber-optic transmission systems, the distance was mainly limited by the fiber loss. Much research had then gone into both minimizing the fiber loss and maximizing the amplification of the optical signal. Table 1.1 summaries the evolution of the fiber loss over different wavelength regions.

Table 1.1 Summary of the evolution of the fiber loss over different wavelength regions.

Generation	Year	Wavelength (nm)	Loss (dB/km)	Repeater spacing (km)
1st	1975	850	2	10
2nd	Early 1980s	1310	0.5	50
3rd	1990	1550	0.2	60~70

The fiber loss of the third generation fiber-optic transmission systems was already closed to the fundamental limit of about 0.16-dB/km of silica fibers. The erbium-doped fiber amplifier (EDFA) , invented in 1987, not only replaced the cumbersome and low-speed optical-electrical-optical (OEO) conversion but also paved the way for wavelength division multiplexing (WDM) as EDFA can simultaneously amplifier multi-wavelengths within its broad gain spectrum [6]. Fiber-optic communication systems evolved to its fourth generation characterized by using EDFA and WDM to extend the maximum reach and system capacity. Although some efforts are still put into minimizing the fiber loss, the fiber loss is not longer a major issue for current fiber-optic communication systems.

1.1.2 Noises

The noises are generated from optical amplifiers and photodetectors. Although optical amplifiers can compensate the fiber loss periodically for the data transmission over tens of thousands kilometers without OEO generation [7], they also introduce amplified spontaneous emission (ASE) noise that corrupts the optical signals. In addition, the photodetectors convert the incident optical power into electric current but the conversion is not noise free. It introduces shot noise and thermal noise as well. An intuitive way to combat the noises is to improve the signal-to-noise ratio (SNR) by increasing the signal powers. Nonetheless, the optical fiber is a nonlinear medium. Under large launch powers, the fiber nonlinearity effects will become dominant impairments, leading to other signal distortions. Therefore, there is a maximum limit for the launched signal powers. Another effective way to suppress the ASE noise is to employ a filter in the receiver. However, the filter only filters out the out-of-band noise and the in-band noise is still a problem. The distributed Raman amplifiers are found to effectively reduce the noise accumulation because the signal amplification occurs along the signal transmission path and then the separations between the amplifiers are reduced [2]. However, since the Raman effect is a nonlinear process, the Raman amplification requires very high pump powers and has a relatively poor pumping efficiency [8]. Forward error correction (FEC) is another effective way to correct the errors in any noise limited system. Recently the third generation FEC was report to have a 10-dB coding gain, which may correct a BER of 10^{-2} up to 10^{-13} [9]. Nonetheless, no matter how sophisticated technology is used, the noise is still an unavoidable impairment and is always a fundamental limit for fiber-optic communication systems.

1.1.3 Fiber chromatic dispersion

Dispersion refers to the phenomenon that light of different spectral components or different polarization components within pulses travels at different speeds, leading to pulse broadening. Dispersion in optical fibers can be categorized into three main types, namely material dispersion, waveguide dispersion and modal dispersion. Both material dispersion and waveguide dispersion are frequency-dependent dispersion, causing the group velocity changing with the wavelength. Therefore, they are also called chromatic dispersion. Several approaches have been employed to compensate the chromatic dispersion. The dispersion-shifted fibers (DSF) are realized by carefully optimizing of the fiber parameters to increase the waveguide dispersion in an optical fiber such that the sum of material and waveguide dispersion becomes zero at 1550 nm [5]. However, in WDM systems, where the optical channels are equally spaced, the fibers with zero dispersion suffer from severe penalties from nonlinearity effects, such as four-wave mixing. Therefore, the nonzero dispersion-shifted fibers (NZDSF) designed to have a small amount of residual dispersion at 1550 nm are more often used. Compared to the standard single mode fibers (SSMF), although the NZDSF could reduce the dispersion of the fibers, they also reduced the nonlinearity tolerance of the systems. Moreover, as the SSMF are already widely deployed, it is cost-prohibitive to re-deploy the NZDSF. Dispersion compensation fiber (DCF) is an effective solution to the chromatic dispersion problem. Similar to DSF, DCF are made available by controlling the fiber parameters such that the sum of material and waveguide dispersion exhibits a large negative value at 1550 nm. DCF can work with any type of fiber, e.g. NZDSF and SSMF, and can be placed in anywhere in the link depending on the dispersion maps. However, DCF will introduce extra loss to the system. In addition, DCF lack flexibility as they are not tunable and they cannot adaptively compensate the dispersion if the length of the link changes. Consequently, chromatic dispersion compensation is a challenging issue for current systems.

1.1.4 Polarization related effects

The PMD, resulted from modal dispersion in the fiber, causes random broadening of pulses because of a group delay between different polarization states [5]. In the early 1980s, the systems were operating on multimode fibers and the bit rate was limited at 100-Mb/s due to modal dispersion [2]. By replacing the multimode fibers with the single mode fibers, the modal dispersion was significantly reduced. However, the single mode fibers are not truly single mode - they can support two degenerate modes in two orthogonal polarizations. Therefore, the PMD is still a major source of impairment for the systems with a bit rate beyond 10-Gb/s. The difficulty involved in compensating the PMD is that it varies with time and wavelength. An optical PMD compensator based on a feedback loop is able to track the PMD variation with time. It firstly splits PMD-distorted signal into two components and then introduces an adjustable delay in one component based on the error signals from the feedback loop. The two components are finally combined again [2]. The drawback with this optical PMD compensator is that it cannot compensate multi-channel's PMDs simultaneously. A multi-channels' PMD compensation technique was proposed by using fast polarization scrambling and FEC. It transforms PMD-induced outage times to some short error bursts which can be corrected by the FEC. However, this technique works well with systems of fixed differential group delay (DGD) and may not be directly applied to practical systems where the DGD is varying with time and wavelength [10]. Therefore, the PMD is a major impairment for current high-speed fiber-optic systems.

The polarization dependent loss (PDL) is another key polarization dependent impairment. When the optical signal passes through a component with different losses towards different states of polarization (SOP), the signal will suffer PDL effect. PDL is defined as the difference between a component's minimum and maximum polarization dependent insertion loss. PDL occurs mainly in components such as modulators, amplifiers, couplers, filters, attenuators, and isolators. Although the amount of PDL is relatively small for each component, the accumulative PDL may cause the output signal to have a large power fluctuation changing with the SOP of the input signal [2]. PDL, combined with PMD, will lead to not only power fluctuation but also signal distortion.

The polarization dependent frequency shift (PDf) is a main impairment for direct detection phase modulation formats as it usually occurs at the delay interferometer (DI), where the phase modulated signal is demodulated. It originates from the birefringence of the bent fiber in DI. It will introduce a frequency offset between the laser's frequency and the transmissivity peak of DI, thereby leading to power penalty and spectral distortion of the demodulated signal.

1.1.5 Fiber nonlinearities

Fiber nonlinearities originate from the intensity dependence of the refractive index (also called Kerr effect) and stimulated inelastic scattering [5]. The nonlinearity effects generated from Kerr effect are self-phase modulation (SPM), cross phase modulation (XPM) and four-wave mixing (FWM). At a channel with a baud rate of 20 Gbaud and below, these Kerr nonlinearities mainly happen between individually interacting WDM channels. Consequently they are called inter-channel nonlinearities. At the channel with a baud rate beyond 20-Gbaud and with large local dispersion, these Kerr nonlinearities can also take place between individually interacting bits within a single WDM channel. Thus they are called intra-channel nonlinearities [11]. The simulated inelastic scattering can induce stimulated effects such as stimulated Brillouin scattering (SBS) and stimulated

Raman scattering (SRS). However, they are generally not detrimental since the power thresholds are normally higher than the practical launch power in fiber-optic transmission systems. Therefore, most efforts are put in suppressing the Kerr nonlinearities.

A signal experiencing Kerr nonlinearities is usually calculated by integrating a nonlinear Schrödinger equation and may not have a direct relationship with an instantaneous nonlinearity. This makes the optical fiber channels to be nonlinear channels with memory, which are quite different from Shannon's linear memory-less channel model [12]. Mitra proposed a channel capacity limit for the nonlinear fiber-optic channel with memory [12]. Unlike the Shannon limit that the channel capacity increases with the input signal power, the nonlinear fiber-optic channel capacity gets saturated at some input signal power and decreases because of increasing nonlinear interference as shown in Figure 1.1. Therefore, the mitigation techniques for nonlinear effects are trying to approach the nonlinear limit.

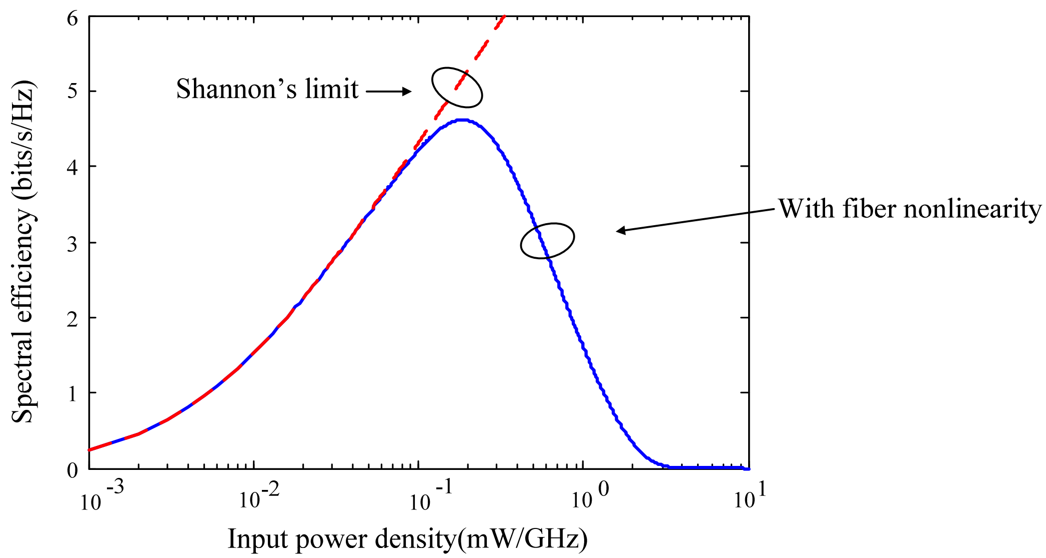

Figure 1.1 Channel capacity limit, evaluated in spectral efficiency, versus input power density for channels without and with fiber nonlinearity. Reproduced by using equation 2 in [12] with the parameters in fig. 1 of [12].

Kerr nonlinearity is a major challenge for current high-speed long haul fiber-optic communication systems and several mitigation approaches were proposed. Dispersion map is an effective way to suppress the Kerr nonlinearities. Dispersion can be used to suppress the FWM since it may destroy the phase matching condition required to generate the FWM [5]. However, the compensation becomes more difficult because of the lack of materials with negative nonlinearity and high group-velocity dispersion simultaneously [13]. Optical phase conjugation (OPC), which inverts the spectrum of the signal in the middle of the transmission link, can cancel out the impairments experienced in the first part of the link with the impairments in the second part of the link. It has been reported that OPC can compensate the SPM and the intra-channel nonlinearities [14]. Nevertheless, wide-band optical phase conjugation exchanges the channel wavelengths, making it complicate for the design and operation of WDM networks. Also, the performance and reliability of prototype conjugators are not yet sufficient for field deployment. Back-propagation was recently proposed to compensate the nonlinear effects. It solves an inverse nonlinear Schrödinger equation through the fiber to estimate the transmitted signal and has been shown to enable higher launched power and longer system reach in DWDM transmission. The main drawbacks of back-propagation are its excessive computation complexity and the difficulty in applying it in the presence of PMD [15]. Thus, the Kerr nonlinearity is one of the major challenges for the high speed long haul fiber-optic communication systems.

1.2 Advanced Key Enable Technologies

Although the technologies elucidated above were employed to approach the system's maximum reach, the systems' performance is still far from its fundamental limit. More advanced enable technologies were proposed recently to further increase the systems' capacity.

1.2.1 Advance optical modulation formats

Modulation is a technology that facilitates information transmission over a medium. Advanced modulation formats for fiber-optic systems not only enable the system to have a strong resilience to linear and nonlinear impairments but also increase the system's spectral efficiency. In optical fibers, the optical field has three physical attributes that can be modulated: intensity, phase and polarization [11]. These attributes can be modulated separately or jointly. Early fiber-optic transmissions were exclusively using the basic binary intensity modulation – non-return-to-zero on-off keying (NRZ-OOK) as it is the simplest to implement. Lately, return-to-zero (RZ)-OOK was widely used in systems as it slightly increases the pulse spacing and reduces the power per bit, thereby increasing the tolerance to nonlinear distortions. The price to pay is that the RZ signal occupies nearly twice the spectrum of the NRZ signal and require an extra modulator to do the RZ pulse carve. In recent years, phase modulation formats became attractive for high speed long haul fiber-optic transmissions due to their better sensitivity by using balanced detection (e.g. a 3-dB sensitivity improvement using differential phase shift keying (DPSK) and a 1.3-dB sensitivity improvement using differential quadrature phase shift keying (DQPSK)) and their strong robustness to fiber nonlinearities compared to the intensity modulation formats [16]. Among them, the quadrature phase-shift keying (QPSK) was most intensively studied as it can encode 2 bits in one symbol and is one of the few practical multilevel modulation formats that enable increasing the system's spectral efficiency. Polarization division multiplexing (PDM) is another approach employed to double the system's spectral efficiency. It is believed that PDM-QPSK with coherent detection and digital signal processing is the most promising candidate for 100-Gb/s systems over wide area networks at 50-GHz channel grid [17]. Recently, orthogonal frequency-division multiplexing (OFDM) and quadrature amplitude modulation (QAM), are becoming hot topics in optical communication domain, and they are also arguably to be one of the key enabling modulation formats for next-generation fiber-optic transmission to approach the fundamental limit [18].

1.2.2 Electronic dispersion compensation (EDC)

EDC is capable of compensating CD and PMD induced ISI impairments in fiber-optic communication channels by constructing filter structures that match, or adapt to match the channel characteristics of the transmission link [19]. Prior to the introduction of EDC, dispersion compensation in optical communication systems was mainly realized by placing the DCF of proper length at the end of each transmission span. However, these DCF are designed to work in static conditions and cannot cope with the dispersion statistical variations. They also introduce considerable attenuation to the systems and consequently more EDFA are required to compensate for the loss. More ASE noises generated from these EDFA are accumulated in the link, thereby reducing the maximum transmission length. EDC may be a cost-effective and flexible solution. Current transmitter based electronic equalizers are able to compensate dispersion of 5120-km transmission over NZDSF for 10-Gb/s RZ-DPSK without any optical dispersion compensation [20]. The state-of-arts receiver based electronic equalizers can compensate dispersion of 2480-km transmission over SSMF for 40 Gb/s coherent detection PDM-QPSK without optical dispersion compensation [21]. In addition, the EDC can compensate the impairments caused by CD, PMD, SPM and the intra-channel nonlinearities simultaneously, which the DCF fails to accomplish [22][23]. Moreover, modern optical communication networks with different transmission paths may carry light paths of different distances with different amounts of dispersion. The EDC enables the equalization to adapt to the variance of the transmission length, lending more flexibility to the optical network designs [24]. Nowadays, the EDC has been an integrated part of digital signal processing for coherent receivers, which allows the received signal keeping all its information after detection for further processing. They work together towards the fundamental limit of fiber-optic communications.

1.3 Thesis Research Challenges and Objects

As the phase modulation formats are among the most promising modulation formats for future high speed long haul fiber-optic communication systems, it is of great significance to study their performance. Although they have been intensively studied for several years, some of their new issues are recently found and remain unsolved. More specifically, the first issue comes when the DQPSK channel co-propagates with the OOK channels, the DQPSK channel will suffer from severe impairment from XPM because the intensity fluctuations of the OOK channels are converted into the phase noise of the DQPSK channels. Does the fiber type have an impact on the XPM penalty in the co-propagation problem? Does the XPM penalty have a dependence on the dispersion compensation schemes? The second issue is when the phase modulation formats are modulated using direct detection, the birefringence of the fiber-based DI will introduce a PDf which causes a frequency offset between the laser's frequency and the transmissivity peak of DI, degrading the performance of phase demodulation. Will the performance become even worse when the bit rate of phase modulation increases? Will the PDf induced penalty be less if the phase modulation use RZ pulse shaping? The third issue is when using the phase modulation together with the EDC, will the performance be better than that of using the amplitude modulation with the EDC? Can the performance be improved by using the RZ pulse shaping? All of these questions are new and create research challenges for the phase modulation formats.

The objective of this thesis is to provide solutions for the problems enumerated above. In particular, we designed:

- a model for the XPM induced differential phase shift of the DQPSK signal dependence on walk off effect in the co-propagation problem;
- Simulation comparisons of the XPM penalty of the DQPSK channel co-propagating with the OOK channels for different fibers under different dispersion maps;
- Simulation and experimental comparisons of the PDf induced penalty for the DPSK signals with varying bit rates and pulse shaping;
- Simulations of the EDC's CD and PMD compensation capabilities for the direct detection DPSK signals with different pulse shaping.

1.4 Thesis Overview

The thesis is organized as follows:

- **Chapter 2 XPM penalty mitigation for a 40-Gb/s DQPSK channel co-propagating with 10-Gb/s OOK channels**

  In this chapter, we state our motivation in working on the co-propagation of a 40-Gb/s DQPSK channel with adjacent 10-Gb/s OOK channels and review existing solutions to mitigate the XPM penalty of the DQPSK channel. We propose a model of mitigating the XPM penalty by using the walk off effect. Corresponding mathematical analysis and simulation demonstration are provided to verify our model.
- **Chapter 3 Polarization dependent frequency shift induced penalty in DPSK demodulator**

  Starting from the frequency response of the DI, the chapter gives a comprehensive analysis of the PDf induced penalty for the phase modulation formats with different bit rates and different pulse shaping. The experiment results are also presented to support our analysis.
- **Chapter 4 Electronic dispersion compensation for phase modulation formats**

  Based on the principle of electronic dispersion compensation described in the beginning of the chapter, we investigate on the EDC's CD and PMD compensation capabilities for the direct detection NRZ-DPSK signal. The investigation is extended by comparing the results with that of the OOK signal with the EDC. The effect of RZ pulse shaping on the EDC' performance is studied in this chapter as well.

- **Chapter 5 Conclusion & Future work**

  The last chapter concludes the thesis with a brief review of the main contributions of the study presented in the preceding chapters. Based on this work, we also propose future research directions.

References

[1] Shannon C. E., 1948, "A mathematical theory of communications," Bell System Technology Journal, vol. 27, pp. 379-423, 623-656.

[2] Agrawal G. P., 2005, Lightwave Technology, Wiley-interscience Publisher.

[3] Sanferrare R. J., 1987, "Terrestrial Lightwave Systems," AT&T Technology Journal, vol. 66, no.1, pp. 95-107.

[4] Fan C. and Clark L., 1995, Optics & Photonics News, vol. 6, no.2, pp. 26.

[5] Agrawal G. P., 2007, Nonlinear Fiber Optics, Academic Press, pp. 5-9, 13.

[6] Olsson N. A., 1989, "Lightwave systems with optical amplifiers," Journal of Lightwave Technology, vol. 7, no.7, pp. 1071-1082.

[7] Bergano N. S., Aspell J., Davidson C. R., Trischitta P. R., Nyman B. M., Kerfoot F.W., 1991, "Bit error rate measurements of 14000 km 5 Gbit/s fibre-amplifier transmission system using circulating loop," Electronics letters, vol. 27, no. 21, pp. 1889-1890.

[8] Islam M. N., 2004, Raman Amplification in Telecommunications, Springer Publisher, pp. 7.

[9] Mizouchi T, 2005, "Recent Progress in Forward Error Correction for Optical Communication Systems," IEICE Transaction on Communication, vol. E88-B, no.5, pp. 1934-1946.

[10] Bülow H., Xie C., Klekamp A., Liu X. and Franz B., 2009, "PMD Compensation/mitigation techniques for high-speed optical transport," Bell System Technology Journal, vol. 14, no.1, pp. 379-423, 623-656.

[11] Winzer, P. J. and Essiambre R. J., 2006, "Advanced optical modulation formats," Proceedings of the IEEE, vol. 94, no. 5, pp. 952-985.

[12] Mitra P. P. and Stark J. B., 2001, "Nonlinear limits to the information capacity of optical fibre communications," Nature, vol. 411, pp. 1027-1030.

[13] Wei H. and Plant D. V., 2004, "Intra-channel nonlinearity compensation with scaled translational symmetry," Optics Express, vol. 12, no. 18, pp. 4282-4296.

[14] Jansen S. L., Borne D. V. D., Spinnler V., Calabrò S., Suche H., Krummrich P. M., Sohler W., Khoe G. D., and Waardt H. D., 2006, "Optical phase conjugation for ultra

long-haul phase-shift-keyed transmission," Journal of Lightwave Technology, vol. 24, no. 1, pp. 54-64.

[15] Ip E. and Kahn J. M., 2008, "Compensation of dispersion and nonlinear effects using digital backpropagation," Journal of Lightwave Technology, vol. 26, no. 20, pp. 3416-3425.

[16] Ho K. P., 2005, Phase-modulated optical communication systems, Springer Publisher.

[17] Renaudier J., Charlet G., Bertran-Pardo O., Mardoyan H., Tran P., Salsi M. and Bigo S., 2009, "Transmission of 100Gb/s Coherent PDM-QPSK over 16x100km of standard fiber with allerbium amplifiers," Optics Express, vol. 17, no. 7, pp. 5112-5119.

[18] Rosenkranz W., Leibrich J., Serbay M. and Ali A., 2007, "Orthogonal frequency division multiplexing (OFDM) and other advanced options to achieve 100Gb/s ethernet transmission," The 9th International Conference on Transparent Optical Networks (ICTON) 2007, pp. 12-15.

[19] Nielsen X. and Chandrasekhar S., 2004, "OFC 2004 workshop on optical and electronic mitigation of impairments," Journal of Lightwave Technology, vol. 23, no. 1, pp. 131-142.

[20] McGhan D., Laperle C., Savchenko A., Li C. D., Mak G. and O'Sullivan M., 2006, "5120-km RZ-DPSK transmission over G.652 fiber at 10 Gb/s without optical dispersion compensation," Photonics Technology Letters, vol. 18, no. 2, pp. 400-402.

[21] Savory S.J., 2006, "Digital equalization of 40 Gbit/s per wavelength transmission over 2,480 km of standard fiber without optical dispersion compensation," The 32nd European Conference on Optical communications (ECOC) 2006, Th 2.5.5.

[22] Roberts K., Li C. D., Strawczynski L., O'Sullivan M. and Hardcastle I., 2006, "Electronic precompensation of optical nonlinearity," Photonics Technology Letters, vol. 18, no. 2, pp. 403-405.

[23] Weber C., Fischer J.K., Bunge C. A. and Petermann K., "Electronic precompensation of intrachannel nonlinearities at 40 Gb/s," Photonics Technology Letters, vol. 18, no. 16, pp. 1759-1761.

[24] Binh L. N., 2009, Digital optical communications, CRC Press.

Chapter 2 XPM Penalty Mitigation for a 40-Gb/s DQPSK Channel Co-propagating with 10-Gb/s OOK Channels

2.1 Introduction

As the demand increases for high speed internet access and multimedia broadcasting, the capacities of most current 10-Gb/s systems already get filled and fail to keep up with the increasing traffic growth. Systems are now being upgraded to 40-Gb/s and will probably be upgraded to 100-Gb/s in the near future [1]. A smooth upgrade requires operating high speed channels on currently deployed system infrastructures without affecting other presently running 10-Gb/s on-off keying (OOK) channels. Since most current systems are built on 50-GHz DWDM channel grid originally designed for the NRZ-OOK channels modulated at 10-Gb/s, and contain reconfigurable optical add-drop multiplexers (ROADM) which have strong filtering effects [2], a narrow bandwidth modulation format is required in order to fit the high speed channel's spectrum profile into this channel grid. Differential Quadrature phase shift keying (DQPSK) is attractive due to its high spectrum efficiency, good optical signal-to-noise ratio (OSNR) sensitivity, and excellent tolerance to the chromatic dispersion (CD) and the polarization mode dispersion (PMD). But compared to the OOK modulation format, transmitters and receivers of the DQPSK modulation are more complex, leading to higher cost. Thus, out of the cost-effectiveness consideration, the service providers may not upgrade all the channels to 40-Gb/s. In the future, the 10-Gb/s OOK channels will still co-exist with the 40-Gb/s DQPSK channels over the same fiber, as shown in Figure 2.1.

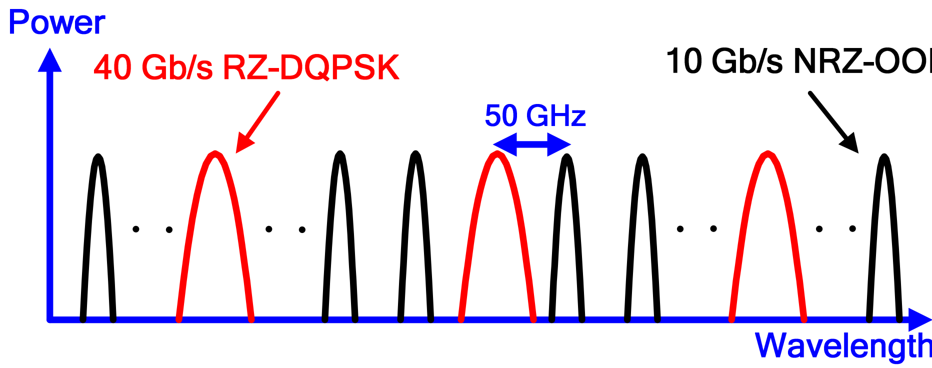

Figure 2.1 Channel plan example for the co-propagation of 40-Gb/s DQPSK channels and 10-Gb/s OOK channels over the same fiber.

2.2 XPM penalty for the DQPSK channels in the co-propagation

When co-propagating with the OOK channels, the DQPSK channels suffer severe limitation from cross phase modulation (XPM) nonlinearity effect, through which the pattern dependent intensity fluctuations of the OOK channels are converted into the phase noise in the DQPSK channels. Figure 2.2 and Figure 2.3 illustrate the XPM penalty for a 40-Gb/s RZ-DQPSK channel when co-propagating with 16 adjacent 10-Gb/s NRZ-OOK channels. The DQPSK channel locates amid the 16 OOK channels on 50-GHz channels spacing. The simulated transmission length is 6 spans, with 80-km-long standard single mode fiber (SSMF) per span. The dispersion is fully compensated using dispersion compensation fiber (DCF) at the end of each span, meaning that there is no residual dispersion per span. The noises included in the simulation are the amplified spontaneous emission (ASE) from EDFAs at the end of each span, shot noise and thermal noise at the photodetector. We assume the system is ASE noise dominated. The noise figure of each EDFA is 6-dB.

2.2.1 Performance evaluation metric

The performance is evaluated in term of Q factor. According to Nyquist's sampling theorem and the sample rate setting in our simulation tool - Optisystem, 32-samples per bit is required to accurately simulate multi-channels' XPM effect. However, due to the limitation of computation time and complexity, with 32-samples per bit, the simulation program is unable to generate enough bits to directly count the bit error rate (BER). (In chapter 5, we can direct count the BER because 2-samples per bit is sufficient to simulate single channel's dispersion effect and so more bits can be generated.) The Q factor is therefore used to estimate the BER by evaluating the signal's statistical fluctuation. In ASE limited system, the noise distribution is Chi-square [3]. However, it has been shown that Gaussian approximation gives fairly good results for intensity modulated formats such as OOK. Therefore, assuming at the receiver, the dispersion is fully compensated, meaning that there is no inter-symbol interference, we may use the standard Q factor to estimate BER for the OOK channels. The standard Q factor is defined as [4]:

$$Q = \frac{\mu_1 - \mu_0}{\sigma_1 + \sigma_0} \tag{2.1}$$

where μ_1, σ_1 and μ_0, σ_0 are the mean and standard deviation of the received variables around the logical "1" and "0" levels, respectively. Under Gaussian approximation, the BER can be estimated by:

$$\mathrm{BER} = \frac{1}{2}\mathrm{erfc}\left(\frac{Q}{\sqrt{2}}\right) \tag{2.2}$$

where $\mathrm{erfc}(\cdot)$ is the complementary error function. However, it has been shown in that BER estimation based on the standard Q factor for differential phase modulation formats is not accurate because of the non-Gaussian nature of the noise distribution in the output of the balanced detector [5][6][7]. Two methods have been employed to estimate BER when the noise distribution is not Gaussian. One is to use closed-form formula in derived from Marcum's Q function [8][9]. The other method is to use differential phase Q factor (DP-Q) [5][6]. Here we use DP-Q because the first method is difficult to calculate for small BER [8]. The idea behind DP-Q is the Gaussian distribution of the noise at the differential phase eye diagram of the received signal. DP-Q has been applied in RZ-DPSK systems [5][6] and RZ-DQPSK systems [10]. A correction factor has been suggested to be applied on DP-Q to avoid underestimation of the BER value [11]. According to [10], for DQPSK systems, the DP-Q is defined as:

$$Q_{\Delta\phi^{(I,Q)}} = \frac{c_f \cdot \pi}{2(\sigma_{\Delta\phi_0^{(I,Q)}} + \sigma_{\Delta\phi_1^{(I,Q)}})} \tag{2.3}$$

where c_f is the correction factor, $\sigma_{\Delta\phi_0^{(I,Q)}}$ and $\sigma_{\Delta\phi_1^{(I,Q)}}$ represent the standard deviation of differential phase $\Delta\phi^{(I,Q)}$ for the "0" and "1" bit rails, respectively. The distribution of

$\Delta\phi^{(I,Q)}$ can be seen as a superposition of two Gaussian distributions with positive (+) and negative means (-). They may have different standard deviations. Therefore, the BER for the I and Q components can be estimated by:

$$\mathrm{BER}^{(I,Q)} = \frac{1}{4}\left[\mathrm{erfc}\left(\frac{Q_{\Delta\phi_{+}^{(I,Q)}}}{\sqrt{2}}\right) + \mathrm{erfc}\left(\frac{Q_{\Delta\phi_{-}^{(I,Q)}}}{\sqrt{2}}\right)\right] \tag{2.4}$$

Assuming Gray mapping, the overall BER is given by:

$$\mathrm{BER} = \frac{1}{2}\left[1 - \left(1 - \mathrm{BER}^{(I)}\right)\left(1 - \mathrm{BER}^{(Q)}\right)\right] \tag{2.5}$$

By comparing the estimated BER with BER of direct counting, a good fit is found when $c_f = 0.76$. In order to be able to compare with the Q factor of OOK channels, the BER for the DQPSK signal is converted back to the standard Q factor by using Equation (2.2). With the third-generation FEC, the BER would become better than 10^{-13} when the signal has a Q factor of 8.5-dB (FEC limit) [12].

2.2.2 Characterization of the XPM penalty for the DQPSK channels

In Figure 2.2, the two curves are derived by increasing the launch powers of all channels from -16-dBm per channel to 4-dBm per channel. As shown in Figure 2.2, when the launch powers of all channels increase, in both co-propagation scenarios, the Q factor of the DQPSK channel investigated first increases with its launch power due to the improved OSNR and then decreases because of the nonlinearity effects. The Q factors of the DQPSK channel in both co-propagations have an optimal point where the OSNR improvement and the nonlinear penalty strike a balance. However, it can be seen that, in the case when the DQPSK channel co-propagates with the OOK channels, the DQPSK channel suffers more from the XPM penalty. This penalty can be evaluated in two ways. The first way is the XPM induced Q penalty for a given launch power. For example, in Figure 2.2, at a launch power of 1-dBm per channel, the DQPSK channel co-propagating with the 16 OOK channels suffer 6-dB more penalty than that when it co-propagates with the 16 DQPSK channels. The second way to evaluate the penalty is XPM induced launch power tolerance degradation at the optimal point between the two cases. Usually, the launch power at the optimal point is the operating launch power set for all channels. Obviously, the higher the optimal launch power, the better the channel's OSNR, thereby the longer the maximum reach. Compared to the 17 DQPSK channels co-propagation case, the optimal launch power is 6-dB smaller for the DQPSK channel when it co-propagates with 16 OOK channels. Therefore, the XPM induced launch power tolerance degradation is 6-dB in this configuration.

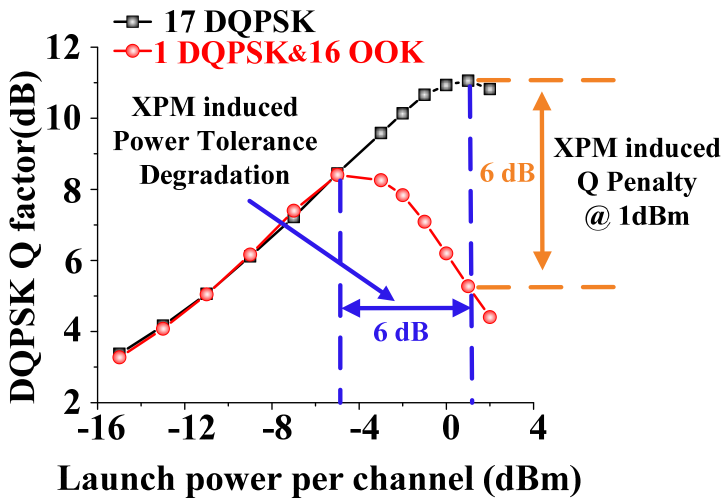

Figure 2.2 Simulated XPM penalty for a DQPSK channel when co-propagating with 16 adjacent OOK channels and with 16 adjacent DQPSK channels, respectively.

The XPM induced penalty in turn restricts the maximum launch power of the OOK channels, thereby limiting the transmission distance of the OOK channels. This can be easily understood from Figure 2.3, which is derived by keeping the launch power of the DQPSK channel at the optimal launch power of -5-dBm and increasing the launch power of the OOK channels. The Q factor of the DQPSK channel decreases due to the increasing XPM penalty while the Q factors of the OOK channels firstly increases and then decreases. The points above the FEC limit can achieve error-free operation by applying FEC coding. In order to attain the best performance for both the DQPSK channel and the OOK channels, the launch power of the cross point of these two curves is utilized. This cross point is -5-dBm, exactly same as the optimal point in the previous analysis. Further increasing the launch power of the OOK channels beyond the launch power of the cross point will lead to a Q factor of the DQPSK channel smaller than the Q factor of the OOK channels and drop below the FEC limit. Consequently, the XPM penalty also set a maximum launch power of the OOK channels, in another word, the maximum reach of the OOK channels.

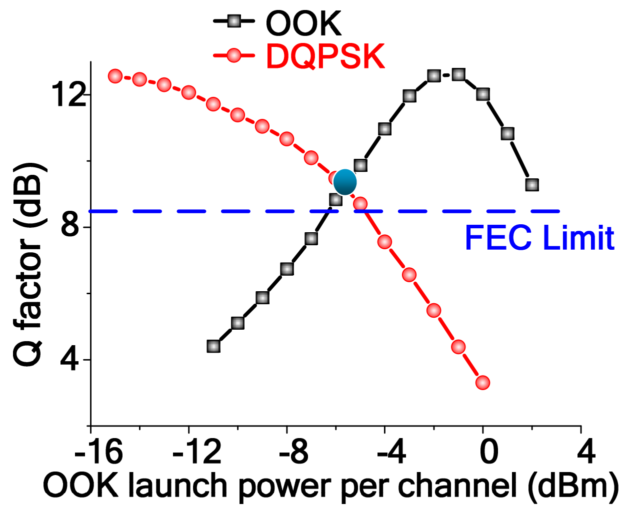

Figure 2.3 The Q factor of the DQPSK channel and the OOK channels when increasing the OOK launch power per channel while keeping the DQPSK channel launch power constant.

Our effort in this chapter aims to find a solution to mitigate the XPM penalty, thereby allowing the cross point to move towards the higher launch power direction.

2.3 Review of current approaches

Extensive researches on mitigation of the XPM penalty in the co-propagation systems have been conducted. A straightforward way is to reduce the launch power of the OOK channels [13], however this will shorten the maximum reach of the OOK channels. Lenihan *et al.* showed that the XPM penalty can be effectively reduced by increasing the channel spacing between the DQPSK and OOK channels [14]. The drawback is that large channel spacing also reduces the spectral efficiency, which is not expected in the upgrade. Similarly, although a guard band can be introduced between the 40-Gb/s DQPSK and the 10-Gb/s OOK channels [15], the approach reduces system spectral efficiency and imposes inflexibility in the channel allocation. An approach which launches the DQPSK channel with orthogonal polarization with respect to its adjacent OOK channels was proposed to suppress the XPM penalty [14]. The difficulty with this approach is that it would involve a complicated polarization control in the transmitter. The study was further extended to the DQPSK coherent receiver [16]. The coherent receiver shows a higher susceptibility to the XPM effect induced by the co-propagating 10-Gb/s NRZ channels than direct detection receiver because the XPM induced phase noise can severely impair the carrier phase estimation in the coherent receiver. Bertran-Pardo *et al.* investigated on the XPM penalty for 40-Gb/s PDM-QPSK with coherent detection over 1600-km-long SSMF transmission. They found that the optimization of the CPE process and the introduction of bandgaps in the multiplex are not sufficient to compensate for the induced penalties in hybrid 10/40-Gb/s systems and thus not yielding enough margins for actual industrial operation [17]. Recently, an experiment of co-propagating transmission for different dispersion maps showed that a good performance can be achieved when the system has a large residual dispersion percentage per span (RDPS) [15]. Several models have been proposed to study this dependence of the XPM penalty on the fiber dispersion and dispersion maps. In [18], the model is used to analyze the XPM efficiency which depends on the fiber dispersion. In [19], the XPM process is modeled as linear filter with a frequency response depending on both fiber dispersion and dispersion management. In [20], the model looks at the XPM suppression factor due to channel walk-off. The results presented in this thesis model the direct relationship between the XPM induced phase shift of the DQPSK channel and the walk-off bits. The model describes the dependence of XPM penalty on the fiber dispersion and residual dispersion per span. Using this model, we find that an amount of residual dispersion corresponding to a one bit walk-off in each span is sufficient to suppress the XPM penalty.

2.4 Model of XPM mitigation approach based on walk off effect

XPM occurs when the intensity pulses of the DQPSK and OOK channels are overlapped in the time domain. We assume that the pulse spreading in the DQPSK and OOK channels is small during the transmission, which is true for most dispersion management systems. Therefore, the intensity envelope in the DQPSK channel remains constant and the XPM-induced nonlinear phase shift on the DQPSK signals occurs only when an intensity pulse (“1” bit) is present in the neighboring OOK channels, particularly the nearest neighbors.

2.4.1 Physical model of the XPM penalty for the DQPSK channel

As shown in Figure 2.4, the red pulse represents a “1” level bit in the NRZ-OOK channel in time domain while the blue pulse represents a phase pulse in the DQPSK channel in phase domain. At the beginning, the two pulses of different channels start at the same point. The nonlinear phase shift is being imposed on the blue pulse (phase pulse) of the

DQPSK channel due to the XPM effect initiated by the co-propagating red pulse (intensity pulse) in the OOK channel. Meanwhile, due to the dispersion effect, the blue pulse in the DQPSK channel is gradually walking off the red pulse in the OOK channel. The XPM effect ceases to happen when the blue pulse completely walks through the red pulse. However, during the walk off time, the blue pulse already accumulated some phase shift. Suppose a preceding blue pulse is co-propagating with a "0" level bit in the OOK channel, no XPM effect occurs between the DQPSK and OOK channels, thereby no phase shift is imposed on this blue pulse. Since different bits in the DQPSK channel will experience different amounts of nonlinear phase shift depending on the bit pattern of the neighboring OOK channels, an accurate phase decision will be difficult to make.

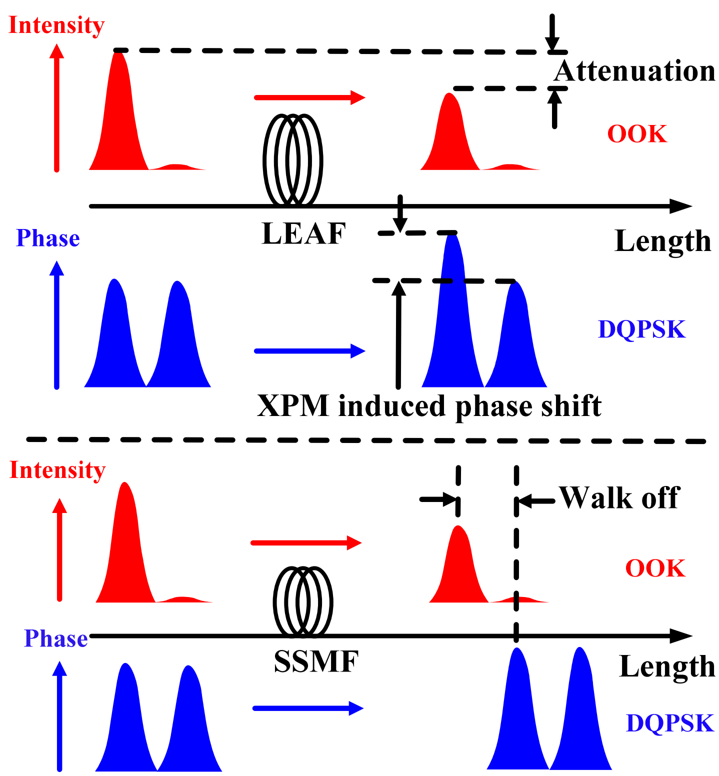

Figure 2.4 Illustration of the walk off between the OOK channel and the DQPSK channel in LEAF and SSMF.

2.4.2 Physical model of our XPM mitigation approach

Our solution to the above problem is to introduce large walk off between the DQPSK and OOK channels, so that the blue pulse can walk off as many OOK bits as possible. Assuming equal probabilities of "1's" and "0's", statistically different bits in the DQPSK channel will experience nearly the same amount of nonlinear phase shifts if the walk-off effect occurs over sufficient bits of the OOK channels.

Two ways can be used to introduce large walk off. A straightforward way is to use large dispersion fiber, e.g. SSMF, instead of small dispersion fiber, e.g. large effective area fiber (LEAF), as the walk off is directly related to the fiber dispersion. The other way is to leave some residual dispersion in each span. This can be understood from Figure 2.5: No residual dispersion per span means the chromatic dispersion in each span is fully compensated. Since the dispersion value of DCF is negative, the DCF will exhibit an opposite walk off effect, which we describe as walk back. Therefore, due to the walk back, the blue pulse in DQPSK channel and the red pulse in OOK channel, which are already separated from each other during the transmission in SSMF, will start to overlap again after passing the DCF, leading to even more accumulated phase shift on the same blue pulses in DQPSK channel in the later on transmission.

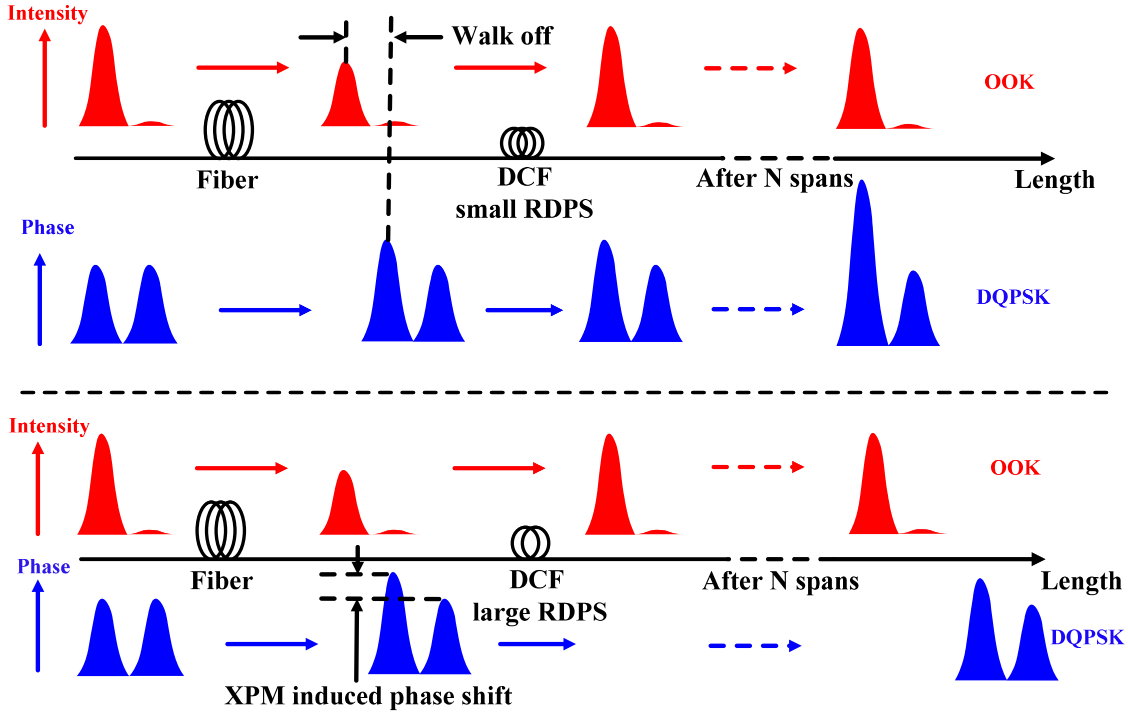

Figure 2.5 Illustration of the walk off between the OOK channel and the DPSK channel for different dispersion schemes.

2.4.3 Mathematical modeling of the XPM penalty's dependence on walk off effect

In order to quantitatively evaluate our mitigation approach, a relation between the walk off bits and the fiber dispersion, the residual dispersion per span is provided. The walk off parameter between these two channels d_W is defined as [21]:

$$d_W = \frac{1}{v_{OOK}} - \frac{1}{v_{DQPSK}} \tag{2.6}$$

where v_{OOK} and v_{DQPSK} are the group velocity of the OOK channel and DQPSK channel respectively. In the nonzero dispersion region, $d_W \approx D \cdot \Delta\lambda$, where D is the fiber dispersion coefficient and $\Delta\lambda = \lambda_{DQPSK} - \lambda_{OOK}$ is the channel spacing between DQPSK channel and OOK channel [22]. And the walk off length L_W, which is the length that a DQPSK bit transmitted before completely walking through an OOK bit, is defined as [21]:

$$L_W = \frac{T_{OOK}}{d_W} = \frac{\frac{1}{B_{OOK}}}{D \cdot \Delta\lambda} = \frac{1}{B_{OOK} \cdot D \cdot \Delta\lambda} \tag{2.7}$$

where the T_{OOK} is the pulse width of OOK bit, B_{OOK} is the baud rate of OOK channel. Thus, the total number of fiber dispersion induced walk off bits in one span with a length of L km is:

$$n_D[bit] = \frac{L}{L_W} = \frac{L[km]}{\frac{1}{B_{OOK}[bit/ps] \cdot D[ps/nm/km] \cdot \Delta\lambda[nm]}} = L \cdot B_{OOK} \cdot D \cdot \Delta\lambda[bit] \tag{2.8}$$

It can easily be seen from above equation that the total number of walk off bits is directly proportional to the fiber dispersion. However, this result does not take into account the dispersion compensation. In the presence of dispersion compensation, the number of walk off bits due to the residual dispersion n_C needs to be added to above formula. (n_D-n_c) is the number of the walk back bits per span due to DCF. Consider a transmission link with N_A spans, the total number of walk off bits including the dispersion compensation effect is:

$$n = N_A \cdot n_D - (N_A - 1) \cdot \left(n_D - n_C\right) = n_D + (N_A - 1)n_c \tag{2.9}$$

Therefore, large dispersion compensation, in another word, large n_C will lead to the reduction of the number of total walk off bits.

From the traditional definition of nonlinear phase shift due to XPM effect [21]:

$$\phi = n_2 k_0 L(2\left|E\right|^2) \tag{2.10}$$

Dividing the span length to n times the walk off length L_W, the accumulated XPM induced phase shift in the case of n bits walk off can be given by [23]:

$$\phi_m = \sum_{k=1}^{n_{OOK}} \left(2\gamma \sum_{j=1}^{N_A} \sum_{i=1}^{n_{D_k}} \int_{(i-1)\cdot L_{W_k}}^{i\cdot L_{W_k}} P_i(z) \cdot N_k \left[m - 1 + i \cdot j - (j-1) \cdot (n_{D_k} - n_{c_k}) \right] dz \right) \tag{2.11}$$

where n_{OOK} is the number of co-propagating OOK channels. γ is the nonlinear parameter of the fiber. P_i is the power profile of the co-propagating *i*th bit in the adjacent OOK channel. Due to the fiber attenuation, P_i changes with the co-propagation length. N is the bit pattern in OOK channel. For the DQPSK channel co-propagating with multiple OOK channels, according to Equation (2.7) and (2.8), the walk off length L_{W_k}, the number of the walk off bits n_{D_k} and the number of the walk back bits n_{c_k} depend on the channel spacing between the OOK channel and the DQPSK channel investigated.

Since in the DQPSK modulation format, the information is modulated in the phase difference between the adjacent bits, we care more about the differential phase shift between the adjacent bits. Therefore, the XPM induced differential phase shift is:

$$\Delta\phi = \phi_m - \phi_{m-1} \tag{2.12}$$

where m is the bit order in DQPSK channel. Take (2.11) into (2.12), we can get the XPM induced differential phase shift.

2.4.4 Analytical simulations of the dependence of XPM induced differential phase shift on walk off effect

Based on this model, we conducted a simulation of XPM induced differential phase shift vs. bit pattern of DQPSK channel for different fiber dispersions and different dispersion compensation schemes. The parameters in the simulation are shown in Table 2.1.

Table 2.1 Simulation parameters.

Span length	$L = 80km$
Number of spans	$N_A = 12$
Baudrate of OOK channel	$B_{OOK} = 10GBaud/s = 10^{-2} bit/ps$
Baudrate of DQPSK channel	$B_{DQPSK} = 20GBaud/s = 2\times10^{-2} bit/ps$
Dispersion of LEAF fiber	$D_{LEAF} = 4 ps/nm/km$
Dispersion of SSMF fiber	$D_{SSMF} = 16 ps/nm/km$
Launch power per channel per span	$P_{in} = -4dBm$
Attenuation of the fiber (SSMF and LEAF)	$\alpha = 0.2dB/km$
Nonlinear parameter (SSMF and LEAF)	γ=1.4×10^{-3}(*1/(W·m)*)
Number of co-propagating OOK channels	$n_{OOK} = 8$
Channel spacing	50GHz ($\Delta\lambda \approx 0.4nm$)

Although SSMF and LEAF have different nonlinear parameters and effective areas, we set the same values for these two different fibers because we only want to focus on the mitigation effect due to the large walk off effect and eliminate the impacts from other fiber properties. And this setting will not affect our conclusion for real systems as LEAF has a larger nonlinear parameter and a small effective area, meaning that the signal transmitting over LEAF suffers even more from the nonlinear effect in real system. Out of the same reason, we neglect the pulse spreading of OOK pulses due to the dispersion and dispersion compensation. We compared the XPM induced differential phase shift for consecutive 10^4 bits in the DQPSK channel. The results are shown in form of histogram. In order to make the results legible, we only chose a small amount of bits (100 bits) to visualize how the XPM induced differential phase shift varies in each bit.

2.4.4.1 The dependence of XPM induced differential phase shift on fiber dispersion

Figure 2.6 and Figure 2.7 compare the XPM induced differential phase shift for the DQPSK channel over SSMF and LEAF in 12 spans, respectively. A less distorted signal should have its XPM induced differential phase shift distributed within a small area around zero. As it can be seen from Figure 2.6, the XPM induced differential phase shift for the DQPSK channel over LEAF is generally larger than that over SSMF. The Probability density in Figure 2.7 gives a quantitative comparison. For zero residual dispersion case, the standard deviation of XPM induced differential phase variance for SSMF is 0.34 radian while for LEAF, the standard deviation of XPM induced differential phase variance can reach 0.82 radian.

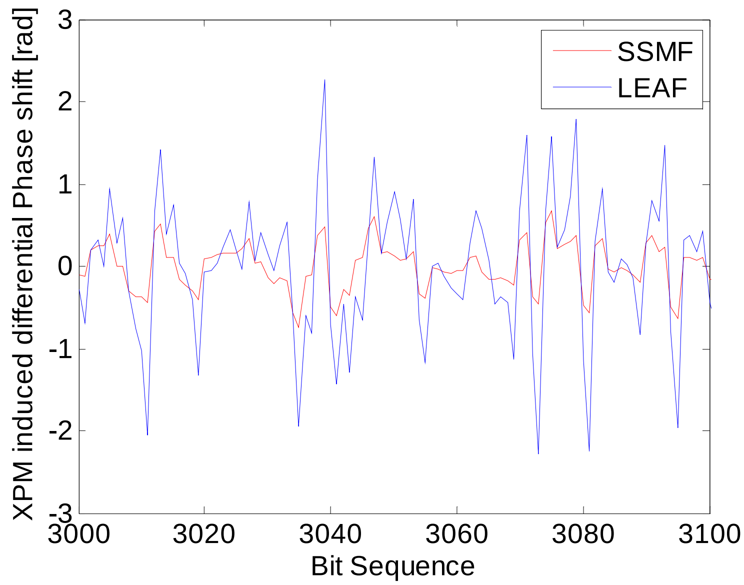

Figure 2.6 The XPM induced differential phase shift for the DQPSK channel transmitted over LEAF and SSMF.

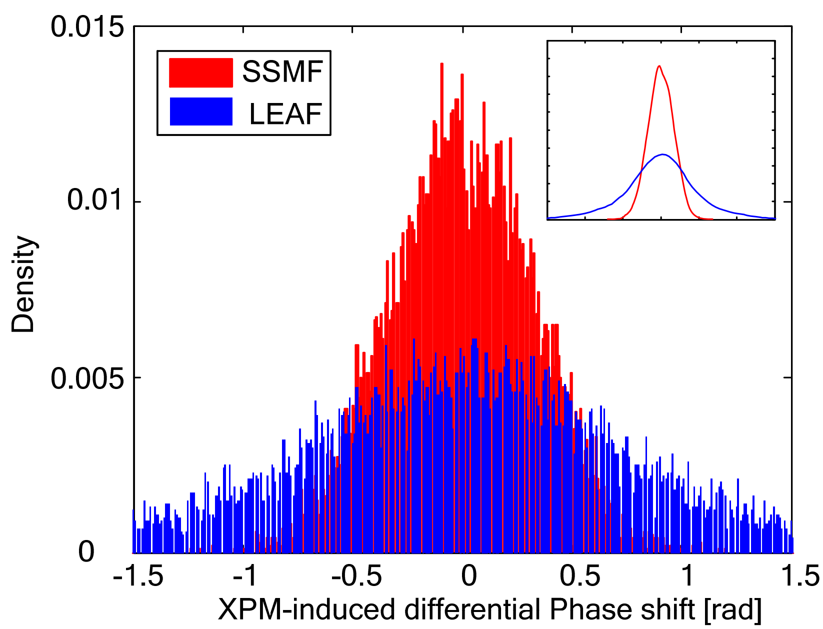

Figure 2.7 Probability density of the XPM induced differential phase shift for the DQPSK channel transmitted over LEAF and SSMF. The inset figure shows the profile of the probability density.

2.4.4.2 The dependence of XPM induced differential phase shift on dispersion compensation

As shown in Section 2.4.3, for a DQPSK channel co-propagating with a pair of neighboring OOK channels, the residual dispersion can be evaluated in the number of relatively walk off bits. However, when the DQPSK channel co-propagates with many pairs of neighboring OOK channels, the relation between the residual dispersion and the number of the walk off bits will depend on the channel spacing between the OOK channel and the DQPSK channel investigated. Figure 2.8 shows the standard deviation of XPM-induced differential phase variance versus residual dispersion percentage per span and its corresponding number of walk off bits in the nearest pair of neighboring OOK channels (n_{c1}) when the channels are co-propagating over SSMF. It can be seen that with residual dispersion per span, the XPM-induced differential phase variance is dominated by the nearest neighboring OOK channels. This can be understood that, for the same amount of dispersion compensation, the larger the channel spacing between the OOK channel and the DQPSK channel, the more relatively walk off bits between these two channels. As it will be analyzed later, one bit walk off is sufficient to suppress the XPM induced differential phase shift. The suppression of the XPM induced differential phase shift due to more walk off bits is negligible. Therefore, when the DQPSK channel co-propagates with many pairs of neighboring OOK channels, the residual dispersion can still be evaluated in the number of residual dispersion induced walk off bits in the nearest pair of neighboring OOK channels (n_{c1}).

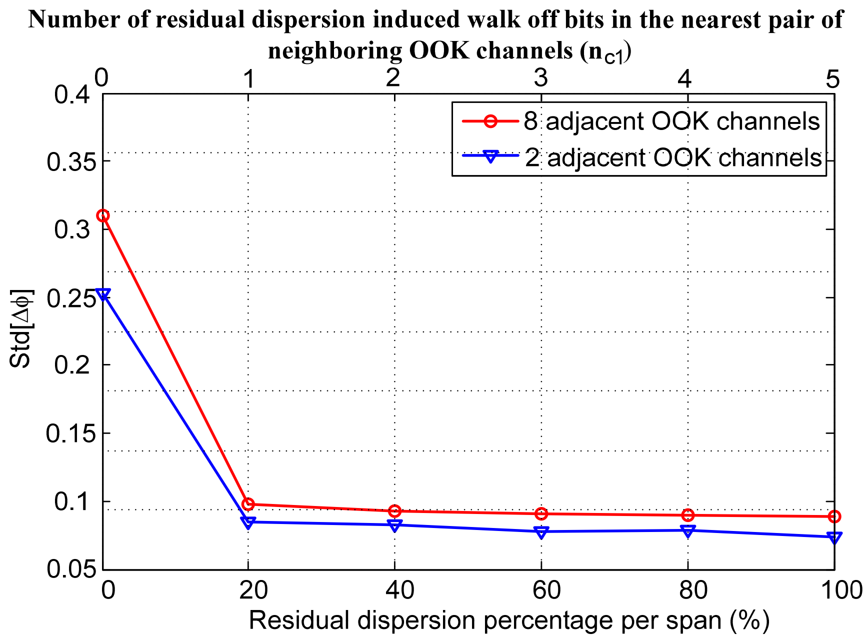

Figure 2.8 Standard deviation (Std) of XPM-induced differential phase variance versus residual dispersion percentage per span and its corresponding number of walk off bits in the nearest pair of neighboring OOK channels (n_{c1}) for different number of adjacent OOK channels.

Figure 2.9 and Figure 2.12 compare the XPM induced differential phase shift after a transmission over 12 spans under different dispersion map scenarios. Figure 2.9 and Figure 2.10 show the suppression of the XPM induced differential phase shift in SSMF from the residual dispersion induced walk off. The XPM induced differential phase shift at the residual dispersion leading to one bit walk off has a variance that is three times smaller than that in the absence of walk off. This can be explained by noting that with some amount of residual dispersion, the DQPSK bits may advantageously see a different bit pattern per span. With full dispersion compensation however, the DQPSK bits will walk back and encounter exactly the same bit pattern as was experienced in previous span.

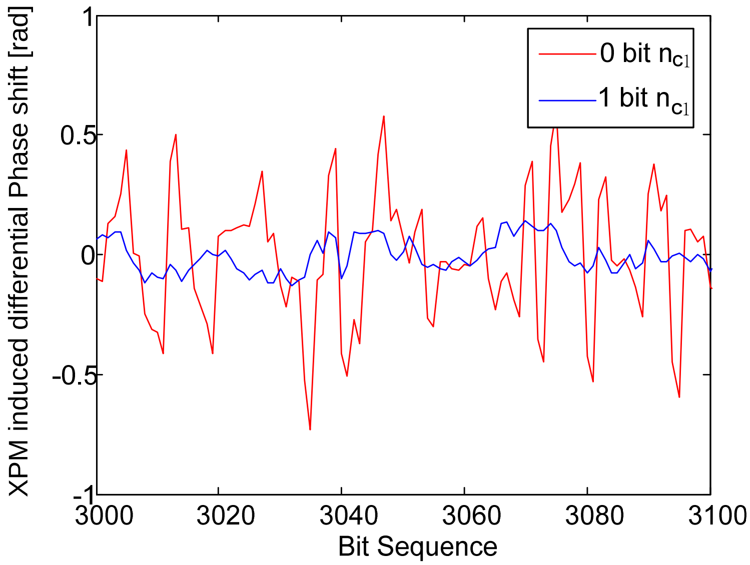

Figure 2.9 The XPM induced differential phase shift for the DQPSK channel transmitted in a link with and without residual dispersion.

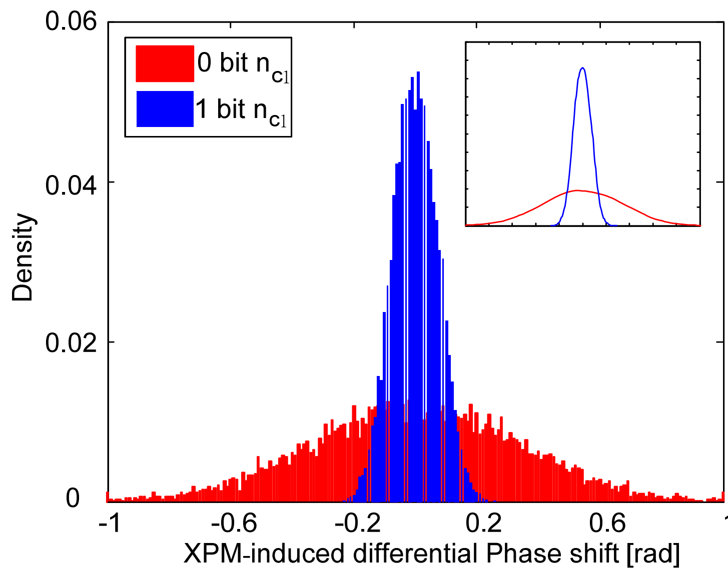

Figure 2.10 Probability density of the XPM induced differential phase shift for the DQPSK channel transmitted in a link with and without residual dispersion. The inset figure shows the profile of the probability density.

Another interesting result is that further increasing residual dispersion induced walk off beyond one bit does not lead to more suppression of the XPM induced differential phase shift. As shown in Figure 2.11 and Figure 2.12, the XPM induced differential phase shift in the transmissions with residual dispersion leading to one bit walk off and residual dispersion leading to three bits walk off almost have the same density distribution. This can be seen from Figure 2.13 that, in both SSMF and LEAF, when residual dispersion induced walk off is equal to or larger than one bit, the standard deviations of XPM-induced differential phase variance are nearly the same. This is reasonable because with one bit walk off, the bit pattern that the DQPSK bit encounters is already different from the bit pattern in the previous span. More walk off bits do not help in increasing the difference. Therefore, residual dispersion leading one bit walk off in each span is sufficient to suppress the XPM induced differential phase shift. This explains why the XPM suppression in [24] saturates at a 60% dispersion compensation ratio. This dispersion compensation value is equivalent to residual dispersion leading to one bit walk off. In Figure 2.14, we compare the standard deviations of XPM-induced differential phase variance in LEAF for different residual dispersion induced walk off in order to validate our model. The result agrees well with that in [24].

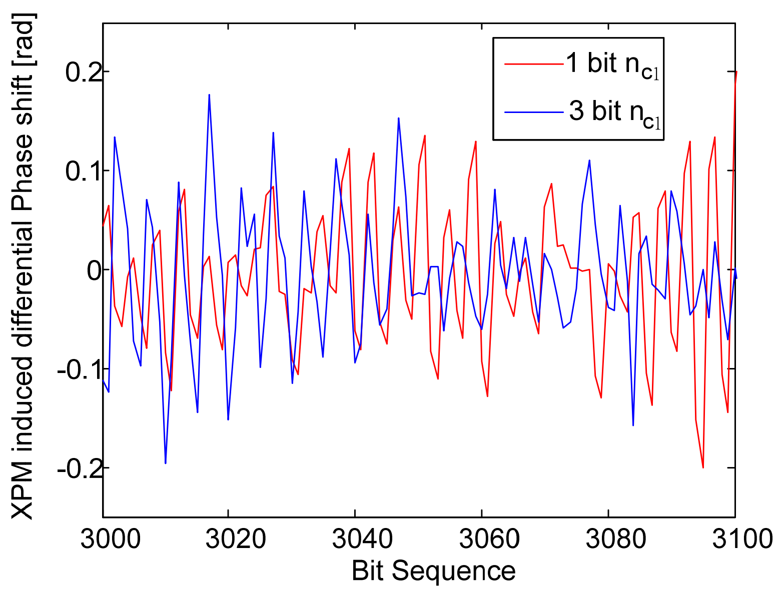

Figure 2.11 The XPM induced differential phase shift for the DQPSK channel transmitted in a link with different residual dispersion.

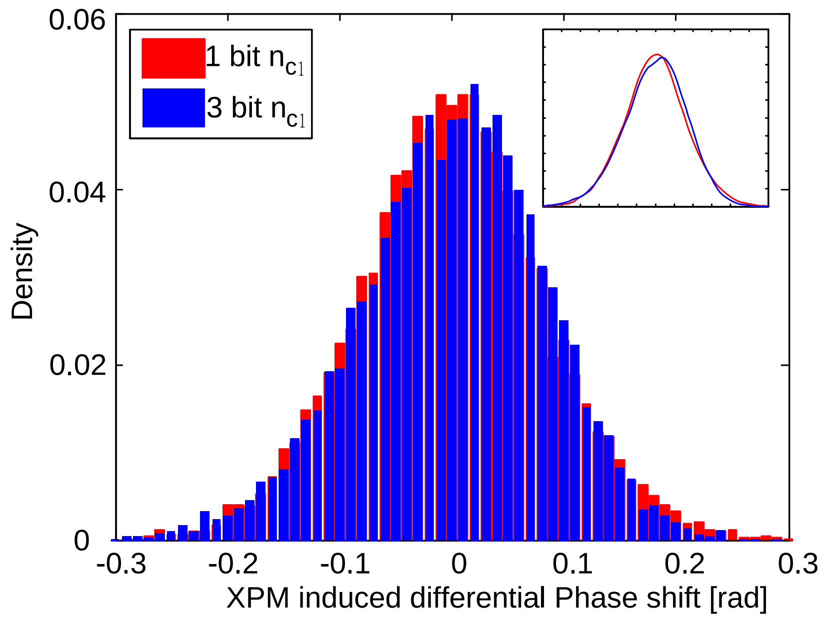

Figure 2.12 Probability density of the XPM induced differential phase shift for the DQPSK channel transmitted in a link with different residual dispersion. The inset figure shows the profile of the probability density.

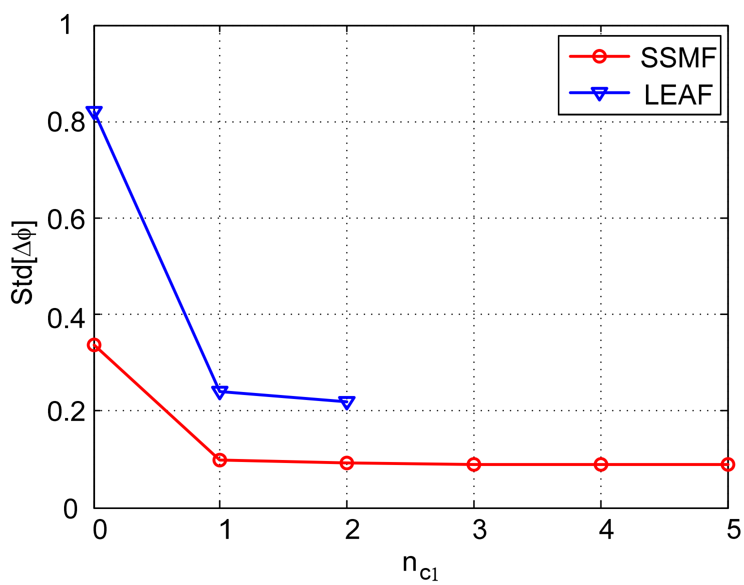

Figure 2.13 Standard deviation of XPM-induced differential phase variance versus n_{c1} for different fiber types (less points in LEAF is due to its large walk-off length).

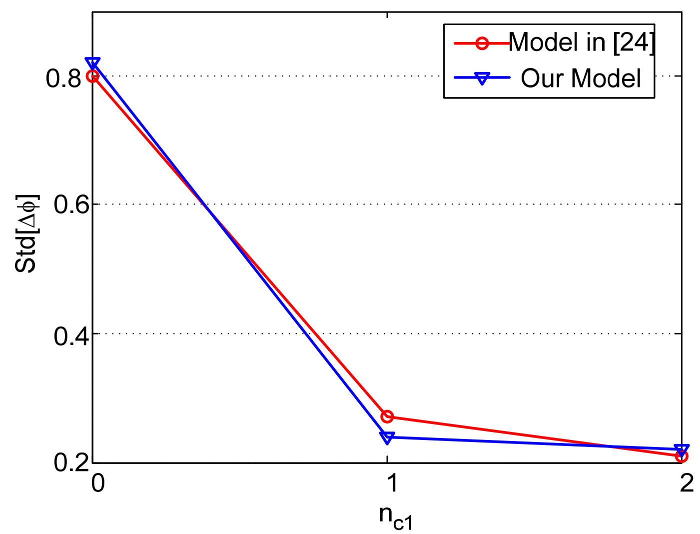

Figure 2.14 Comparison of standard deviations of XPM-induced differential phase variance in LEAF versus n_{c1} between the model in [24] and our model.

2.4.4.3 The effect of channel plan on XPM induced differential phase shift

The above analysis is performed assuming that the DQPSK channel is located amidst the OOK channels. Another widely employed channel plan is that the DQPSK channels are interleaved with the OOK channels on 50-GHz grid. Figure 2.15 compares the standard deviation of XPM-induced phase variance under various dispersion maps for different channel plans. It can be seen from the figure that, with full dispersion compensation per span, the channel plan that the DQPSK channels are interleaved with the OOK channels, may help suppress the XPM induced differential phase shift. However, when there is a residual dispersion leading to more than a one bit walk off in each span, the interleaving channel plan does not offer notable improvement over the amidst channel plan.

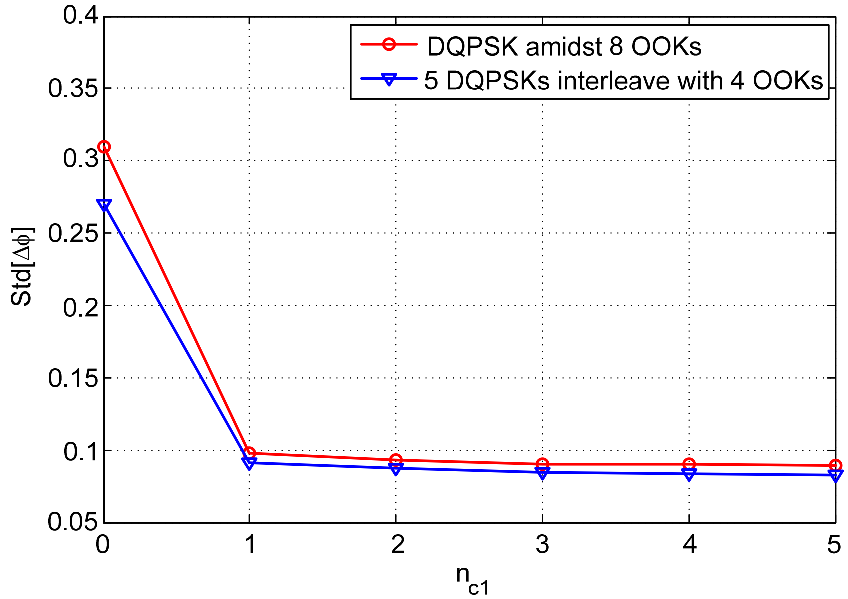

Figure 2.15 Standard deviation of XPM-induced differential phase variance versus n_{c1} for different channel plans

2.5 System simulation demonstration [25]

In order to verify our analysis and results, we simulate the XPM penalty for real system using a third party simulation tool – Optisystem 7. The hybrid system setup is shown in Figure 2.16. The transmitter consists of 17 channels generated by distributed feedback lasers (DFB) in the C-band ranging from 193.1 THz to 193.9 THz spaced by 50 GHz on the ITU-T dense wavelength division multiplexing (DWDM) grid. All channels are modulated with 10.7-Gb/s NRZ-OOK format except the center one (λ_9) being modulated with 42.7-Gb/s 33% RZ-DQPSK. The DQPSK channel has the worst-case XPM penalty in this kind of channel occupancy [15]. The NRZ-OOK format is generated with a single drive Mach-Zehnder modulator (MZM) driven with 2^{15}-1 length pseudo random bit sequences (PRBS) at 10.7-Gb/s. The multi-wavelength NRZ-OOK signals are de-correlated by transmitting through 10-km SSMF. To produce the RZ-DQPSK format, the first dual-drive MZM is driven sinusoidally with a 10.7-Gb/s clock signal generating 33% RZ pulse and the second nested $LiNbO_3$ MZM is driven by two 21.3-Gb/s PRBS precoded data of length of 2^{15}-1 bits. By tuning the variable optical attenuators (VOA), the channel's launch power can be varied to study the XPM penalty. The polarization controllers are used to adjust the polarization of each channel so that all channels are launched co-polarized to study the worst case XPM penalty. A 50-GHz arrayed waveguide grating (AWG) wavelength multiplexer combines all channels into the recirculating loop.

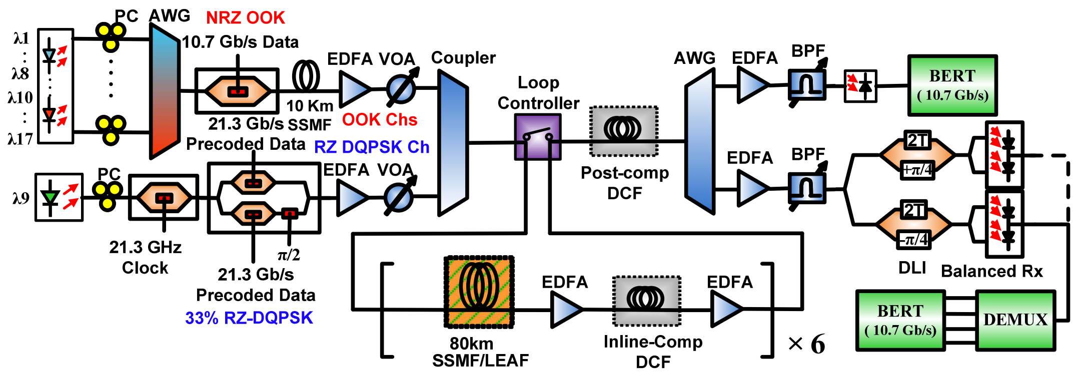

Figure 2.16 Schematic of the hybrid system setup.

The recirculating loop consists of six 80-km-long spans of a given fiber (SSMF or LEAF). By changing the fiber type, we compare the XPM penalties for different fiber types. Additionally, by changing the residual dispersion per span, we can evaluate the XPM effect for different dispersion maps. The location and length of the DCF are optimized according to the dispersion maps being investigated.

After transmission, a 50-GHz AWG wavelength demultiplexer separates the 10.7-and 42.7-Gb/s channels. The DQPSK signal is pre-amplified and the out-of-band noise is filtered out with a 0.3-nm tunable optical band pass filter (BPF). Differential demodulation is performed using an optical two-bits (one-symbol) delayed Mach-Zehnder interferometer. The two outputs of I or Q component are differentially detected with a balanced receiver.

Firstly, we compared the XPM penalty over the two different fiber types (SSMF and LEAF) with different local dispersion (16.7-ps/nm/km and 4-ps/nm/km). First, optimal launch power of the DQPSK channel need to be determined for both types of fiber. As mentioned in section 2.2, the optimal launch power is the launch power that makes the OSNR improvement and the nonlinear penalty of the DQPSK channel strike a balance. In other words, it is the DQPSK channel launch power where the Q factor of the DQPSK channel reaches its maximum in the absence of XPM. In order to emulate quasi single-channel operation, we set the launch power of all the OOK channels to -15-dBm so that the XPM effect from the OOK channels is negligible. Then we sweep the launch powers of the DQPSK channel to find the optimal launch power. For both fiber types, when increasing the launch power in the DQPSK channel, the Q factor of the DQPSK channel first increases due to improved OSNR and then decreases due to SPM. We found that at 50% RDPS, the maximum Q factor for the DQPSK channel over SSMF is 11.5-dB when the launch power of the DQPSK channel is 2-dBm. While the maximum Q factor for the DQPSK channel over LEAF is 12-dB when the launch power is -1-dBm. We set the launch power of the DQPSK channel to its optimal launch power for each type of fiber and simulate the Q factor penalty of the DQPSK channel measured with respect to the OOK channel launch power shown in Figure 2.17. As expected, the Q penalty for both types of fiber increases with the OOK channels' launch power due to the XPM effect. Moreover, the DQPSK signal co-propagating in LEAF always suffers more XPM penalty than in SSMF. This result matches well with our previous analysis that low local dispersion of LEAF is insufficient to provide enough walk-off between the OOK and the DQPSK channels to suppress the accumulation of XPM induced differential phase shit.

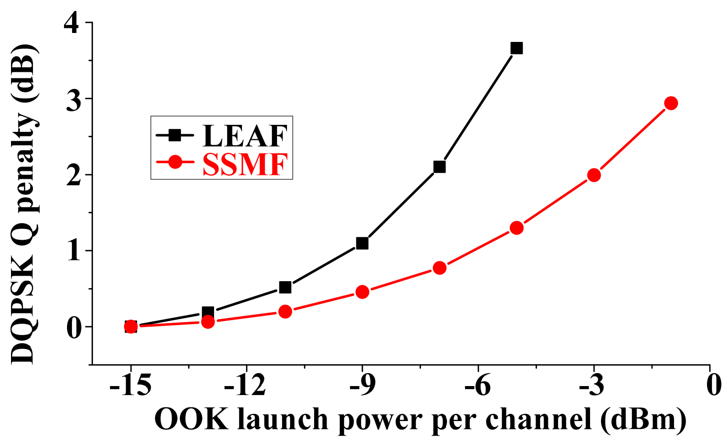

Figure 2.17 Q penalty on the DQPSK channel versus OOK channel launch power.

The XPM penalty was further compared for different dispersion map schemes over the two types of fiber. Chromatic dispersion and dispersion compensation are linear processes. Hence, dispersion compensation can be inserted at any location as long as the total amount of compensation is equal to the total amount of fiber dispersion. By changing the length of DCF in the loop, we can set different RDPS values while the total residual dispersion is compensated through post-compensation. Figure 2.18 shows the different dispersion compensation schemes and their corresponding transmission performances for the DQPSK channel over the LEAF. The result for the SSMF case is shown in Figure 2.19. The Q penalty of DQPSK channel at a given OOK launch power for both types of fiber decreases as the RDPS increases. This is slightly different from our previous analysis. Actually two mechanisms are involved in these simulations that can suppress XPM penalty. Our previous model is based on walk off effect only and assumes no power spreading of the OOK pulses. However, the large local dispersion and large residual dispersion at the same time can also lead to the power spreading of the OOK pulses, thereby making the envelope of the OOK channels to be more constant. The constant envelope of OOK channel reduces the bit pattern dependent XPM induced differential phase shift. Therefore, further increasing residual dispersion beyond the amount that provides one bit walk off can still mitigate the XPM penalty, but because of power spreading of OOK pulses rather than the walk off effect. This can explain why in both Figure 2.18 and Figure 2.19, for the same OOK launch power, the difference of the Q penalty between 0% RDPS and 50% RDPS is more than that between 50% RDPS and 100% RDPS.

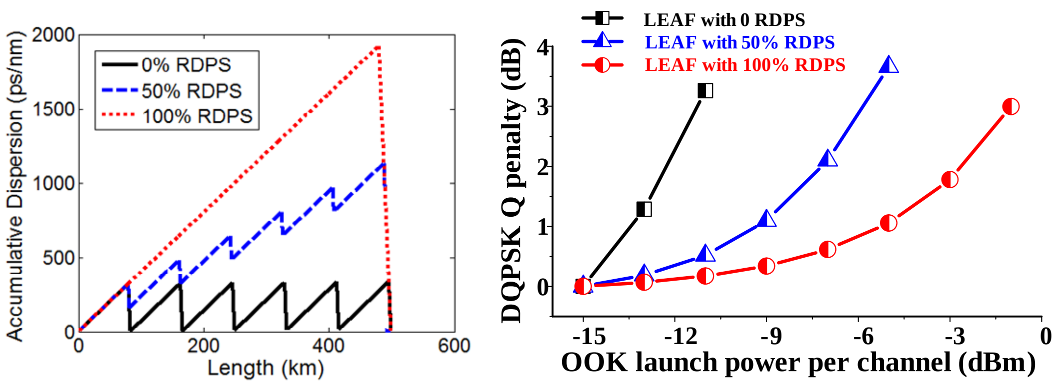

Figure 2.18 The different dispersion compensation schemes and their corresponding transmission performances for the DQPSK channel co-propagating over LEAF fibers.

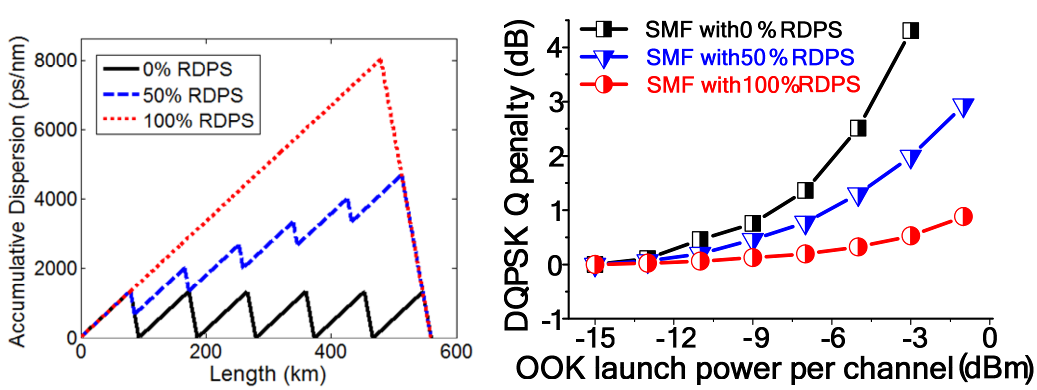

Figure 2.19 The different dispersion compensation schemes and their corresponding transmission performances for the DQPSK channel co-propagating over SSMF fibers.

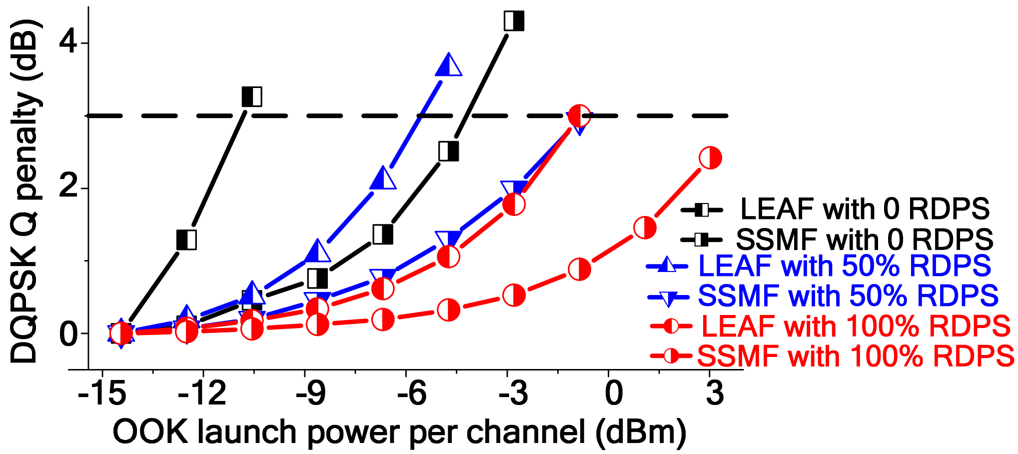

Figure 2.20 The XPM penalty for the DQPSK channel transmitted over different fibers with different dispersion compensation schemes.

Figure 2.20 compares the XPM penalty for the DQPSK channel transmitted over different fibers with different dispersion compensation schemes. As can be seen, by using SSMF and large residual dispersion, the XPM induced Q penalty for the DQPSK channel can stay below 3-dB for OOK launch power per channel up to 3-dBm.

To quantitatively compare the performance, Figure 2.21 shows the OOK launch power per channel at which the XPM penalty of the DQPSK channels reaches 3-dB for different RDPS values. When the RDPS is increased from 0% to 75%, the OOK launch power tolerance is increased by 6-dB for the DQPSK channel in both LEAF and SSMF. For the same RDPS value, the DQPSK channel in SSMF has a larger power tolerance than in LEAF. The largest tolerance to the OOK launch power is 1-dBm/ch, occurring when the co-propagation of the OOK and the DQPSK channels are transmitted over SSMF with 75% RDPS value. This is due to the co-effect of the walk off and the power spreading of OOK pulses. The price to pay for using SSMF and large RDPS is that post-compensation techniques, either optical or electrical, are required at the receivers.

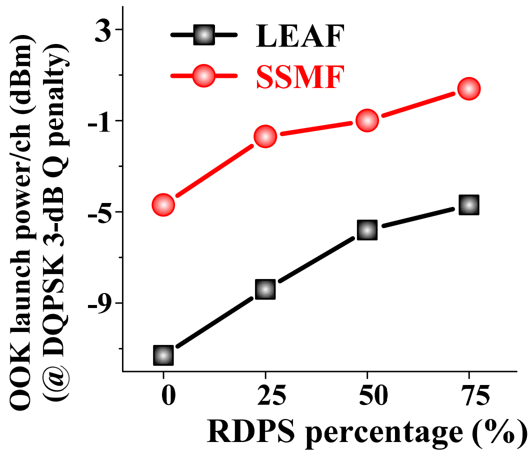

Figure 2.21 OOK launch power per channel at DQPSK 3-dB Q penalty.

2.6 Summary

In this chapter, XPM penalty on 40-Gb/s DQPSK channel in 10-/40-Gb/s hybrid system over SSMF and LEAF fiber has been investigated for different dispersion map schemes. The comparison results show that the XPM penalty has a large dependence on the walk-off between the co-propagating channels. Because of low local dispersion, LEAF is often thought to be superior to SSMF. However, this advantage becomes a drawback when the LEAF is used in 10-/40-Gb/s hybrid systems because the low dispersion of LEAF is insufficient to provide enough walk-off between channels. Using SSMF, together with one bit walk-off of residual dispersion per span, XPM penalty can be reduced to smaller than 3-dB at practical launch power levels.

In the selection of optical fiber, SSMF, which is currently the most widely deployed fiber, was thought not the good solution for future fiber-optic communication systems due to its large local dispersion. However, by our study we found SSMF actually works well in the hybrid DWDM system and is believed to be the best choice for the future optical network. Thus, the fiber in the current optical network is not needed to be redeployed for future DWDM optical network. With the design of dispersion maps, residual dispersion can not only suppress the XPM penalty but also allow the dispersion to be compensated using the inexpensive electronic dispersion compensation, which has already become the trend of current dispersion compensation techniques. Therefore, this guideline offers an optimum and economical solution for future DWDM systems.

References

[1] IEEE P802.3ba 40Gb/s and 100Gb/s Ethernet Task Force.

[2] Pardo O. B., Renaudier J., Mardoyan H., Tran P., Charlet G. and Bigo S., 2008, "Investigation of design options for overlaying 40Gb/s coherent PDM-QPSK channels over a 10Gb/s system infrastructure," The Optical Fiber communication/National Fiber Optic Engineers Conference (OFC/NFOEC) 2008, OTuM5.

[3] Humblet P.A. and Azizoglu M., 1991, "On the bit error rate of lightwave systems with optical amplifiers," Journal of Lightwave Technology, vol. 9, no. 11, pp. 1576-1582.

[4] Agrawal G. P., 2005, Lightwave Technology, Wiley-interscience Publisher.

[5] Wei X., Liu X. and Xu C., 2003, "Numerical simulation of the SPM penalty in a 10-Gb/s RZ-DPSK system," Photonics Technology Letters, vol. 15, no. 11, pp. 1636-1638.

[6] Xu C., Liu X. and Wei X., 2004, "Differential phase-shift keying for high spectral efficiency optical transmissions," Journal of Selected Topics in Quantum Electronics, vol. 10, no. 2, pp. 281-293.

[7] Bosco G. and Poggiolini P., 2004, "On the Q factor inaccuracy in the performance analysis of optical direct-detection DPSK systems," Photonics Technology Letters, vol. 16, no. 2, pp. 665-667.

[8] Ho K. P., 2004, "The effect of interferometer phase error on direct-detection DPSK and DQPSK signals," Photonics Technology Letters, vol. 16, no. 1, pp. 308-310.

[9] Ho K. P., 2005, Phase-modulated optical communication systems, Springer Publisher.

[10] Costa N. M. S. and Cartaxo A. V. T., 2007, "Novel approach for BER evaluation of DQPSK systems using differential phase Q," The 20th Annual Meeting of the IEEE Lasers and Electro-Optics Society (LEOS 2007), MP3.

[11] Hiew C. C., Abbou F. M., Chuah H. T., Majumder S. P. and Hairul A. A. R., 2004, "BER estimation of optical WDM RZ-DPSK systems through the differential phase Q," Photonics Technology Letters, vol. 16, no. 12, pp. 2619-2621.

[12] Charlet G., Mardoyan H., Tran P., Klekamp A., Astruc M., Lefrancois M. and Bigo S., 2005, "Upgrade of 10 Gbit/s ultra-long-haul system to 40 Gbit/s with APol RZ-DPSK modulation format," Electronic Letter, vol. 41, no. 22, pp. 1240-1241.

[13] Fürst C., Elbers J. P. and Camera M., 2006, "43 Gb/s RZ-DQPSK DWDM field trial over 1047 km with mixed 43 Gb/s and 10.7 Gb/s channels at 50 and 100GHz channel spacing," The 32nd European Conference on Optical communications (ECOC 2006), Th 4.1.4.

[14] Lenihan A. S., Tudury G. E., Astar W. and Carter G. M., 2005, "XPM-induced impairments in RZ-DPSK transmission in a multi-modulation format WDM system," Conference on Lasers and Electro-Optics (CLEO 2005), CWO5.

[15] Chandrasekhar S. and Liu X., 2007, "Impact of channel plan and dispersion map on hybrid DWDM transmission of 42 Gbps DQPSK and 10Gbps OOK on 50-GHz grid," Photonics Technology Letters, vol. 19, no. 22, pp. 1801-1803.

[16] Tanimura T., *et al.*, 2008, "Non-linearity tolerance of direct detection and coherent receivers for 43 Gbs RZ-DQPSK signals with co-propagating 11.1 Gbs NRZ Signals over NZ-DSF," The Optical Fiber communication/National Fiber Optic Engineers Conference (OFC/NFOEC 2008), OTuM4.

[17] Bertran-Pardo O., Renaudier J., Charlet G., Mardoyan H., Tran, P. and Bigo, S., 2008, "Nonlinearity limitations when mixing 40-Gb/s coherent PDM-QPSK channels with preexisting 10-Gb/s NRZ channels," Photonics Technology Letters, vol. 20, no. 15, pp. 1314-1316.

[18] Chiang T. K., Kagi N., Marhic M. E., and Kazovsky L. G., 1996, "Cross-phase modulation in fiber links with multiple optical amplifiers and dispersion compensators," Journal of Lightwave Technology, vol. 14, no. 3, pp. 249-260.

[19] Bononi A., Bertolini M., Serena P. and Bellotti G., 2009, "Cross-phase modulation induced by OOK channels on higher-rate DQPSK and coherent QPSK channels," Journal of Lightwave Technology, vol. 27, no. 18, pp. 3974-3983.

[20] Liu X. and Chandrasekhar S., 2008, "Suppression of XPM penalty on 40-Gb/s DQPSK resulting from 10-Gb/s OOK channels by dispersion management," The Optical Fiber communication/National Fiber Optic Engineers Conference (OFC/NFOEC) 2008, OMQ6.

[21] Agrawal G. P., 2007, Nonlinear Fiber Optics, Academic Press.

[22] Cartaxo A. V. T., 1999, "Cross-phase modulation in intensity modulation-direct detection WDM systems with multiple optical amplifiers and dispersion compensators," Journal of Lightwave Technology, vol. 17, no. 2, pp. 178-190.

[23] Xu X., Tian Z., Liboiron-Ladouceur O. and Plant D. V., 2010, "Suppression of XPM-Induced nonlinear phase shifts using a walk-off effect in DQPSK/OOK hybrid systems," submitted to The Conference on Lasers and Electro-Optics and The Quantum Electronics and Laser Science Conference (CLEO/QELS) 2010.

[24] Tao Z., Yan W., Oda S., Hoshida T. and Rasmussen J. C., 2009, "A linear model for nonlinear phase noise induced by cross-phase modulation," Optics Express, vol. 17, no. 16, pp.13860-13868.

[25] Xu X., Liboiron-Ladouceur O. and Plant D.V., 2008, "XPM penalty mitigation for a 42.7-Gb/s DQPSK channel co-propagating with 10.7-Gb/s OOK channels using SSMF and dispersion map," The 21st Annual Meeting of the IEEE Lasers and Electro-Optics Society (LEOS 2008), WH4.

Chapter 3 Polarization Dependent Frequency Shift Induced Penalty in DPSK Demodulator

3.1 Introduction

For phase modulation formats, such as DPSK, the information is encoded in the phase of the optical field. However, photodetectors only detect the optical power and are insensitive to the optical phase. Therefore, a conversion from the optical phase information to the optical intensity information should be performed before photodetection. This process is also called demodulation. The DPSK demodulation can be categorized into two main types, coherent detection and direct detection. Direct demodulation of DPSK signal has attracted particular attention in the application of 10-Gb/s and 40-Gb/s optical metro networks due to its simplicity, cost-effectiveness and maturity. A DPSK direct demodulator is a Mach-Zehnder delay interferometer (DI) with a one bit delay in one arm, such that the phase in one time slot interferes with that of the successive time slot to convert the phase signal to an intensity signal [1]. A typical schematic of a fiber-based DPSK demodulator is illustrated in Figure 3.1 [2]. It is comprised of two 3-dB wavelength insensitive couplers with two bended fiber arms of different lengths between them to introduce a specified delay. A thin film heater is directly deposited on the optical fiber to control the phase of the interferometer so that the transmissivity of the DI can be tuned to align with the laser frequency. The bending of the fibers can result in birefringence through the photoeleastic effect. Birefringence causes the polarization dependency, thereby introducing a polarization dependent frequency shift (PDf). The PDf will lead to a frequency offset between the laser frequency and the transmissivity peak of the DI, degrading the performance of DPSK demodulation [2].

In this chapter, we study the PDf of a 10-GHz DPSK demodulator induced penalty on a 10-Gb/s NRZ-DPSK signal and the PDf of a 40-GHz DPSK demodulator on a 40-Gbps NRZ-DPSK signal respectively. The comparison results reveal that PDf ratio, defined as PDf over free spectral range (FSR), plays a predominant role in determining the performance of the demodulator. We further investigate the PDf of a 40-GHz DPSK demodulator on a 40-Gb/s RZ-DPSK signal to study PDf incurred optical filtering effect on the RZ-DPSK signal. The experiment result shows that for the same PDf, the RZ signal suffers more degradation because of the more spectrum distortion induced by the PDf of the demodulator.

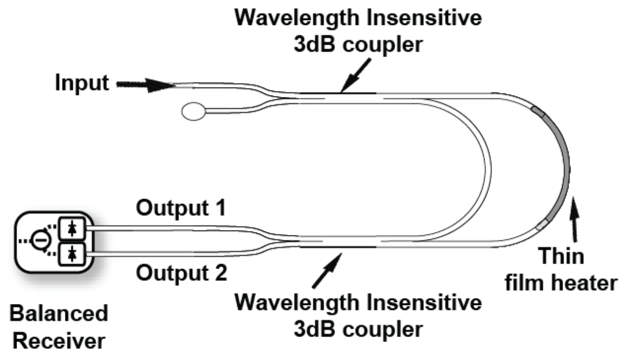

Figure 3.1 Schematic of a fiber-based DPSK demodulator [2].

3.2 Model of PDf in a DPSK demodulator

A DI, in principle, makes two adjacent bits interfere with each other such that the two bits can interfere constructively if they are in phase and interfere destructively if they are out of phase [1]. The balanced photodetector followed the DI can therefore determine whether there is an amplitude change between two consecutive bits and give the corresponding logic estimation. The interferometer has two intensity outputs that are logically conjugated, which are the constructive port and the destructive port. Assume one bit period of a DPSK signal is T_s, the delay between the two arms of a DI is equal to the symbol duration if the DI is perfectly tuned. The optical field at the constructive port is $E_c(t) = E_{in}(t) + E_{in}(t - T_s)$ and the optical field at the destructive port is $E_d(t) = E_{in}(t) - E_{in}(t - T_s)$, where $E_{in}(t)$ is the incident optical field at the time T. The transfer function of the DI $D(f)$ has a cosinusoidal/sinusoidal frequency response from the input to the constructive/destructive ports and is given by [3]:

$$D_{c/d}(f) = \frac{E_{c/d}(f)}{E_{in}(f)} = \frac{1}{2}\left[1 \pm \varepsilon \exp\left(\frac{j2\pi f}{FSR}\right)\exp(-j\Delta\phi)\right] \tag{3.1}$$

where ε is related to the DI extinction ratio, the sign $\pm$ applies to the constructive and destructive ports, respectively. FSR is the spectral period of a cycle of the transfer function and is often chosen to be equal or close to the bit rate, such that the delay between the two arms of the interferometer is around one bit period. $\Delta\phi$ is the optical phase difference between the two arms. The birefringence of the DI causes a random polarization dependent phase difference $\Delta\phi$ between the two arms and is related to the PDf by: $\Delta\phi = 2\pi\frac{PDf}{FSR}$. The maximum PDf is the frequency shift induced by two orthogonal states of polarization (SOP) and it is usually called the measured PDf for commercial DIs. In Figure 3.2, $D(f)$ at the constructive and destructive ports are plotted for two orthogonal SOP of a DI with a FSR=10-GHz and measured PDf=1-GHz. The frequency response $D(f)$ of the DI is usually called transmissivity.

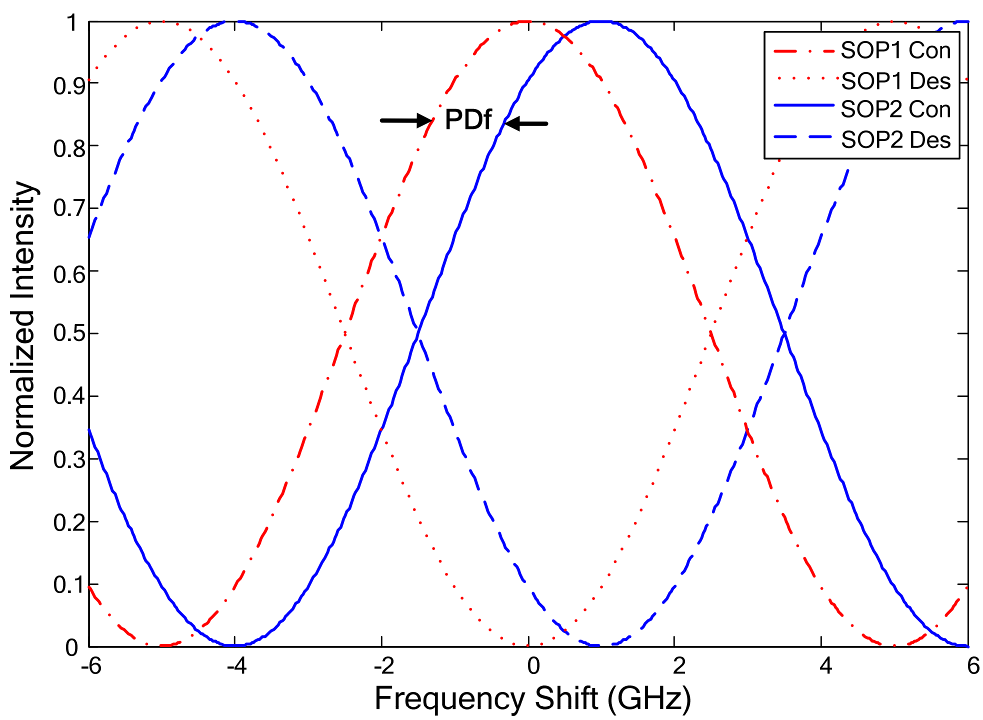

Figure 3.2 The frequency response at the constructive and destructive ports for two orthogonal SOP of a DI with FSR=10-GHz and measured PDf=1-GHz.

As seen from the FSR spectrum in Figure 3.2, the transmissivity of the DI is shifted by PDf due to the polarization dependent effect. If the DI is tuned to align its transmissivity (red dot line) peak with the spectrum peak of one of the SOP of a laser, no penalty can be seen when the signal passes through the DI. However, during the transmission, the SOP of the signal will probably change to another SOP. Due to the PDf, the FSR of the DI will be shifted depending on the incoming signal's SOP. Then the PDf will impose penalty on the signal. The penalty can be divided into two parts. Assume the received DPSK signal has the same spectrum profile with the DI's transmissivity, the spectrum profile of the received DPSK signal after the DI is shown in Figure 3.3. The red dash dot line shows the transmissivity of the DI when it is aligned to the SOP of the laser. As the received DPSK signal has the same spectrum profile with the DI's transmissivity, the red dash dot line also represents the spectrum profile of the received DPSK signal. The blue dash line illustrates the polarization induced shifted transmissivity of the DI seen by the received DPSK signal. Therefore, the common part is the spectrum profile of the DPSK signal after passing the DI. As it is shown in the vertical shade area of Figure 3.3, part of the signal power is being cut off due to the random polarization dependent spectral shift. It means that more signal power is required in order to maintain the same bit error rate level. Thus, one part of the penalty is from power filtering due to the shifted DI's transmissivity. The other part of the penalty is from the spectrum distortion. As it can be seen from the horizontal shade area of Figure 3.3, although this part of the power has not been cut off by the shifted DI's transmissivity, it does not have its counterpart in the negative side of the spectrum with respect to the laser frequency. Therefore, it is not useful part of the signal power, but just a distortion to the signal's spectrum.

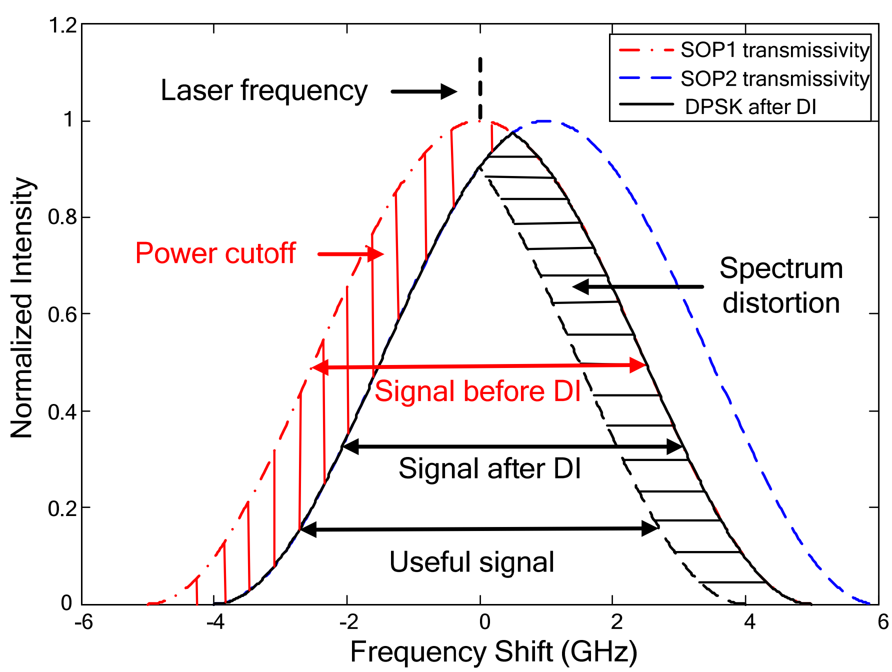

Figure 3.3 The spectrum profile of the received DPSK signal after the DI and the PDf induced penalty.

The PDf induced penalty not only depends on the PDf of the DI, but also has a strong correlation on the FSR of the DI. The PDf ratio, which is defined as $\frac{PDf}{FSR}$, is a key parameter to evaluate the PDf induced penalty in a DI. Figure 3.4 compares the transmissivity at the constructive port of two DIs. They both have a PDf of 1-GHz, but one DI has a FSR of 10-GHz while the other one has a FSR of 40-GHz. If there are two DPSK signals with bit rates of 10-Gb/s and 40-Gb/s respectively, passing the corresponding DIs, the output spectrums of the DIs can be illustrated in Figure 3.5. The red dot dash line and the red solid line show the spectrum profile of the 10-Gb/s DPSK signal before and after the 10-GHz DI respectively. The blue dot dash line and the blue solid line illustrate the spectrum profile of the 40-Gb/s DPSK signal before and after 40-GHz DI respectively.

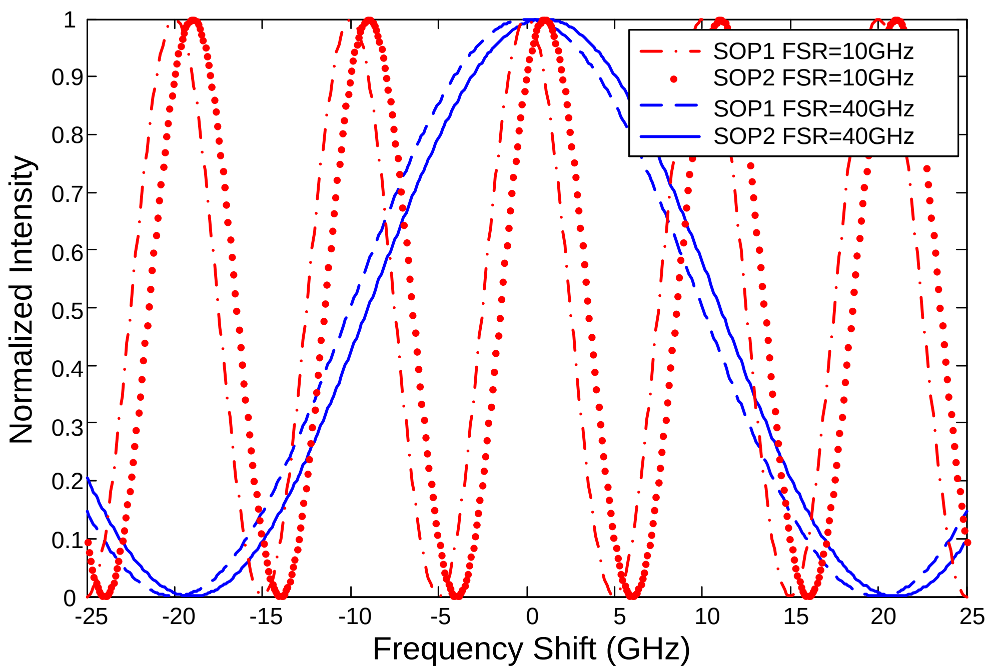

Figure 3.4 The transmissivity at the constructive port of the DIs with FSR=10-GHz and FSR=40-GHz for different SOP.

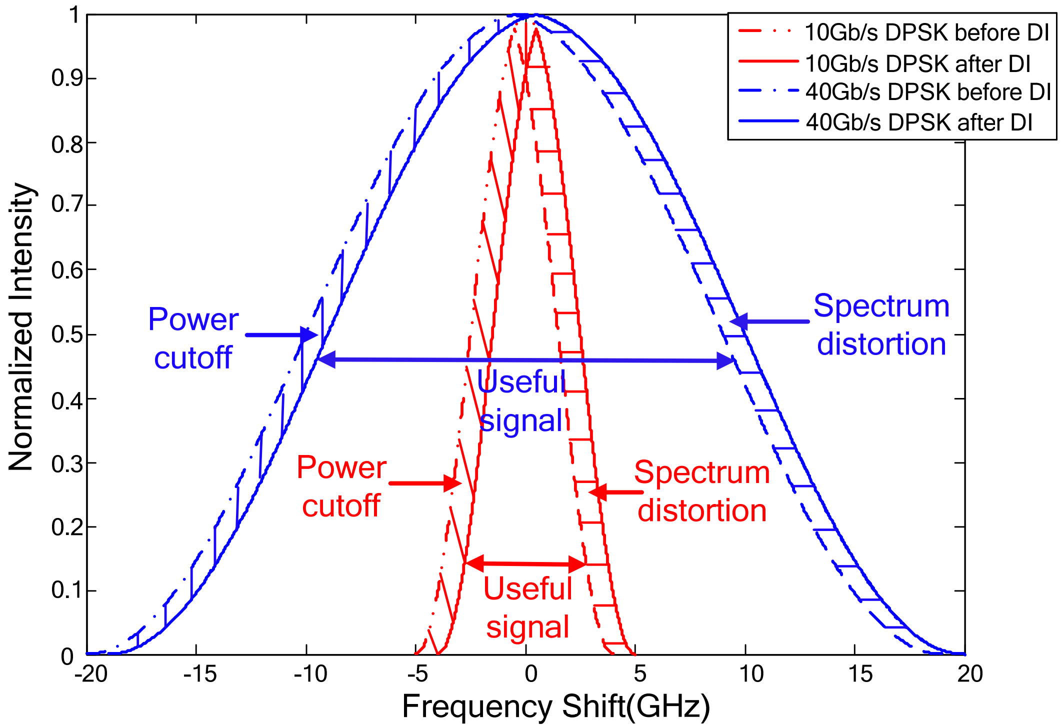

Figure 3.5 The comparison of the spectrum of the demodulated signal at the constructive port of the DIs with FSR=10-GHz and FSR=40-GHz and the PDf induced penalty.

To quantitatively evaluate the PDf induced penalty, we define two parameters called power cut off ratio $C_{cutoff}(\%) = \frac{P_{cutoff}}{P_{total}} \cdot 100\%$ and spectrum distortion ratio $C_{distortion}(\%) = \frac{P_{distortion}}{P_{total}} \cdot 100\%$ where P_{cutoff} is the power being cut off by PDf, $P_{distortion}$ is the power of the distortion part in the spectrum and P_{total} is the total power of the DPSK signal before passing through the DI. According to the Figure 3.3 and the Figure 3.5, $P_{cutoff} \approx P_{distortion}$. Therefore, the total penalty ratio is $C_{penalty}(\%) = \frac{P_{cutoff} + P_{distortion}}{P_{total}} \cdot 100\% \approx \frac{2 \cdot P_{cutoff}}{P_{total}} \cdot 100\%$. Obviously, smaller C_{cutoff} means smaller PDf induced penalty. From Figure 3.5, we may calculate that at PDf = 1-GHz, the DI with 10-GHz FSR has a $C_{penalty} = 38.6\%$ while the DI with 40-GHz FSR has a $C_{penalty} = 10\%$. We also calculate the PDf ratio for the two DIs. The comparison of PDf induced penalty and the PDf ratio for both DIs is shown in Table 3.1. It can be seen that the PDf induced penalty ratio is approximately four times of the PDf ratio, for both the 10-GHz DI and the 40-GHz DI. Although the PDf for both DI are the same, the DI which has a smaller FSR (larger PDf ratio) imposes more severe penalty on the signal because more portion of the signal power is being cut off and being distorted. Therefore, the smaller the PDf ratio is, the smaller the PDf induced penalty we should see.

Table 3.1 The comparison of PDf induced penalty and the PDf ratio for DIs with different FSR

FSR of DI	PDf induced penalty ratio ($C_{penalty}$)	PDf ratio ($\frac{PDf}{FSR}\cdot 100\%$)	$C_{penalty}/(\frac{PDf}{FSR})$
10-GHz	38.6%	10%	3.86
40-GHz	10%	2.5%	4

The actual DPSK signal may not have exactly the same spectrum profile as the transmissivity of the DI. For example, if the spectrum bandwidth of the DPSK signal is larger than the bandwidth of the DI's transmissivity, the signal after passing the DI should have the same spectrum profile with the shifted transmissivity of the DI, as shown in the black solid line in Figure 3.6. As it can easily be seen that the power penalty does not change but the horizontal shade area becomes larger, meaning that the signal's spectrum is even more distorted. This is the reason why RZ-DPSK signal is even more sensitive to the PDf of the DI.

When RZ-DPSK signal passes through the DI, the DI has a strong filtering effect on the signal as the spectrum width of RZ-DPSK signal is nearly twice FSR bandwidth of the DI. Meanwhile, the PDf of the DI introduces an extra impairment for the RZ-DPSK signal. The reason is that, different from the spectrum of the NRZ-DPSK signal which has a sharp top, the spectrum of the RZ-DPSK signal has a relatively constant top within the bandwidth of the transmissivity of the DI. Therefore, the spectrum of the RZ-DPSK signal after the DI has the same shape of the shifted transmissivity of the DI, just like the black solid line in Figure 3.6. Thus, in the presence of the PDf, the spectrum of the RZ-DPSK signal is more asymmetrical with respect to the laser frequency. As a result, the RZ-DPSK signal has a smaller tolerance to the PDf of the DI.

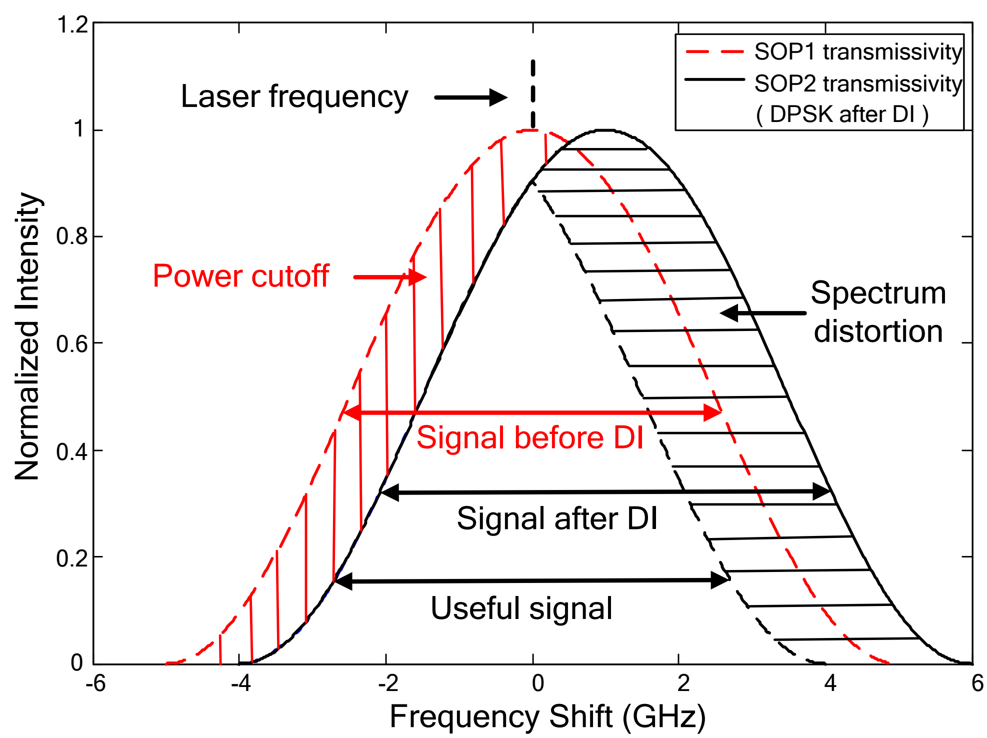

Figure 3.6 The spectrum profile of the received RZ-DPSK signal after the DI and the PDf induced penalty.

If the bandwidth of the DI's transmissivity is larger than the spectrum bandwidth of the DPSK signal, from the PDf ratio, we would expect a smaller PDf induced penalty. This can be verified by the results shown in Figure 3.7. The red dash dot line shows the spectrum profile of the DPSK signal before DI. The blue dash line illustrates the spectrum profile of the signal after DI with a FSR of 10-GHz and a PDf of 1-GHz. The black line represents the spectrum profile of the signal after DI with a FSR o f 11-GHz and a PDf of 1-GHz. As it can be seen from Figure 3.7, with the same amount of PDf, the DI with a FSR of 1-GHz larger than the bit rate generally has a smaller penalty than the DI with a FSR equals to the bit rate. Table 3.2 shows the PDf induced penalty ratio dependence on the FSR of DI. At the PDf = 1-GHz, by increasing FSR of 1-GHz, the PDf induced penalty ratio $C_{penalty}$ can be mitigated by 9.8% and 2.5% for the 10-Gb/s DPSK signal and 40-Gb/s DPSK signal. However, the FSR cannot be increased unlimitedly and it should be close to the bit rate so that the demodulation can be correctly performed. Therefore, a trade off should be made between the demodulation penalty and PDf induced penalty. Actually a FSR slightly larger than the bit rate has been reported to be advantageous in the presence of improper optical filtering and chromatic dispersion [4][5]. We believe a FSR slightly larger than bit rate also help reduce the penalty due to PDf.

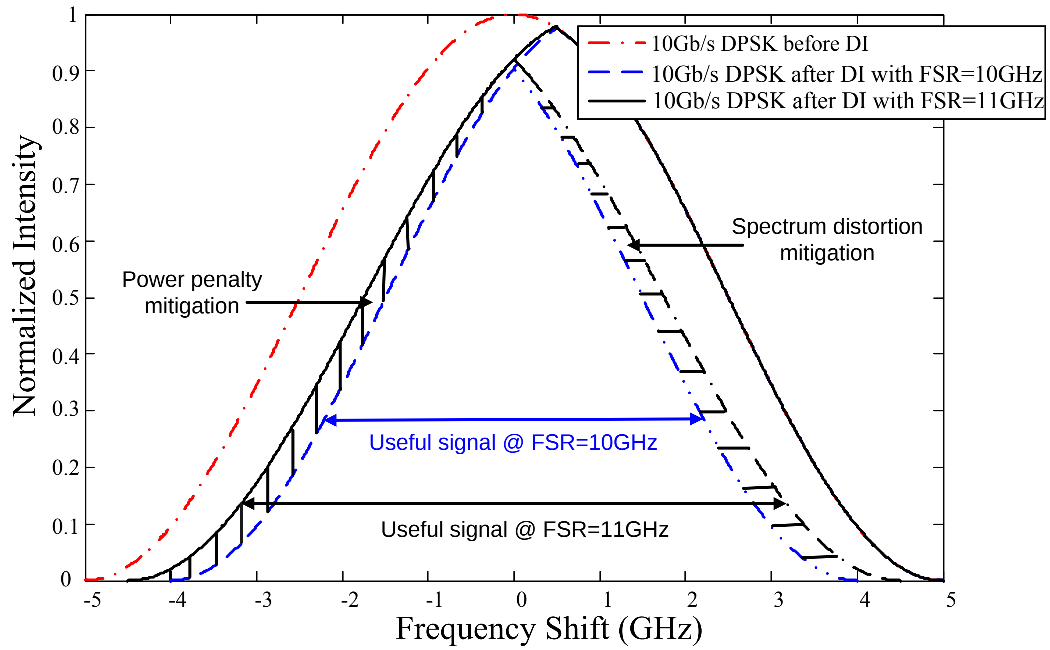

Figure 3.7 The comparison of the PDf induced penalty for the DIs with FSR=10-GHz and FSR=11-GHz.

Table 3.2 The PDf induced penalty ratio dependence on the FSR of the DI.

FSR of DI (GHz)	PDf induced penalty ratio ($C_{penalty}$)
10	38.6%
11	28.8%
12	19%
40	10%
41	7.5%
42	5%

3.3 Experiment on polarization dependent frequency shift induced penalty for DPSK demodulator [6]

3.3.1 Experiment Setup

In order to verify our analysis above, we conduct measurements of the penalty of a

10-Gbps DPSK signal from the PDf of a 10-GHz DPSK demodulator and the penalty of a 40-Gbps DPSK signal from the PDf of a 40-GHz DPSK demodulator respectively. The experiment setup is shown in Figure 3.8. The light is generated from a distributed feedback (DFB) laser with a central frequency at 1551.7-nm, and modulated with a Mach-Zehnder modulator (MZM) at 10-/40-Gb/s, appropriately biased to create DPSK modulated data. The MZM is driven by a pseudorandom bit sequence with a length of 2^{31}-1. The second MZM is driven by a 10-/40-GHz clock signal to generate 10-/40-Gb/s RZ pulses. The EDFA is used to compensate the losses of the modulators and the out-of-band noise generated is filtered out by using a 1-nm bandpass filter (BPF). A variable optical attenuator (VOA) is used to compensate the PDL of the 95/5 splitter as well as the demodulator such that the bit error rate (BER) floor, is the same for all states of polarization (SOP). The polarization controller (PC) before the DI is employed to change the SOP of the light entering the DI. In order to track the signal's SOP, a polarization analyzer (PA) is utilized. The 10-GHz DI has a measured PDf of 360-MHz and the 40-GHz DI has a measured PDf of 600-MHz. The DI is followed by a balanced detector.

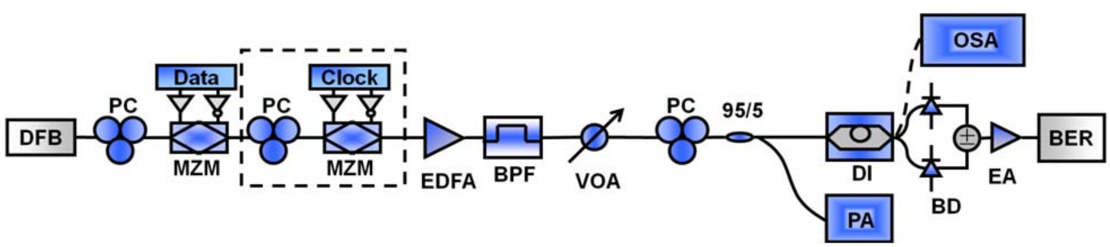

Figure 3.8 Schematic of the experiment setup.

3.3.2 Methodology

The first and foremost step is to find a 2-tuple of orthogonal SOPs that provides the maximal PDf in the DI. There are two ways that we can find this pair of SOPs. The first method does not require a high resolution optical spectrum analyzer (OSA). For a DI, the phase difference between the two arms depends on both the applied voltage on the thin film heater and the state of SOP of the signal. We can tune the DI's peak transmissivity to align it with the laser's frequency for any arbitrary SOP by applying voltage on the thin film heater to thermo-electrically compensate the PDf effect [7]. In order to find out the two orthogonal SOPs, we need to cover as many different SOPs as possible. The Poincare sphere, shown in Figure 3.9, is a graphical, three-dimensional representation of SOPs. Any SOP can be uniquely represented by a point on the sphere. The coordinates ($S1, S2, S3$) are the three normalized Stokes parameters that describes the SOP. Thus, we choose a set of points that uniformly cover the Poincaré sphere to obtain different SOPs as shown in Figure 3.9. To set the laser frequency fixed, for each SOP, we apply a voltage on the thin film heater such that the peak transmissivity of DI will align with the laser frequency. Since there is a linear relation between the applied voltage and frequency shift, the PDf can be given by the maximal difference in applied voltage multiplied by a conversion factor. Thus, the two SOPs that provide the maximal difference are considered to be orthogonal.

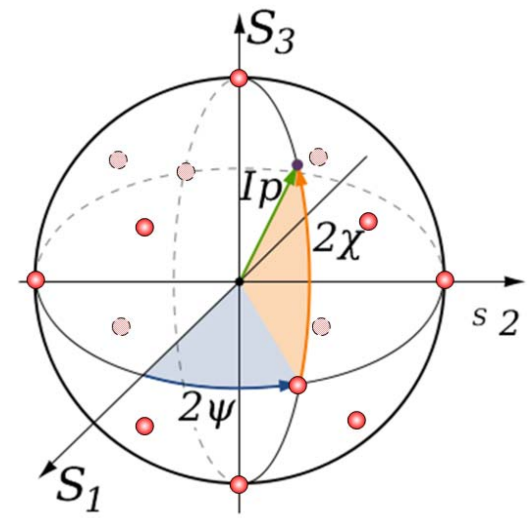

Figure 3.9 Set of SOPs that uniformly cover the Poincaré sphere [8].

The second method involves a high resolution OSA to see the details of the signal spectrum. In our experiment, we use a complex OSA with a fine resolution of 0.16-pm (20-MHz). To observe small frequency shifts of the optical spectrum, the measurements were done at the peaks and nulls of the spectrum, where the spectrum exhibits sharper and more abrupt transitions. By looking at the signal spectrum of the destructive port, we can tune the DI's peak transmissivity to align it with the laser's frequency for any arbitrary SOP. By looking at the signal spectrum of the constructive port, we can monitor the polarization dependent frequency shifts. By adjusting the PC in front of the DI, we set the SOP of the signal entering the DI to cover the entire Poincaré sphere. We then record a 2-tuple of orthogonal SOPs that provides the maximal frequency shift. These two SOPs represent the fast and the slow axis of the DI.

Our second step tuned the DI to maximally transmit one of these two SOP, such that the signal will experience the worst BER penalty due to PDf. To quantify this BER penalty, we have to measure the impact of a frequency offset of the laser on BER. The measurement consisted of detuning the laser's frequency to align the DI peak transmissivity at one of above two SOPs and measuring the BER for both SOPs. Figure 3.10 shows the aligning process and the measured PDf of 600 MHz.

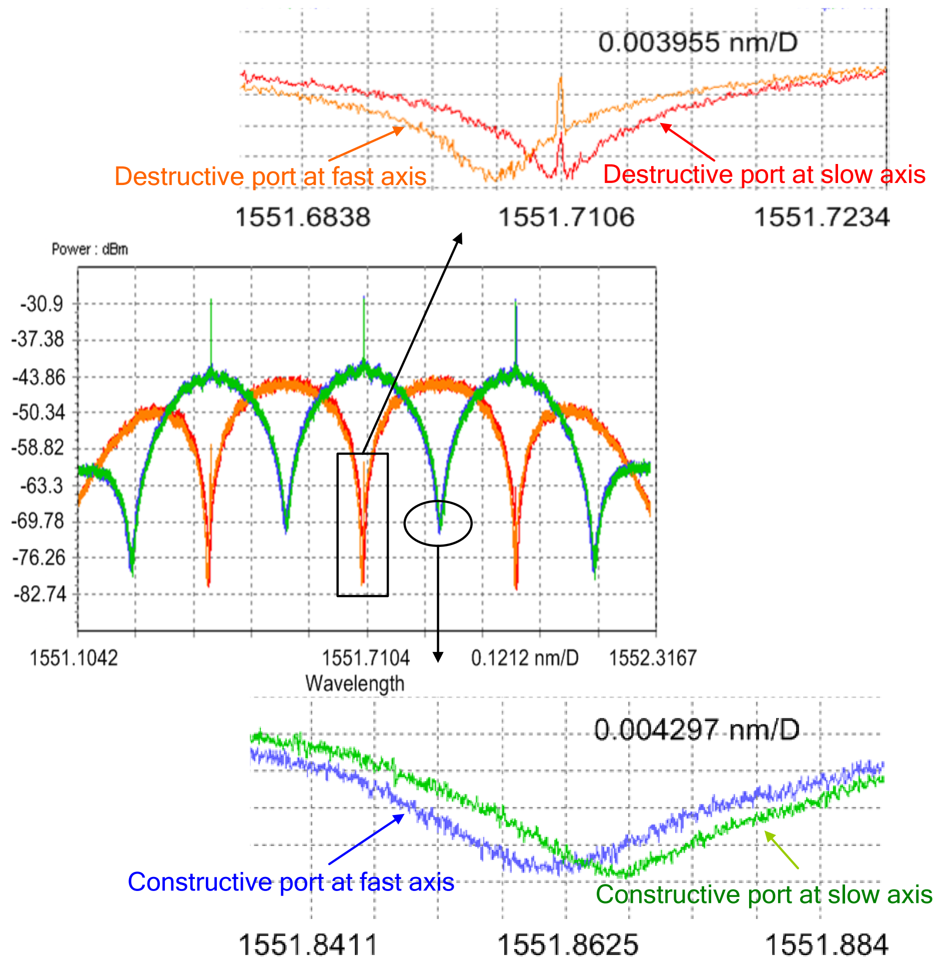

Figure 3.10 The aligning process and the PDf measurement.

3.3.3 Experiment Result

First, we compare the PDf induced BER penalty for a 10-Gb/s NRZ-DPSK signal and a 40-Gb/s NRZ-DPSK signal. The BER penalty is defined as $10\cdot(\log(\mathrm{BER}_1)-\log(\mathrm{BER}_2))$, where BER_1 and BER_2 are the BER at zero-frequency shift point for the two orthogonal SOPs respectively. Figure 3.11 shows the plot of log(BER) versus frequency detuning for the fast and slow polarization axis of two DI, one with a FSR of 10-GHz and the other one with a FSR of 40-GHz. In the zoom-in figure, we can see that the 10-GHz DI has a maximal PDf of 360-MHz while the 40-GHz DI has a maximal PDf of 600-MHz from the BER measurement. It is clear from the figure that the 10-Gb/s NRZ-DPSK signal is more sensitive to laser-DI misalignments. As shown in the zero-frequency shift point, the BER penalty of the maximal PDf for 10-GHz DI is around 0.85-dB while it is 0.15-dB for the 40-GHz DI. This effect can be explained by the PDf ratio. The PDf ratio of the 10-GHz DI is 0.04 while that of the 40-GHz DI is only 0.0175. This ratio enables us to compare DPSK demodulators with different PDf and FSR characteristics. The smaller the PDf ratio is, the smaller PDf induced BER penalty will be. This agrees well with our previous analysis.

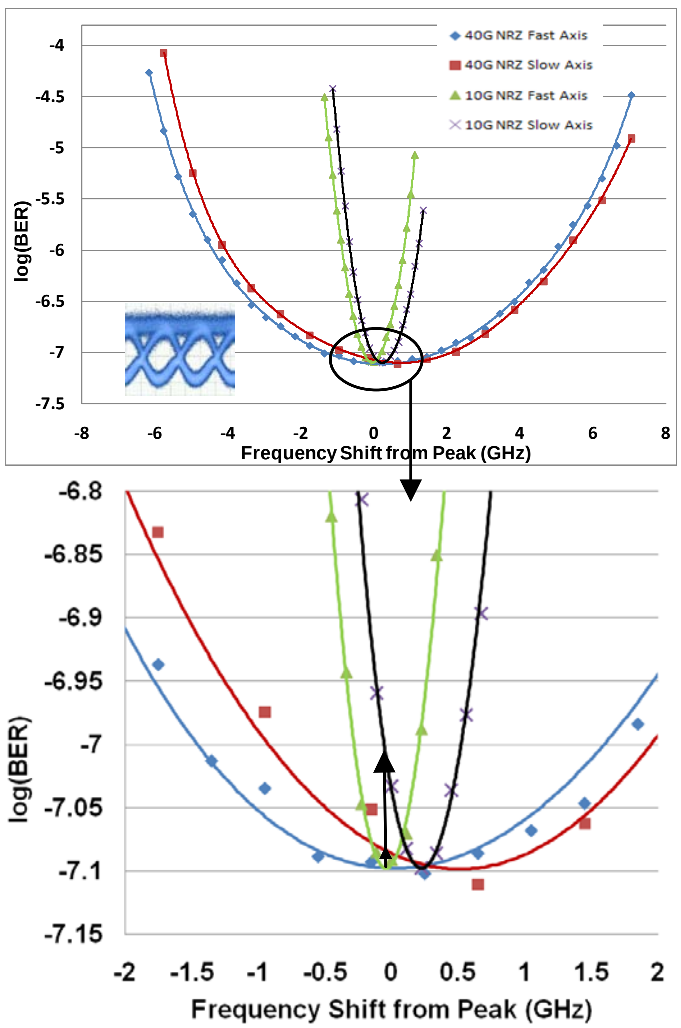

Figure 3.11 BER versus frequency detuning for the fast and slow polarization axis for the10-GHz and 40-GHz DI and the zoom-in at the frequency range of -2-GHz to 2-GHz.

The PDf induced penalty is further compared for 40-Gb/s NRZ-DPSK signal and 40-Gb/s RZ-DPSK signal to study the penalty incurred from PDf when the FSR of the DI is smaller than the bandwidth of the signal. Figure 3.12 shows the comparison of the spectrum of a 40-Gb/s NRZ-DPSK signal and a 40-Gb/s RZ-DPSK signal before and after the DI without PDf. As it can been seen from the red line, the RZ-DPSK signal before the DI has a much wider spectrum width than that of the NRZ-DPSK signal and has a lot of power in the side lobes. However, after passing the DI, the RZ-DPSK demodulated signal suffers more from optical filtering imposed by the shifted transmissivity of DI, as it is shown in green line in Figure 3.12. To measure the penalty induced by the PDf of the DI, we have to set the minimal BER to be the same for both NRZ and RZ. This implies that in the case of RZ, the required OSNR to achieve the same BER level is greater to account for the power lost from optical filtering.

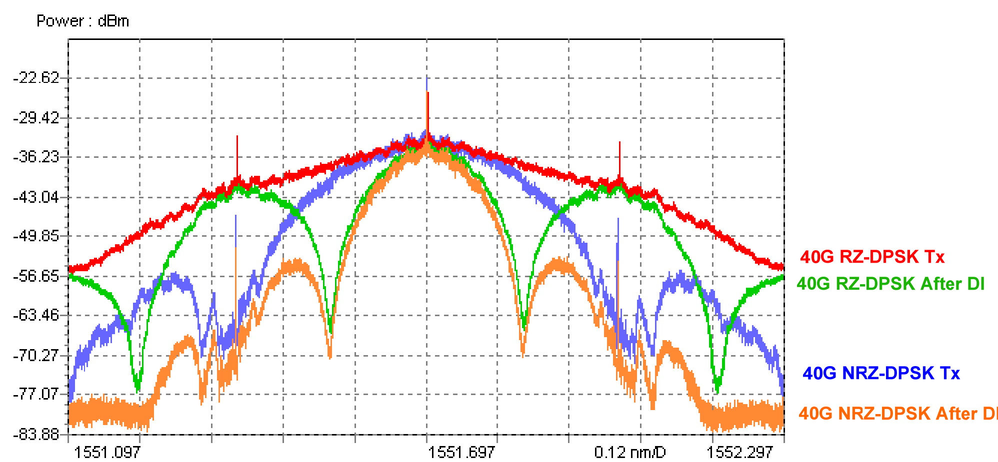

Figure 3.12 Comparison between the 40-Gb/s NRZ-DPSK and RZ-DPSK signals, both modulated and demodulated spectrums at no frequency shift.

As it is shown in Figure 3.12, for both the NRZ-DPSK and RZ-DPSK signals, if the peak transmissivity of the demodulator is perfectly aligned with the laser frequency, the spectral filtering is symmetrical and the demodulated signals will keep their symmetry. However, any small variations of the alignment will break this symmetry, leading to the power filtering and spectrum distortion. As it can be seen from Figure 3.13, for the same frequency shift (we deliberately increase the frequency shift to make the results legible), the RZ-DPSK signal suffers more from the spectrum distortion as its spectrum is more asymmetrical with respect to the laser frequency than that of the NRZ-DPSK signal. This is exactly what has been analyzed. Figure 3.14 shows the comparison of BER penalty between a 40-Gb/s RZ-DPSK and a 40-Gb/s NRZ-DPSK signal. As we can see from the figure, the measured PDf induced BER penalty for the 40-Gb/s NRZ-DPSK signal is measured to be 0.15-dB. While for the 40-Gb/s RZ-DPSK case, the PDf induced BER penalty is measure to be 0.4-dB. Therefore, the RZ-DPSK signal is more sensitive to the PDf of the DI.

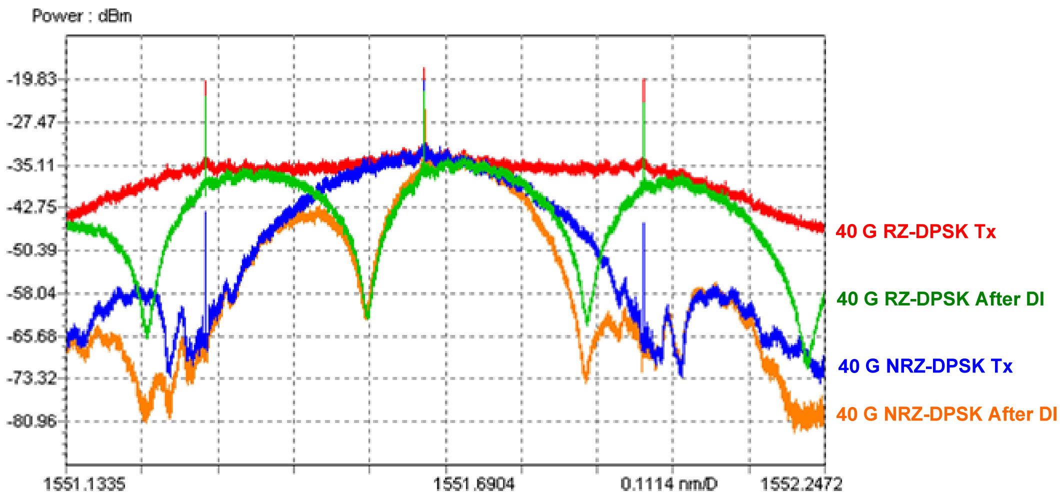

Figure 3.13 Comparison between the 40-Gb/s NRZ-DPSK and RZ-DPSK signals, both modulated and demodulated spectrums at a frequency shift of 11.425-GHz.

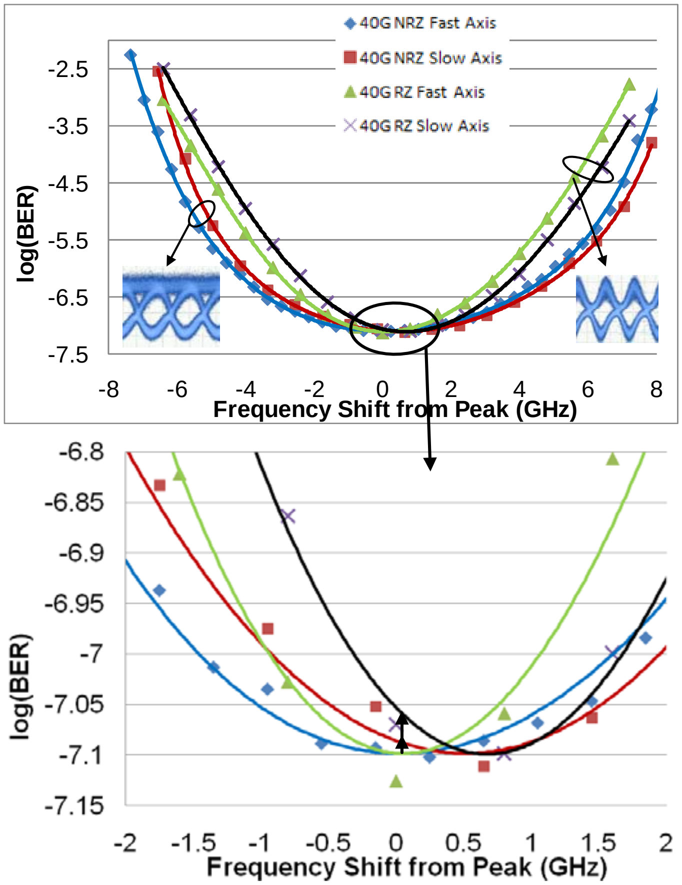

Figure 3.14 BER versus frequency detuning for the 40-Gb/s NRZ-DPSK and RZ-DPSK signals for the fast and slow polarization axis of a 40-GHz DI and the zoom-in at the frequency range of -2-GHz to 2-GHz .

3.4 Summary

In this chapter, we provide several possible solutions to mitigate the PDf induced penalty in a DI. Starting from the PDf induced penalty dependency on the PDf ratio, we suggested that using a DI with either small PDf or large FSR will help mitigate the penalty. However, PDf is usually determined by devices and the FSR should be closed to the data rate. Under such condition, we found that a DI with a FSR slightly larger than the signal bit rate will help suppress the PDf induced penalty due to less power cutoff and less spectrum distortion. Using NRZ-DPSK signal instead of RZ-DPSK signal actually improves the performance due to the smaller spectrum distortion of the NRZ-DPSK signal when passing the DI. In order to verify our analysis, we then conducted an experiment to measure the PDf induced penalty of a 10-GHz DPSK demodulator on a 10-Gb/s NRZ-DPSK signal, and a 40-GHz DPSK demodulator on a 40-Gb/s NRZ-DPSK signal, respectively. The experimental results show that the smaller the PDf ratio is, the smaller the PDf impact on the BER penalty will be. And degradation for the RZ signal has been found in the presence the PDf. These match well with our analysis. Other possible solution includes tuning the DI to maximally transmit an optical signal with an SOP that was in the mid-range of frequency shifts so that the absolute frequency shift of the peak transmissivity is halved. The effective PDf can therefore be reduced by a factor of two [7].

References

[1] Gnauck A. H. and Winzer P. J., 2005, "Optical phase-shift-keyed transmission," Journal of Lightwave Technology, vol. 22, no. 1, pp. 115-130.

[2] Lizé Y. K., Faucher M., Jarry É., Ouellette P.,Villeneuve É., Wetter A. and Séguin F., 2007, "Phase-tunable low-loss, S-, C-, and L-Band DPSK and DQPSK demodulator," Photonics Technology Letters, vol. 19, no. 23, pp. 1886-1888.

[3] Malouin C., Bennike J. and Schmidt T. J., 2007, "Differential phase-shift keying receiver design applied to strong optical filtering," Journal of Lightwave Technology, vol. 25, no. 11, pp. 3536-3542.

[4] Mikkelsen B., Rasmussen C., Mamyshev P. and Liu F., 2006, "Partial DPSK with excellent filter tolerance and OSNR sensitivity," Electronics Letters, vol. 42, no. 23, pp. 1363–1364.

[5] Lize Y. K., Christen L., Wu X., Yang J. Y., Nuccio S., Wu T., Willner A. E. and Kashyap R., 2007, "Free spectral range optimization of return- to-zero differential phase shift keyed demodulation in the presence of chromatic dispersion," Optics Express, vol. 15, pp. 6817–6822.

[6] Cotruta D., Xu X., Liboiron-Ladouceur O. and Plant D. V., 2009, "Polarization dependent frequency shift induced BER penalty in DPSK demodulators," The 22nd Annual Lasers and Electro Optics Society Meeting (LEOS 2009), WM1.

[7] Cotruta D., Liboiron-Ladouceur O., Lize Y. K. and Plant D. V., 2009, "Polarization dependent power penalty in DPSK demodulation," The Conference on Lasers and Electro-Optics and The Quantum Electronics and Laser Science Conference (CLEO/QELS) 2009, JThE78.

[8] http://en.wikipedia.org/wiki/File:Poincar%C3%A9_sphere.svg

Chapter 4 Electronic Dispersion Compensation for Direct Detection Phase Modulation Formats

4.1 Introduction

As mentioned in Chapter 1, chromatic dispersion (CD) and polarization mode dispersion (PMD) can cause inter-symbol interference (ISI), which is one of the detrimental impairments for reliable high speed fiber-optic communication systems. Traditionally, CD has been controlled by the optical channel itself using the dispersion compensation fiber (DCF). Recently the electronic dispersion compensation (EDC) became an alternative solution that may offer a more flexible and cost-effective solution. EDC is done at either the transmitter or the receiver and is designed to reduce the ISI without knowing the cause of it. Thus, EDC is capable of simultaneously compensating the CD and the PMD.

EDC in the transmitter and the receiver have different functions. The transmitter based EDC, also called dispersion pre-compensation, is to compensate for CD by pre-filtering the signal with the inverse of the fiber transfer function. As both the amplitude and the phase of the transmitted signal can be pre-distorted by using arbitrary waveform generation, an ideal signal can be obtained at the receiver. Consequently it can compensate not only the dispersion, but also some nonlinear impairments [1][2][3]. However, it requires a good knowledge of the transmission channel and is not able to compensate time-variant impairments, such as the PMD. Therefore, the receiver based EDC can be an alternative to overcome the limitation. The receiver based EDC, also known as dispersion post-compensation or electronic equalizer, bear the potential of being made adaptive and thereby capable of estimating the channel response. The price to pay is that for the direct detection systems, the loss of phase information after the square law photodetection limits the amount of CD and PMD that can be effectively compensated. This problem can be addressed if coherent detection is employed.

4.2 History of electronic dispersion compensation

EDC for optical fiber communications was first proposed in 1990 [4][5]. However, the multi-gigabit-per-second data rates in optical communications were beyond the capabilities of high-speed electronics [6]. With the advances of the state-of-the-art high-speed electronics and fast digital signal processing technologies, electronic dispersion compensation technologies became feasible in fiber-optic communication systems. For example, nowadays, with the commercial availability of high-speed BiCMOS and CMOS processes of 130nm or smaller feature size, high-speed analog-to-digital and digital-to-analog converters (ADC/DAC) are made possible with a sampling rate over 20-Gb/s with sufficient resolution. They can be integrated with multi-million gate to undo fiber impairments for date rate of 10-Gb/s and beyond [7]. A 24-GSamples/s ADC with 6-bit resolution was made available in 90-nm CMOS according to [8]. Equalizers demonstrated in early experiments were mostly based on feed-forward equalizers (FFE) and decision feedback equalizers (DFE). In 2000, Buchali *et al.* at Alcatel Germany presented at ECOC 2000 that they demonstrated 10-Gbit/s dispersion mitigation using DFE [9]. Franz *et al.* also at Alcatel Germany reported the mitigation of CD and PMD in 43 Gbit/s optical transmission systems using a 5-tap FFE and a novel 1-tap DFE in 2006 [10]. In January 2008, Fludger *et al.* at Coreoptics and Khoe's group used FFE with coherent detection and POLMUX-RZ-DQPSK to achieve a successful robust 100-GE transmission over 2375km [11]. In 2004, maximum likelihood sequence estimator (MLSE) was reported. Färbert *et al.* presented at ECOC 2004 a 10.7-Gb/s receiver with digital equalizer using MLSE to compensate chromatic dispersion. A reach of 150-km was shown for NRZ transmission using a 4-state MLSE at the receiver [12]. Kupfer *et al.* showed at OFC 2007 that the dynamic PMD compensation capability has also been experimentally demonstrated. The results showed that an MLSE update rate of 2 kHz is suitable to compensate for a polarization rotation rate of up to 0.25-rad/ms with first order PMD [13]. And Gene *et al.* demonstrated joint PMD and chromatic dispersion compensation using an MLSE and showed that MLSE in a 10.7-Gb/s NRZ system improves by 60-70% the tolerance to first-order PMD in the presence of residual chromatic dispersion [14]. More recently, optical orthogonal frequency-division multiplexing (OFDM) technique was shown to be a very effective electronic dispersion compensation technique [15][16][17].

In this chapter, we provide a complete study of the EDC performance for direct detection phase modulation formats. In particularly, we investigate on the EDC's CD and PMD compensation capabilities for the DPSK signals. We then compare the performance of the EDC between intensity modulation format and phase modulation format. The EDC's capability for the CD compensation of different pulse shapes (RZ vs. NRZ) is also studied.

4.3 Principle of Electronic Dispersion Post-compensation

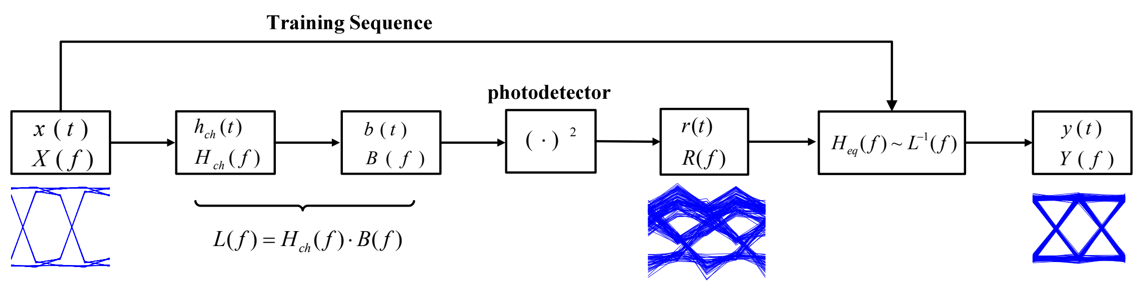

Figure 4.1 Model for a typical baseband communication system.

Figure 4.1 shows the model for a typical baseband communication system. Consider the input is a set of modulated signal $x(t)$. The transmission channel is assumed to be linear with an impulse response $h_{ch}(t)$. Since we only consider dispersion here, we neglect the noise added by the optical channel. The front end of the receiver consists of a bandpass filter with an impulse response $b(t)$. The received signal after the bandpass filter is $r(t) = b(t) \otimes h_{ch}(t) \otimes x(t)$ with an expression in frequency domain of $R(f)$. Let $L(f) = H_{ch}(f) \cdot B(f)$ denote the frequency response between the transmitted signal and the received signal $l(t) = h_{ch}(t) \otimes b(t)$ [18]. If we assume that the photodetector can detect the amplitude rather than the power of the signal, then when the frequency response of the equalizer satisfies $H_{eq}(f) = L^{-1}(f)$, the signal after the equalization in frequency domain becomes:

$$Y(f) = H_{eq}(f) \cdot R(f) = H_{eq}(f) \cdot L(f) \cdot X(f) = L^{-1}(f) \cdot L(f) \cdot X(f) = X(f) \tag{4.1}$$

The transmitted signal can be correctly recovered. The equalizer output $y(t)$ is then sampled at a rate of $1/T = k/T_s$, where T_s is the symbol duration. In the time domain, the signal after equalization is:

$$y(t)=h_{eq}(t)\otimes r(t)=\sum_{n=0}^{N-1}h_{eq}(nT)r(t-nT)=\sum_{n=0}^{N-1}C_n r(t-nT) \tag{4.2}$$

where $N\cdot T$ is the finite duration of the finite impulse response $h_{eq}(t)$. $h_{eq}(t)$ can be implemented with a finite impulse response (FIR) filter as shown in Figure 4.2. In the FIR filter, N is the number of taps, C_n are the tap coefficients (also called tap weights) and T is the tap delay. The output of the FIR filter is simply the weighted sum of a multiple samples of the time delayed inputs. The most important aspect for FIR filter is to obtain optimized coefficients. If the transfer functions of the pulse shaping, the fiber channel and the bandpass filter are known, it is easy to set the coefficients by mathematically inverting the frequency response of $L(f)$. However, the photodetector follows a square law, meaning that it only detects the power of the signal. Therefore, the transfer function $H_{eq}(f)$ should be the square of the transfer function $L(f)$ and it is where the phase information is lost. The reason why we use $H_{eq}(f)\sim L^{-1}(f)$ instead of $H_{eq}(f)=L^{-1}(f)$ is that the equalizer tries to approximate the nonlinear relationship. Consequently, it is not possible anymore to get the optimal FIR coefficients by mathematically inverting the transfer function of $L(f)$. A possible solution is to use adaptive equalizers that can automatically optimize the coefficients based on the coefficients adaptation algorithm. Another advantage of using these adaptive equalizers is that they are very effective in mitigating the time-variant PMD.

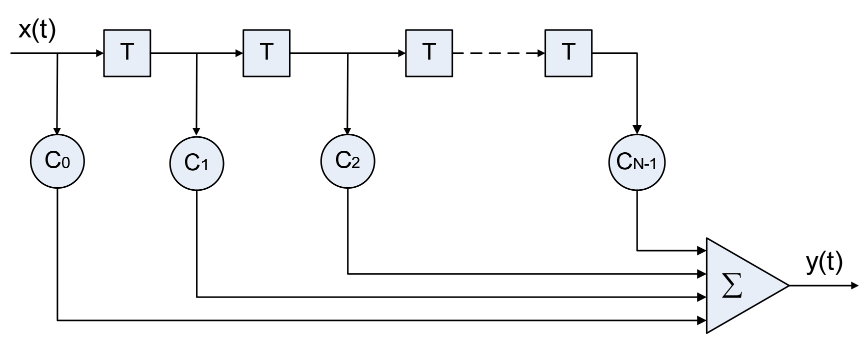

Figure 4.2 Schematic of FIR filter.

4.3.1 Types of adaptive equalizers

There are three main kinds of adaptive equalizers, namely feed-forward equalizer (FFE), decision feedback equalizers (DFE) and maximum-likelihood sequence estimation (MLSE) respectively. In this chapter, we focus on the performance of the FFE and DFE for phase modulation formats. The FFE, also called linear equalizer, is simply a FIR filter with a coefficients adaptation algorithm, as shown in Figure 4.3. The equalizer first calculates the error between the equalized signal and the expected signal. In the training mode, the error signal is the difference between the equalized signal and the training signal. After the training mode, the equalizer enters the decision directed mode, in which, the update of the tap weights occurs based on the previous decision result. The error signal then comes from the comparison between the equalized signal before and after the decision. Based on an adaptation criterion, such as least-mean-square (LMS) error or recursive least-square (RLS) error, the FFE can adjust its tap coefficients to set its frequency response to an optimum in terms of ISI compensation. However, the FFE is only able to remove the ISI cause by the symbols after the present estimation. That is why the DFE is introduced. The DFE consists of two filters, a feed-forward filter and a feedback filter, shown in Figure 4.4. The feed-forward filter is identical to the FFE. The feedback filter has its input from previously detected symbols and is used to remove that part of the ISI from the present estimate caused by previously detected symbols. The DFE is actually a nonlinear equalizer because the feedback filter contains previous detected symbols. The output of the DFE can be expressed as:

$$y(t)=\sum_{n=0}^{N_1-1}C_n x(t-nT)-\sum_{m=1}^{N_2}B_m y(t-mT_s) \tag{4.3}$$

where C_n and B_m are the tap coefficients of the feed-forward and feedback filters respectively. N_1 and N_2 are the length of the feed-forward and feedback filters. Note that in the feedback filter, the tap delay is the symbol duration T_s rather than the sample duration T because the feedback signal is the detected symbols, not the output samples.

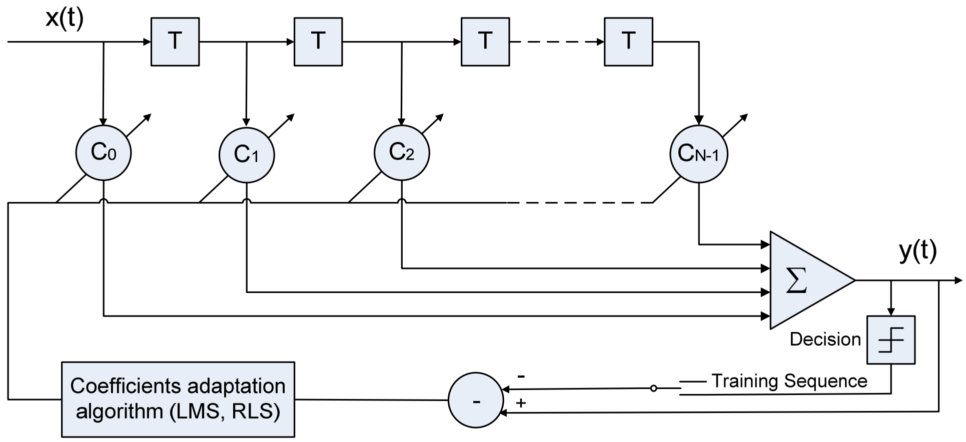

Figure 4.3 Schematic of FFE equalizer.

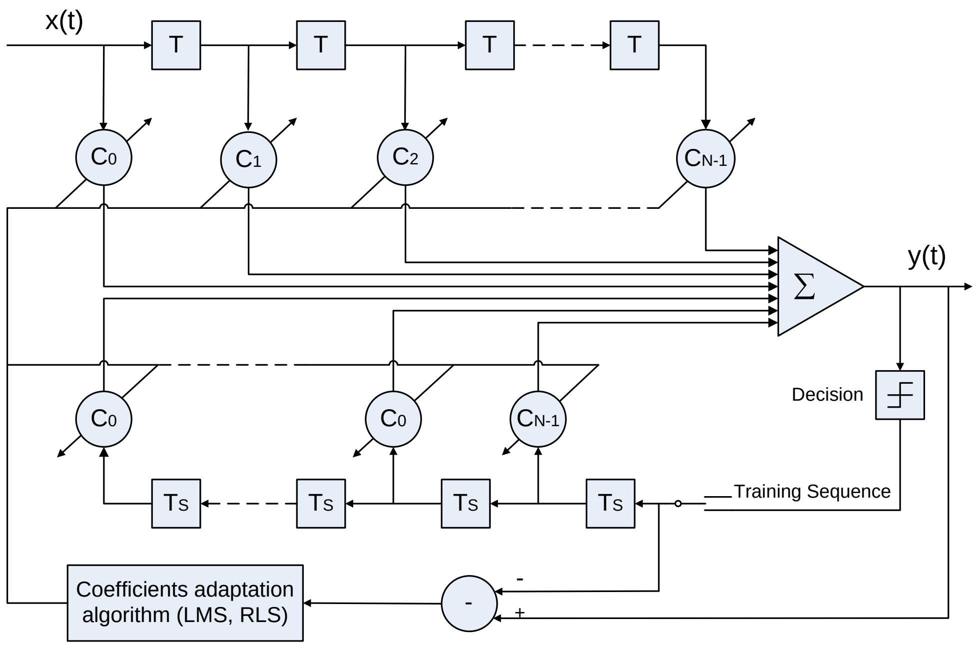

Figure 4.4 Schematic of DFE equalizer.

4.3.2 Coefficients Adaptation algorithm

This section is to obtain the tap coefficients adaption algorithm according to reference [19]. Assume we have an initial set of tap coefficients of

$$\mathbf{C}^T(t) = \left[C_0(t) \quad C_1(t) \quad \ldots \quad C_{(N-1)}(t) \right] \tag{4.4}$$

Let the received data at the equalizer input samples in the tapped delay line be:

$$\begin{aligned} \mathbf{r}(t) &= [r_0(t) \quad r_1(t) \quad \ldots \quad r_{N-1}(t)]^T \\ &= [r_0(t) \quad r_0(t-1) \quad \ldots \quad r_0(t-N+1)]^T \end{aligned} \tag{4.5}$$

where r_N is the r_0 signal at the tap delay N.

Let the equalizer output be:

$$\mathbf{y}(t) = \sum_{n=0}^{N-1} C_n(k) \cdot r_0(t-n) = \mathbf{C}^T(t)\mathbf{r}(t) \tag{4.6}$$

Then the error signal is:

$$\begin{aligned} e(t) &= \mathbf{s}(t) - \mathbf{y}(\mathrm{t}) \\ &= \mathbf{s}(t) - \mathbf{C}^T(t)\mathbf{r}(t) \end{aligned} \tag{4.7}$$

where $\mathbf{s}(t)$ is the training sequence. The equalizer requires a criterion to determine whether the tap coefficients achieve the optimal performance or not. Here, we use LMS error criterion which minimizes the mean square error between the transmitted signal and the equalized signal. The mean square error cost function is defined as:

$$\begin{aligned} J^{MSE} &= E\left\{e^2(t)\right\} \\ &= E\left\{\mathbf{s}^2(t) - 2\mathbf{s}(t)\mathbf{y}(t) + \mathbf{y}^2(t)\right\} \\ &= E\left\{\mathbf{s}^2(t)\right\} - 2E\left\{\mathbf{s}(t)\mathbf{C}^T(t)\mathbf{r}(t)\right\} + E\left\{\mathbf{C}^T(t)\mathbf{r}(t)\mathbf{r}^T(t)\mathbf{C}(t)\right\} \end{aligned} \tag{4.8}$$

When the filter coefficients are fixed, the cost function can be rewritten as follows:

$$\begin{aligned} J^{MSE} &= E\left\{\mathbf{s}^2(t)\right\} - 2\mathbf{C}^T \underbrace{E\left\{\mathbf{s}(t)\mathbf{r}(t)\right\}}_{\mathbf{p}} + \mathbf{C}^T \underbrace{E\left\{\mathbf{r}(t)\mathbf{r}^T(t)\right\}}_{\mathbf{R}} \mathbf{C} \\ &= E\left\{\mathbf{s}^2(t)\right\} - 2\mathbf{C}^T\mathbf{p} + \mathbf{C}^T\mathbf{R}\mathbf{C} \end{aligned} \tag{4.9}$$

Where $\mathbf{p}$ is the cross-correlation vector and $\mathbf{R}$ is the input signal correlation matrix. The gradient of the MSE cost function with respect to the equalizer tap weights is defined as follows:

$$\begin{aligned} \nabla_C J^{MSE} &= \frac{\partial J^{MSE}}{\partial \mathbf{C}} = \left[\frac{\partial J^{MSE}}{\partial C_{\mathbf{0}}} \quad \frac{\partial J^{MSE}}{\partial C_1} \quad \cdots \quad \frac{\partial J^{MSE}}{\partial C_{N-1}} \right] \\ &= -2\mathbf{p} + 2\mathbf{R}\mathbf{C} \end{aligned} \tag{4.10}$$

Using steepest descent algorithm, the equalizer can adjust its tap weights in direction of the negative gradient as follows:

$$\mathbf{C}(t+1) = \mathbf{C}(t) + \mu \cdot \left(-\nabla_C J^{MSE}\right) \tag{4.11}$$

where μ is weights' step size that controls the speed and accuracy of the equalizer tap adaptation.

$$
\begin{aligned}
\nabla_C J^{MSE} &= -2\mathbf{p} + 2\mathbf{RC} \\
&= -2\mathbf{s}(t)\mathbf{r}(t) + 2\left\{\mathbf{r}(t)\mathbf{r}^T(t)\right\}\mathbf{C}(t) \\
&= -2\mathbf{r}(t)\underbrace{\left\{\mathbf{s}(t) - \mathbf{r}^T(t)\mathbf{C}(t)\right\}}_{e(t)} = -2e(t)\mathbf{r}(t)
\end{aligned}
\tag{4.12}
$$

Thus, the equalizer tap adjustment is as follow:

$$
\mathbf{C}(t+1) = \mathbf{C}(t) + \mu \cdot \left(-\nabla_C J^{MSE}\right) = \mathbf{C}(t) + \mu \cdot e(t)\mathbf{r}(t) \tag{4.13}
$$

Therefore, by knowing the training sequence and the received signal and properly setting the weights' step size, the equalizer can automatically adjust its tap weights until the error signal is zero, meaning that the equalized signal is identical to the transmitted signal.

4.4 Performance study of electronic dispersion compensation for phase modulated optical communication systems

4.4.1 Simulation setup

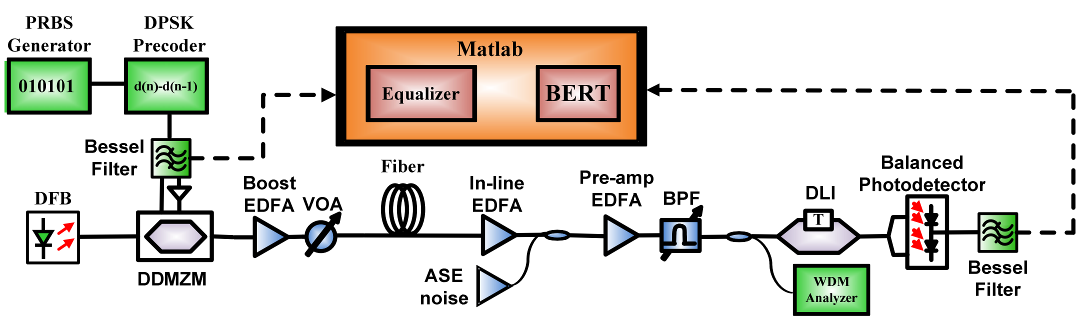

Figure 4.5 Simulation setup.

As shown in Figure 4.5, the simulation is carried out by the co-simulation on OptiSystem and Matlab. OptiSystem is used to generate, transmit and receive the modulated optical signal in optical fiber transmission system. While the EDC for the received signal is implemented in Matlab by using the equalizers and adaptation algorithms we analyzed in section 4.3.

To be specific, in OptiSystem, the electrical data is generated from a pseudo-random bit sequence (PRBS) generator with a pattern length of 2^{15}-1. To generate a DPSK signal, the data is encoded to be differential by utilizing a DPSK pre-coder following the PRBS generator. To make the simulation closed to real system, which normally does not have a sharp rising/falling edges, the signal pulse of the data is shaped by employing a 5th order Bessel filter with a cut-off frequency of 0.8×bit rate according to [20]. The signal at the output of the Bessel filter is used to modulate the optical signal. A copy of the signal is save to file, which is later post-processed in Matlab as the training sequence $\mathbf{s}(t)$.

The optical continuous-wave (CW) light is generated from a distributed feedback (DFB) laser with a linewidth of 2-MHz and an output power of 0-dBm. The wavelength of the CW light is set to 1550.12-nm according to the ITU-T DWDM grid. The electrical signal is modulated on the CW light by using a dual-drive Mach-Zehnder modulator (DDMZM) biased at the minimum of its transfer characteristic. The extinction ratio of MZM is set to 30-dB. A boost erbium-doped fiber amplifier (EDFA) with a noise figure of 6-dB is employed to compensate for the loss of the MZM and its output power is kept constant at 5-dBm. A variable optical attenuator follows the EDFA with an attenuation varied from 15-dB to 0-dB, corresponding to the OSNR ranging from 5-dB to 20-dB at the receiver.

The transmission link consists of SSMF and an in-line EDFA. The length of SSMF is varied depending on the dispersion value we investigate. The dispersion for SSMF is set to 16-ps/nm/km with a dispersion slop of 0.075-ps/nm^2/km. The attenuation for SSMF is 0.2-dB/km@1550nm. The nonlinear effect of SSMF is neglected. The gain of the in-line EDFA is adjustable such that the attenuation of SSMF can be fully compensated. The noise figure of the in-line EDFA is set to 6-dB.

At the receiver, an EDFA is employed to inject amplifier spontaneous emission noise in order to set the OSNR level between 5-dB and 20-dB. A pre-amp EDFA is used to amplifier the received signal to 3-dBm. A 2nd order Bessel optical filter with a 3-dB filtering bandwidth of 0.4-nm (50-GHz) is followed. Right after the optical filter, a WDM analyzer is added to record the OSNR level. The resolution bandwidth of the WDM analyzer is set to 0.1-nm. Differential demodulation of the DPSK signal is performed using an optical one-bit delayed Mach-Zehnder interferometer (MZI). The two outputs of MZI are differentially detected with a balanced photodetector with a responsivity of 1-A/W. The dark current of the photodetector is set to 10-nA and the thermal noise is set to 10^{-24}-W/Hz. A 5th order Bessel filter with a cut-off frequency of 0.8×bit rate is utilized after the balanced photodetector. The output of Bessel filter is saved to a file and post-processed in Matlab as $\mathbf{r}(t)$.

In Matlab, based on the two sequences $\mathbf{s}(t)$ and $\mathbf{r}(t)$ from OptiSystem, the program can calculate the $e(t) = \mathbf{r}(t) - \mathbf{s}(t)$. By properly setting the parameters, namely, the number of taps, training sequence ratio, step size of tap weight, samples per bit and the type of equalizer and then substituting $e(t)$ and $\mathbf{r}(t)$ into equation 4.13 iteratively, the program can derive a set of optimum tap weights for the equalizer. After the training mode, the equalizer will work on decision-directed mode based on the tap weight derived. In the decision-directed mode, the program starts counting the BER by comparing the equalized sequence with the transmitted sequence. Due to the limit of the computer speed and memory, the minimal BER is 3×10^{-5}. This is sufficient since we will calculate the required OSNR at BER=10^{-3}. Two important things must be considered in the implementation of the equalizer. First, $\mathbf{s}(t)$ and $\mathbf{r}(t)$ should be synchronized. Due to the filter induced delay, $\mathbf{r}(t)$ does not necessarily start from the same bit as $\mathbf{s}(t)$. A cross-correlation between $\mathbf{s}(t)$ and $\mathbf{r}(t)$ should be performed to find the relative delay. Second, the power of the transmitted signal and received signal should be at the same level. If not, the power level of the received signal should be normalized to the power level of the transmitted signal. The program will then send these coefficients to the equalizer. The eye diagrams of the unequalized signal and equalized signal are provided so as to visually compare the performance the electronic dispersion compensation.

4.4.2 Equalizer parameters

There are four important parameters in the design of the equalizers, namely, samples per bit, the number of taps, step size of tap weight, training sequence ratio.

4.4.2.1 Samples per bit

Ideally, the equalizer can achieve the best performance if it has all the information of the signal. However, the simulation tools, like OptiSystem and Matlab, cannot have unlimited number of points to represent the signal. They can only sample a limited number of points of the signal at a given sample rate. Therefore, a number of samples are grouped together to form a bit. Samples per bit specify the number of samples dedicated to each bit. The number of samples per bit should be an integer, with the minimum being one, which is referred as bit rate sample. Of course, the more samples per bit, the more information of the signal can be preserved. Nevertheless, too many samples per bit will lead to complicate computational complexity, while only provides marginal improvement. In order to study the equalizer's performance dependence on samples/bit, we simulated the BER versus OSNR at an accumulate dispersion of 1280-ps/nm (equals to the dispersion of 80-km SSMF) for the unequalized signal and the equalized signal from the equalizers with different samples per bit as shown in Figure 4.6. As it can be seen from the figure, the equalizer at 1-sample/bit is of the worst performance. But no much difference in the performance can be seen between the equalizers working at 2-samples/bit and 8-samples/bit. Thus the equalizer at 2-samples/bit is the optimal one considering the tradeoff between the computation complexity and the performance. In all the following simulations, the equalizer will use 2-samples/bit.

The equalizers working on one sample/bit are called bit-spaced linear equalizer while the equalizers working on multi samples per bit are called fractionally spaced equalizers. A bit-spaced linear equalizer consists of a tapped delay line that stores samples from the input signal. Once per bit period, the equalizer outputs a weighted sum of the values in the delay line and updates the weights to prepare for the next bit period. This class of equalizer is called bit-spaced because the sample rates of the input and output are equal. While for a *K* samples per bit application, a fractionally spaced equalizer receives K input samples before it produces one output sample and updates the weights. The output sample rate is the symbol rate $1/T_s$, while the input sample rate is K/T_s. The weight-updating occurs at the output rate, which is the slower rate.

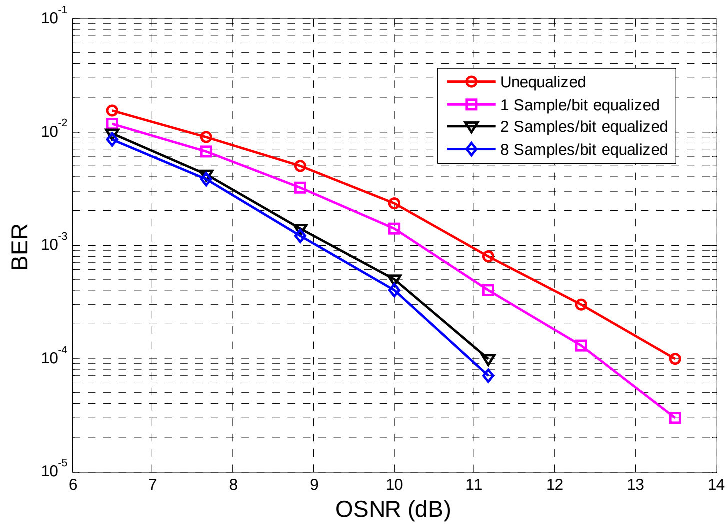

Figure 4.6 BER versus OSNR at an accumulate CD of 1280-ps/nm for the unequalized signal and the equalized signal from the equalizers with different samples per bit.

4.4.2.2 Number of taps

As it has been explained in Section 4.3, the inverted channel frequency response can be realized by using a FIR filter with a finite duration of $N \times T$, where T is the tap delay, or in another word, the sample period, N is the number of taps. Above analysis shows that the optimal sample period is half of the symbol period. If T is fixed, N should be as large as possible such that the sampled impulse response duration will approach the continuous time impulse response duration [21]. Ideally, if N is infinite, the equalizer is able to compensate dispersion of any value. However, due to nonlinear operation of the photodetector, the ISI shows high nonlinearity, probably making the equalizer fail to compensate. In addition, too large N will lead to large computational complexity without further enhancing the performance. To study the equalizer's performance dependence on the number of taps, we conducted a simulation of the BER versus OSNR at an accumulate dispersion of 1280-ps/nm for the unequalized signal and the equalized signal from the equalizers with 5 taps, 7 taps and 9 taps. The result shown in Figure 4.7 reveals that the equalizers with taps number equal to or beyond 5 taps do not exhibit much difference in the performance and compared to the equalizer with 3 taps, they have 0.5 dB gain in the OSNR when BER=10^{-3}. Therefore, the equalizer with 5 taps is sufficient to fully exhibit the dispersion compensation capacity of the equalizer. The following simulations are all based on the equalizers with 5 taps.

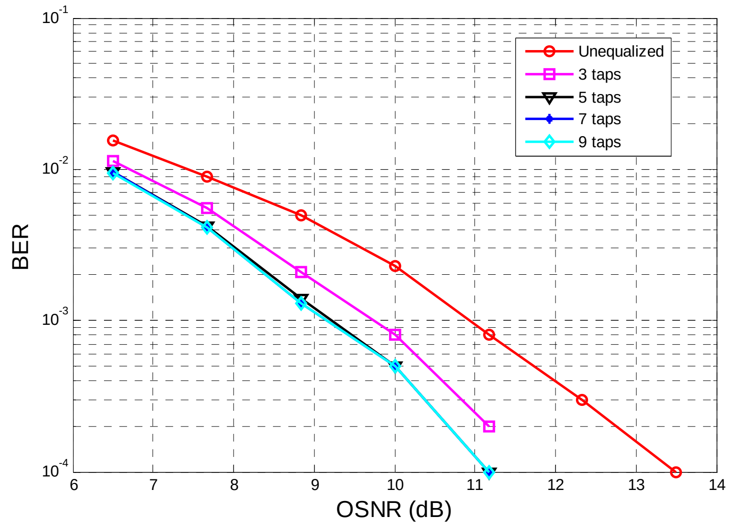

Figure 4.7 BER versus OSNR at an accumulate CD of 1280-ps/nm for the unequalized signal and the equalized signal from the equalizers with 5 taps, 7 taps and 9 taps.

4.4.2.3 Weights step size

According to [22], to ensure the convergence of the steepest-descent algorithm, the weights step size should satisfy the following inequality:

$$0 < \mu < \frac{2}{\lambda_{\max}} \tag{4.14}$$

where $\lambda_{\max}$ is the largest eigenvalue of the autocorrelation matrix of the received signal. Even when the step size is within the range, there is still a tradeoff between the performance of the equalizer and the convergence speed. If the step size is closed to the upper bound, the weights may have a large convergence variance, while if the step size is too small, the convergence speed will be slow. The convergence can be evaluated by plotting the weights to see after the convergence process if the weights reach certain stable values or not. Figure 4.8 illustrates the convergence process of a FFE equalizer compensating a dispersion of 1280-ps/nm. It also shows the convergence speed and variance dependence on the step size of tap weights. Figure 4.8(a) shows the result on the step size of 0.001 while Figure 4.8(b) shows the results on the step size of 0.0001. Although in both cases all the weights are converged, the one with larger step size converges faster but has a larger variance. By making the tradeoff, we found the step size of 0.0001 can ensure the fast convergence of the algorithm while still obtain good performance. It takes about 2000 bits (6% of the total pattern length) to converge to its stable status.

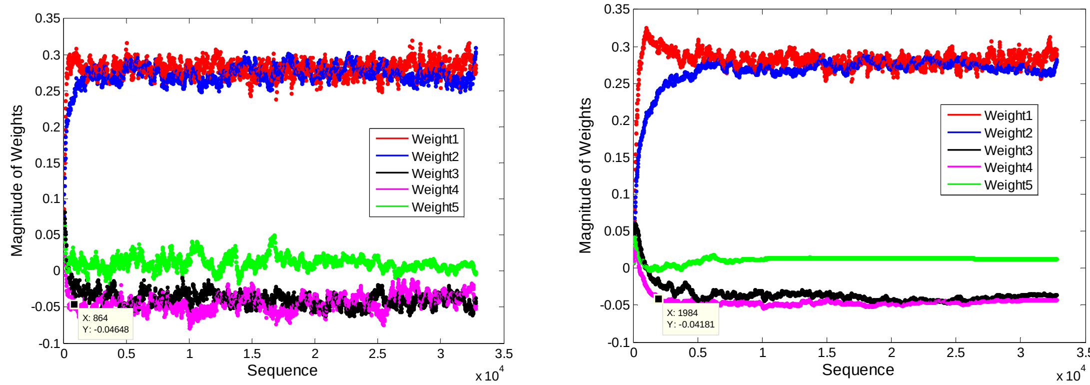

(a) (b)

Figure 4.8 The convergence speed and variance dependence on the step size of tap weights. (a) the result on the step size of 0.001; (b) the results on the step size of 0.0001.

4.4.2.4 Training sequence ratio

The training sequence ratio should be larger than the sequence ratio that is needed for the equalizer to reach its stable status. A precise way to determine the training sequence ratio is to plot the mean square error (MSE). When the MSE drops to an error floor, the training sequence will not affect the performance of the equalizer any more. Figure 4.9 and Figure 4.10 show the MSE before and after a FFE equalizer which compensates the dispersion of 1280-ps/nm, respectively. As it can be seen that, for the equalized signal, after 2000 bits (around 6% of the total length of the sequence), the MSE keeps below -6-dB, 8.4-dB lower than the MSE of the signal without equalization. Thus we set the training sequence ratio at 6%.

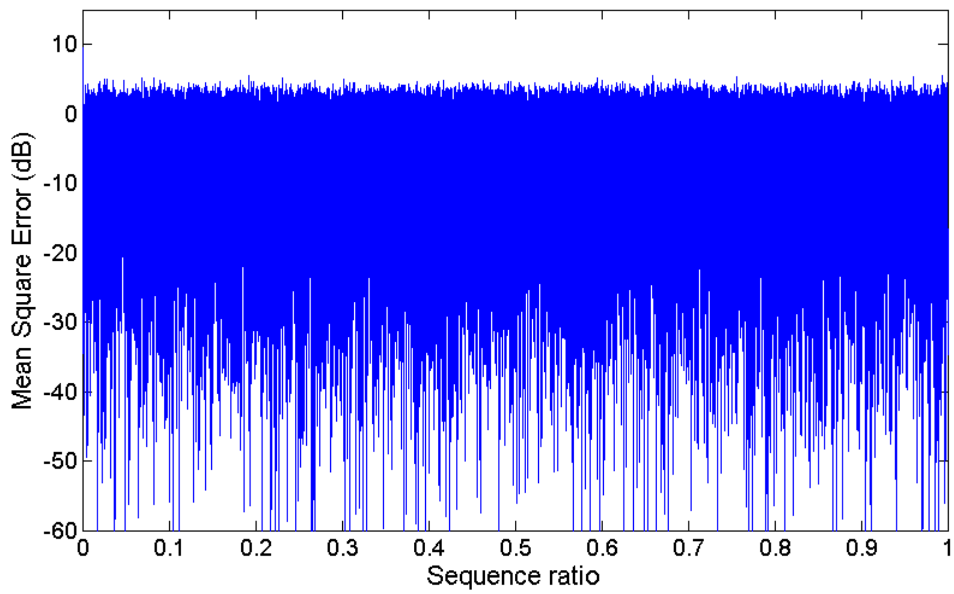

Figure 4.9 The MSE before a FFE equalizer which compensates the dispersion of 1280-ps/nm.

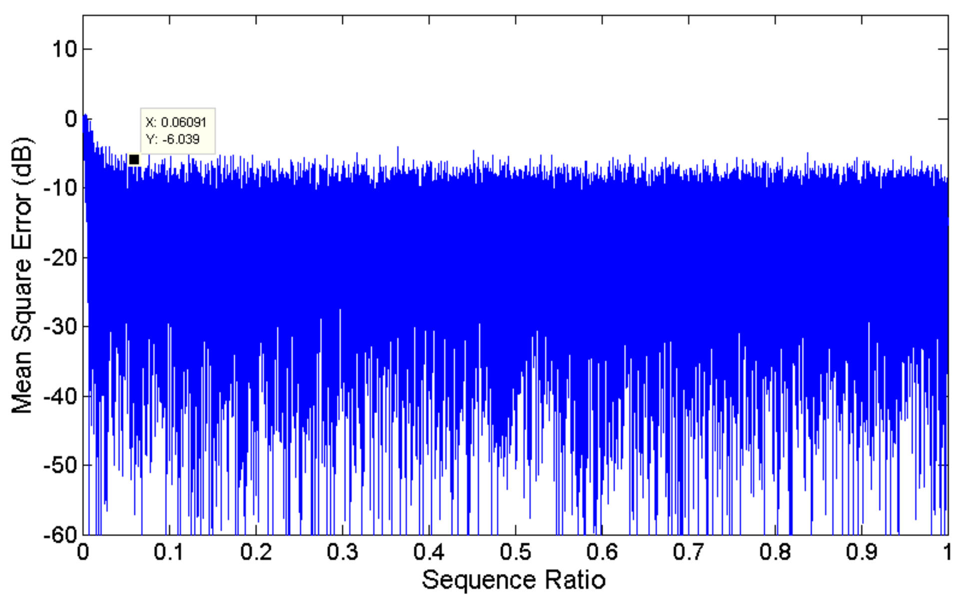

Figure 4.10 The MSE after a FFE equalizer which compensates the dispersion of 1280-ps/nm.

4.4.3 Simulation result

4.4.3.1 CD compensation

Figure 4.11 shows the required OSNR at BER=10^{-3} versus accumulative CD for the NRZ-DPSK signal without equalization, with the FFE equalization and with the DFE equalization. Figure 4.12 shows the corresponding signal eye diagrams at an accumulative CD of 1280-ps/nm (corresponds to the dispersion of around 80-km SSMF) and the OSNR of 13-dB. It can be observed from Figure 4.11 that at an accumulative CD of 1280-ps/nm, the dispersion penalty for the unequalized signal increases dramatically. This is because at this dispersion, the broadening of the pulse already reaches 100-ps, which is equal to the pulse width. At this dispersion, the equalized signal requires around 2-dB less OSNR than the unequalized signal to achieve the same BER level. In another way of comparison, at the same required OSNR level of 11-dB, the equalized signals offer around 300-ps/nm more tolerance to the CD than the unequalized signal. Another conclusion can be drawn from Figure 4.11 is that at an accumulative dispersion of 2000-ps/nm, the DFE equalizer outperforms the FFE equalizer at around 1-dB less required OSNR at BER=10^{-3}. This can be explained by our previous analysis that the DFE equalizer can compensate both the precursor and the postcursor ISI. Another possible reason is that the FFE equalizer can enhance the noise at the frequencies that high gain is needed [23]. For the DFE equalizer, at low OSNR, it has a greater likelihood that the incorrect decision of the feedback filter can be fed back, leading to error propagation. However, lager dispersion generally requires higher OSNR, and at a high enough OSNR, the feedback filter of the DFE almost works at noise free decision, therefore it does not exhibit any noise enhancement. Thus, DFE equalizer can provide better ISI elimination performance than FFE equalizer at a large accumulative dispersion.

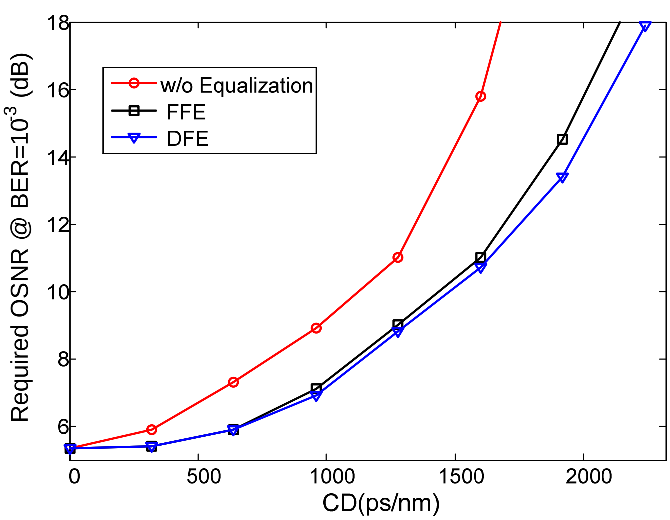

Figure 4.11 The required OSNR at BER=10^{-3} versus accumulative CD for the NRZ-DPSK signal without equalization, with the FFE equalization and with the DFE equalization.

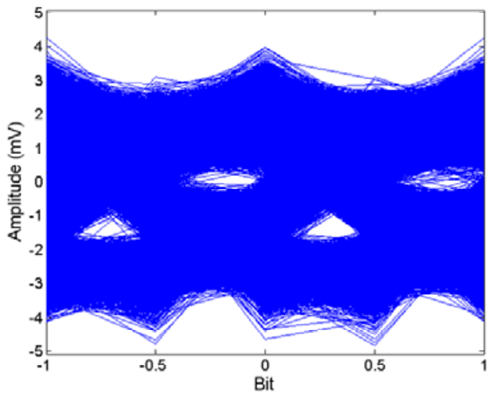

(a)

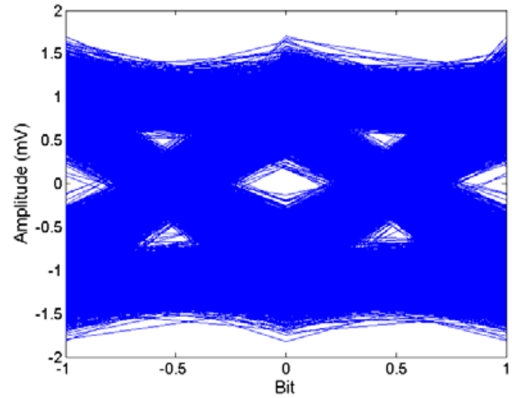

(b)

Figure 4.12 The signal eye diagrams at an accumulative CD of 1280-ps/nm and the OSNR of 13-dB: (a) before equalization; (b) after equalization.

4.4.3.2 PMD compensation

Figure 4.13 depicts the required OSNR at BER=10^{-3} versus differential group delay (DGD) for the NRZ-DPSK signal without equalization, with the FFE equalization and with the DFE equalization. Figure 4.14 shows the corresponding signal eye diagrams at a DGD of 60-ps and the OSNR of 10-dB. It can be seen from Figure 4.13 that at a DGD of 60-ps, the equalized signal requires around 2-dB less OSNR than the unequalized signal to achieve the same BER level. By looking at the same required OSNR at 8-dB, the equalized signal has a 10-ps tolerance to the DGD than the unequalized signal. The DFE equalizer also exhibits slightly better performance over the FFE equalizer in compensating the PMD.

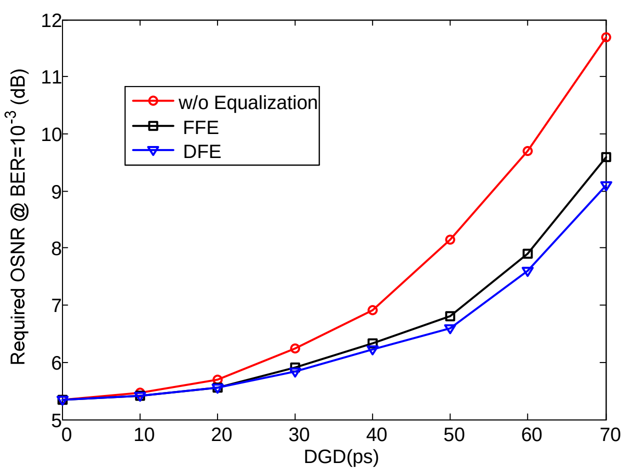

Figure 4.13 The required OSNR@BER=10^{-3} versus DGD for the NRZ-DPSK signal without equalization, with the FFE equalization and with the DFE equalization.

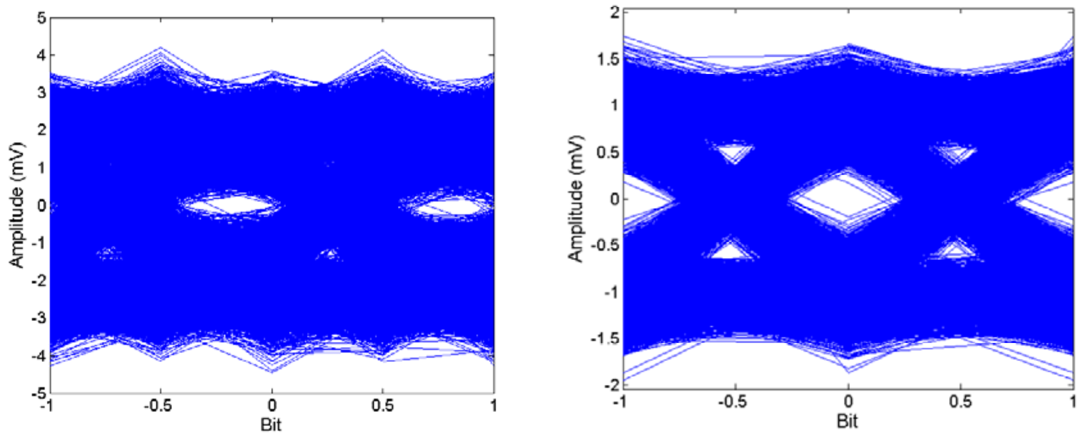

(a) (b)

Figure 4.14 The signal eye diagrams at a DGD of 60-ps and the OSNR of 10-dB: (a) before equalization; (b) after equalization.

4.4.3.3 Modulation formats (1): NRZ-DPSK vs. NRZ-OOK

We further evaluate the performance of the equalizer by comparing the dispersion compensation capacity for different modulation formats. In Figure 4.15, we compare the required OSNR at BER=10^{-3} versus accumulated CD for the NRZ-DPSK signal and the NRZ-OOK signal without equalization, with the FFE equalization and with the DFE equalization. Figure 4.16 shows the eye diagrams for the NRZ-OOK signal without and with equalization at an accumulative CD of 1280-ps/nm and the OSNR of 14-dB. It can be seen that at a dispersion of 1280-ps/nm, the equalizers working with the OOK signal can reduce 4-dB OSNR penalty, while the equalizers working with the DPSK signal only have 2-dB OSNR improvement. Therefore, the equalizers work more effective with the OOK signal. The reason is that the delay interferometer of DPSK receiver introduces strong correlation between the samples with symbol spacing, making the decision samples having a larger variance than those in the OOK signal [24].

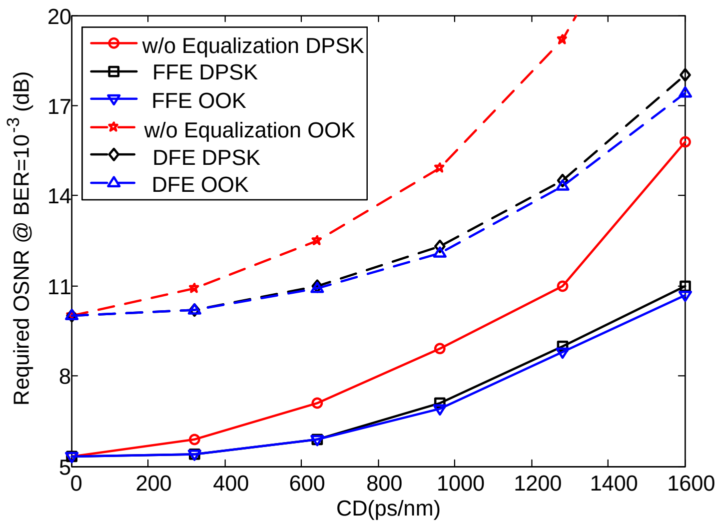

Figure 4.15 The required OSNR at BER=10^{-3} versus accumulative CD for the NRZ-DPSK signal and the NRZ-OOK signal without equalization, with the FFE equalization and with the DFE equalization.

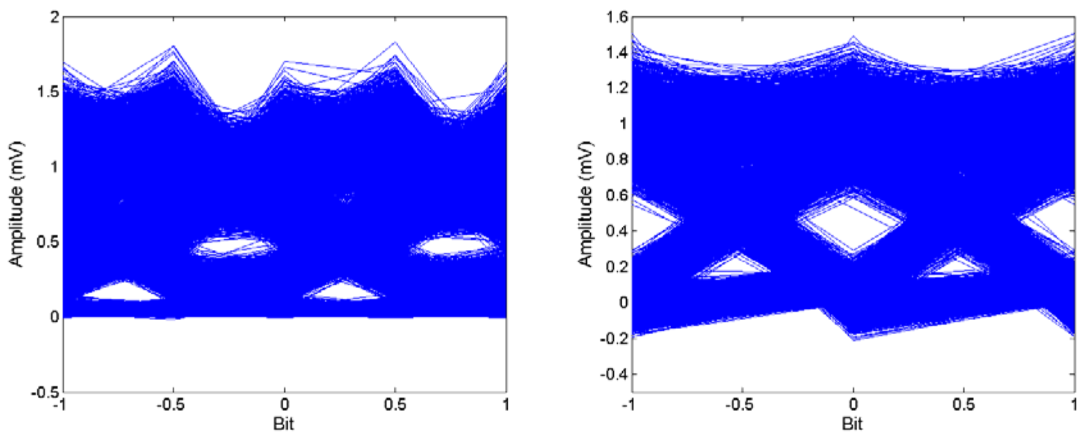

(a) (b)

Figure 4.16 The eye diagrams for the NRZ-OOK signal at an accumulative CD of 1280-ps/nm and the OSNR of 17-dB: (a) before equalization; (b) after equalization.

4.4.3.4 Modulation formats (1): NRZ-DPSK vs. RZ-DPSK

In Figure 4.17, we extend the comparison of the performance of the equalizers to the NRZ-DPSK signal and the RZ-DPSK signal. Figure 4.17 shows the comparison of the required OSNR at BER=10^{-3} versus accumulated CD for the NRZ-DPSK signal and the RZ-DPSK signal without equalization, with the FFE equalization and with the DFE equalization. Figure 4.18 shows the eye diagrams for the RZ-DPSK signal without and with equalization at an accumulative CD of 1280-ps/nm and the OSNR of 14-dB. At the back-to-back case, the RZ-DPSK signal has a slightly better sensitivity than the

NRZ-DPSK signal. However, the RZ-DPSK signal is more sensitive to CD. At a dispersion of 1280-ps/nm, the RZ-DPSK signal has around 3-dB more OSNR penalty than that of the NRZ-DPSK signal. This can be explained that the spectrum width of the RZ-DPSK signal is almost twice of the spectrum width of the NRZ-DPSK signal, meaning that the pulse broadening of the RZ-DPSK is also twice of the pulse broadening of the NRZ-DPSK, leading to much more ISI. Compared to the case of the equalization of the NRZ-DPSK signal, for the RZ-DPSK signal, the DFE equalizer outperforms the FFE equalizer by 1-dB less OSNR penalty. This can be understood that at the same OSNR level, the RZ-DPSK signal has a larger peak power than the NRZ-DPSK signal, thereby making the RZ-DPSK signal more resistant to the noise. This helps the DFE to make more reliable decisions and exhibit better performance.

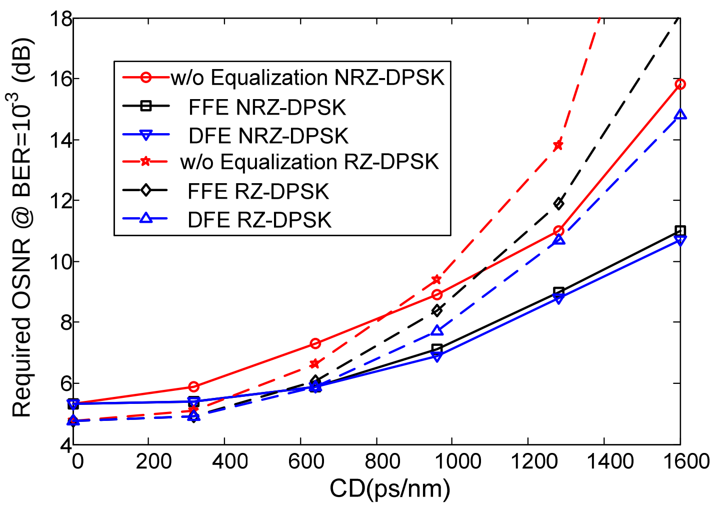

Figure 4.17 The required OSNR at BER=10^{-3} versus accumulative CD for the NRZ-DPSK signal and the RZ-DPSK signal without equalization, with the FFE equalization and with the DFE equalization.

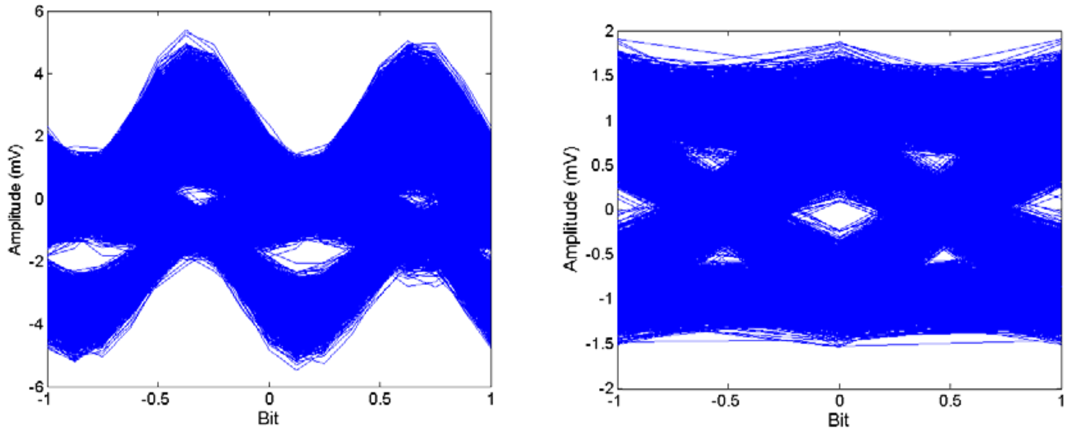

(a) (b)

Figure 4.18 The eye diagrams for the RZ-DPSK signal at an accumulative CD of 1280-ps/nm and the OSNR of 14-dB: (a) before equalization; (b) after equalization.

4.5 Summary

In this chapter, we depict the principle of electronic dispersion post-compensation for direct detection phase modulated signals. Based on this principle, we design in Matlab the adaptive equalizers, including the FFE and the DFE, to compensate various accumulative dispersions for phase modulated signals. Through the co-simulation with OptiSystem and Matlab, we study the EDC's CD and PMD compensation capabilities for the direct detection NRZ-DPSK signal. The simulation result shows that around 300-ps/nm CD and 10-ps DGD can be compensated by employing EDC. However, compared with the OOK signal, the EDC is actually less effective with the DPSK signal because the strong correlation between the samples with symbol spacing introduced by the DI. The investigation is extended to the RZ-DPSK signal and it was found that the DFE exhibits better performance with the RZ-DPSK signal.

References

[1] Roberts K., Li C. D., Strawczynski L., O'Sullivan M. and Hardcastle I., "Electronic precompensation of optical nonlinearity," Photonics Technology Letters, vol. 18, no. 2, pp. 403-405.

[2] Weber C., Fischer J.K., Bunge C. A. and Petermann K., "Electronic precompensation of intrachannel nonlinearities at 40 Gb/s," Photonics Technology Letters, vol. 18, no. 16, pp. 1759-1761.

[3] Chatelain B., Liboiron-Ladouceur O., Gagnon F. and Plant D.V., 2009, "Optimized pulse shaping for mitigating optical nonlinearity," The Conference on Lasers and Electro-Optics and The Quantum Electronics and Laser Science Conference (CLEO/QELS) 2009, CTuL2.

[4] Winters J. H. and Gitlin R. D., 1990, "Electrical signal processing techniques in long-haul fiber-optic systems," IEEE Transaction on Communications, vol. 38, no. 9, pp. 1439-1453.

[5] Winters J. H., 1990, "Equalization in coherent lightwave systems using a fractionally spaced equalizer," Journal of Lightwave Technology, vol. 8, no. 10, pp. 1487-1491.

[6] Gene J. M., Winzer P. J., Chandrasekhar S. and Kogelnik H., 2007, "Dispersion and chromatic dispersion using electronic signal processing," Journal of Lightwave Technology, vol. 25, no. 7, pp. 1735-1741.

[7] Beggs B., 2009, "Microelectronics advancements to support new modulation formats and DSP techniques," The Optical Fiber communication/National Fiber Optic Engineers Conference (OFC/NFOEC) 2009, OThE4.

[8] Schvan P., Bach J., Fait C., Flemke P., Gibbins R., Greshishchev Y., Ben-Hamida N., Pollex D., Sitch J., Wang S. C. and Wolczanski, J., 2008, "A 24GS/s 6b ADC in 90nm CMOS," International Solid-State Circuits Conference (ISSCC) 2008, Digest of. Technical Papers, pp.544-545.

[9] Buchali F., Bulow H. and Kuebart W., 2000, "Adaptive decision feedback equalizer for 10-Gbit/s dispersion mitigation," The 26th European Conference on Optical communications (ECOC 2000), P. 5.2.5.

[10] Franz B., Rosener D., Buchali F., Bulow H. and Veith G., 2006, "Adaptive electronic feed-forward equalizer and decision feedback equalizer for the mitigation of chromatic dispersion and PMD in 43 Gbit/s optical transmission systems," The 32nd European Conference on Optical communications (ECOC 2006), P. 1.5.1.
[11] Fludger C. R. S., Duthel T., Van den Borne D., Schulien C., Schmidt E. D., Wuth T., Geyer J., De Man E., Khoe G. D. and De Waardt H., 2008, "Coherent equalization and POLMUX-RZ-DQPSK for robust 100-GE transmission," Journal of Lightwave Technology, vol. 26, no. 1, pp. 64-72.
[12] Färbert A., 2004, "Performance of a 10.7 Gb/s receiver with digital equaliser using maximum likelihood sequence estimation," The 30th European Conference on Optical communications (ECOC 2004), Th4.1.5.
[13] Kupfer T., Whiteaway J. and Langenbach S., 2007, "PMD compensation using electronic equalizers particular maximum likelihood sequence estimation," The Optical Fiber communication/National Fiber Optic Engineers Conference (OFC/NFOEC) 2007, OMH1.
[14] Gene J. M., Winzer P. J., Chandrasekhar S. and Kogelnik H., 2006, "Joint PMD and chromatic dispersion compensation using an MLSE," The 32nd European Conference on Optical communications (ECOC 2006), We2.5.2.
[15] Lowery A. J., Du L. and Armstrong J., 2006, "Orthogonal frequency division multiplexing for adaptive dispersion compensation in long haul WDM systems," The Optical Fiber communication/National Fiber Optic Engineers Conference (OFC/NFOEC) 2006, PDP39.
[16] Schmidt B. J. C., Lowery A. J. and Armstrong J., 2007, "Experimental demonstrations of 20 Gbit/s direct-detection optical OFDM and 12 Gbit/s with a colorless transmitter," The Optical Fiber communication/National Fiber Optic Engineers Conference (OFC/NFOEC) 2007, PDP18.
[17] Jansen S. L., Morita I., Tadeka N. and Tanaka H., 2007, "20-Gb/s OFDM transmission over 4,160-km SSMF enabled by RF-pilot tone phase noise compensation," The Optical Fiber communication/National Fiber Optic Engineers Conference (OFC/NFOEC) 2007, PDP15.

[18] Ip E. and Kahn J. M., 2007, “Digital equalization of chromatic dispersion and polarization mode dispersion,” Journal of Lightwave Technology, vol. 25, no. 8, pp. 2033-2043.

[19] Simon H., 2002, Adaptive filter theory, 4th edition, New Jersey: Prentice Hall.

[20] Ho K. P., 2005, Phase-modulated optical communication systems, Springer Publisher.

[21] Savory S. J., 2008, “Digital filters for coherent optical receivers,” Optics Express, vol. 16, no. 2, pp. 804-817.

[22] Proakis J. G., 2001, Digital Communications, 4th edition, McGraw-Hill Press.

[23] Nielsen T. and Chandrasekhar S., 2004, “OFC 2004 workshop on optical and electronic mitigation of impairments,” Journal of Lightwave Technology, vol. 23, no. 1, pp. 131-142.

[24] Wang J. and Kahn J. M., 2004, “Performance of electrical equalizers in optically amplified OOK and DPSK systems,” Photonics Technology Letters, vol. 16, no. 5, pp. 1397-1399.

Chapter 5 Conclusion & Future Work

Phase modulation formats are widely acknowledged to be the most promising candidate for future 40-Gb/s and 100-Gb/s long haul optical transmission systems. The unique advantages that phase modulation formats can offer are: (1) a better receiver sensitivity over intensity modulation formats with a balanced detector, e.g., a 3-dB sensitivity improvement using DPSK and a 1.3-dB sensitivity improvement using DQPSK; (2) excellent robustness against fiber nonlinearity; (3) high spectral efficiency when using multilevel phase modulation formats, especially QPSK/DQPSK, which can reduce the symbol rate to half the bit rate while still maintain reasonable required OSNR. However, challenging issues still exist for phase modulated signals. As the information is encoded in the phase, phase modulation formats are sensitive to the phase-related impairments, for example, fiber nonlinearity induced phase shift variance, fiber dispersion introduced intersymbol interference and polarization dependent frequency shift (PDf) of delay interferometer induced penalty during the phase-intensity demodulation. Therefore, our research focuses on these new challenging issues and eventually comes up with some possible solutions.

This chapter concludes the thesis with a brief review of the main contributions of the research presented in the preceding chapters. We also propose future research directions that could improve the performance of phase modulated optical systems.

5.1 Summary

In chapter 1, starting from Shannon's channel capacity limit, we briefly reviewed the technology revolutions of fiber-optic communication systems to approach this fundamental limit. We identified some key research problems facing current fiber-optic communication systems. We pointed out that advanced optical modulation formats, especially the phase modulation formats, are a key enabling technology to address these problems. Recently, electronic equalization and digital signal processing technologies from wireless communications are another supporting technology for future high speed long haul communication systems.

In chapter 2, we firstly identified that the main penalty for the DQPSK channel co-propagating with the OOK channels comes from that the pattern dependent intensity fluctuations of the neighboring OOK channels are converted into the phase noise of the DQPSK channels. We then proposed a model to theoretically analyze the XPM penalty dependence on the walk off effect. Based on this model, we reached two important conclusions: (1) The XPM penalty can be mitigated by using fibers with large local dispersion or intentionally introducing some residual dispersion per span. (2) From walk off effects point of view, the residual dispersion leading to one bit walk off is sufficient to suppress the XPM induced differential phase shift. Further increasing the residual dispersion may help reduce the XPM penalty but not because of the walk off effect. We conducted a simulation of a 42.7-Gb/s DQPSK channel co-propagating with 16×10.7-Gb/s on-off-keying (OOK) channels on different types of fiber with different dispersion maps. The result showed the DQPSK channel co-propagating with the OOK channels in SSMF suffers less XPM penalty than in LEAF. By using different residual dispersion, we found that the XPM penalty decreases with the increase of the residual dispersion, however, the XPM penalty over residual dispersion slope is getting smaller and smaller because the walk off effect does not help mitigate the XPM penalty once the residual dispersion already provides one bit walk off. We also found that less than 3 dB XPM penalty at practical OOK launch powers can be achieved by using SSMF and large residual dispersion per span.

In chapter 3, we started from the transfer function of the DI to analytically explain the penalty dependence on the PDf/FSR ratio of the DI. In order to verify our analysis, we conducted an experiment to measure the PDf induced penalty of a 10-GHz DPSK demodulator on a 10-Gb/s NRZ-DPSK signal, and a 40-GHz DPSK demodulator on a 40-Gb/s NRZ-DPSK signal, respectively. In our experiment, we proposed two methods to find a 2-tuple of orthogonal SOPs. The experiment results showed that the PDf ratio, defined as PDf/FSR, plays a predominant role in determining the performance of the demodulator. The smaller the PDf ratio is, the smaller the PDf impact on the BER penalty will be. We further investigate on the PDf induced penalty for a 40-GHz DPSK demodulator on a 40-Gb/s RZ-DPSK signal to study PDf incurred optical filtering effect and spectrum distortion. Degradation for the RZ signal has been found in the presence the PDf.

In chapter 4, we firstly depicted the principle of electronic dispersion post-compensation for direct detection phase modulated signals. Based on this principle, we designed in Matlab adaptive equalizers, including the FFE and the DFE, to compensate various accumulative dispersions for phase modulated signals. Through the co-simulation with OptiSystem and Matlab, we studied EDC's CD and PMD compensation capabilities for the direct detection NRZ-DPSK signal. The simulation results showed that around 300-ps/nm CD and 10-ps DGD can be compensated by employing the EDC. However, compared to the OOK signal, EDC is actually less effective with the DPSK signal because the strong correlation between the samples with symbol spacing introduced by the DI. The investigation was extended to the RZ-DPSK signal and it was found that the DFE exhibits better performance with the RZ-DPSK signal.

5.2 Future work

In this section, we propose directions for future research that could further improve the performance for phase modulation formats.

Coherent detection

Although EDC turns out to work with the direct detection DPSK signal, the amount of dispersion that EDC can compensate is still far from satisfaction for the long haul transmission system. The main constrain is that EDC cannot exactly invert the frequency response of the optical channel due to the presence of the square-law photodetector. Thus, the solution that EDC provides is not, and will never be optimal for the direct detection phase modulated signals. In order to make significant improvement, the whole information of the signal, including the amplitude, phase and polarization, should be accessible by EDC. We believe with coherent detection, EDC implemented here will be easily to work for long haul transmission system. Coherent detection is a demodulation technique that mixes the weak received signal with a strong optical signal from the local laser oscillator. The local oscillator functions like an optical amplifier to amplify the received signal without noise enhancement. Because of the superior receiver sensitivity over direct detection, coherent detection was extensively studied in the late 1980s and the early 1990s. However, at that time, due to the lack of effective dispersion compensation techniques, the performance of coherent detection was severely affected by the fiber dispersion. Moreover, phase recovery was another major obstacle for coherent detection as the lock of phase coherence between the carriers of transmitter laser source and the local oscillator was difficult to maintain. In the mean time, the advent of EDFA held back the development of coherent detection as EDFA can easily provide the same sensitivity improvement coherent detection can offer. Thanks to the development of high speed integrated circuit and real time digital signal processing techniques in recent years, the dispersion compensation and carrier and phase recovery can be done in the electrical domain after the detection, leading to the revival of coherent detection. Besides the improved receiver sensitivity, another significant advantage that coherent detection can bring is that coherent detection can preserve all the information of the optical field during detection, including the amplitude, phase and polarization, thereby make possible the demodulation for multilevel phase modulation formats (e.g. QPSK) and multi-dimension phase modulation formats (e.g. PDM-QPSK). Therefore, coherent detection is undoubtedly a key technology that can improve the performance of current phase modulated systems to approach the fundamental limit of fiber-optic transmission.

Optical orthogonal frequency-division multiplexing (OFDM)

OFDM is a classic technology in wireless communication and copper cable wire communication, has now become a very hot topic in optical communication domain and it is arguably to be the tendency of next-generation fiber-optic transmission. The great motivations behind optical OFDM are the partially overlap of OFDM subcarriers' spectra allows of very high spectral efficiency; Splitting the waveform into multiple subcarriers thereby reducing the data rate in each subcarrier and adding the cyclic prefix of proper length, OFDM can completely eliminate the ISI caused by CD and PMD; Serial to parallel and parallel to serial conversions of OFDM considerably relieve the electrical bandwidth requirement for the transceiver. Optical OFDM is believed to be a key technology for fiber-optic systems to approach the fundamental limit.

Maximum likelihood sequence estimator (MLSE)

As has been stated in chapter 4, the problem why the FFE and DFE equalizers do not provide an optimal solution is that the FFE and DFE equalizers try to estimate the frequency response of the optical channel, but they will never get the exact frequency response due to the presence of photodetector. Different from the FFE and DFE equalizers, MLSE equalizer does not try to estimate the frequency response of the optical channel, instead, it searches for the most probable transmitted bit stream. In MLSE, the probability of all the transmitted bit combinations is considered and the combination with the highest probability is assumed as the transmitted bit combination. Therefore, the detection performance of MLSE turns out to be optimal. This enables the MLSE to be able to compensate not only the dispersion but also the nonlinear effects. The main problem with the MLSE equalization is that its complexity scales exponentially with its memory, which limits the amount of CD that it can compensate.

Transmitter based EDC

The EDC at the receiver has been shown to increase the dispersion tolerance. However, the loss of the phase information after the square law detection limits the amount of chromatic dispersion that can be effectively compensated. Transmitter based EDC can avoid this limitation as the amplitude and phase of the transmitted signal can be exactly predistorted such that an ideal signal can be obtained at the receiver. In other words, transmitter based EDC can exactly invert the frequency response of the optical channel. Therefore, transmitter based EDC can give an optimal solution for compensating the dispersion. The signal can also be predistorted in such a way that the pulse shape resembles to the RZ pulse in time domain without changing too much spectral characteristics. Therefore, some nonlinear effects can also be mitigated by using transmitter based EDC.

In this thesis, we made several contributions to address key aspects in the direct detection optical phase modulation formats. We covered from dispersion compensation, nonlinearity mitigation to polarization induced frequency shift of the phase demodulator. These works provide a good foundation for our further research on coherent detection and digital signal processing. Many of the works can be applied directly on coherent systems. We believe these enabling technologies makes the direction detection phase modulation systems close to the limit. By employing coherent detection in the future, the systems can get even closer to the limit!